Al Kitab Journal
for Pure Sciences

An academic Semi-annual journal

Volume: 1- Issue :1 /Dec. 2017

Rules and Instructions For Publication In
Al-Kitab Journal For Pure Sciences

First: General requirements

1. The paper is submitted to the Editorial Secretariat directly in four copies with CD-ROM or E-mail of the magazine in MS-Word and PDF file.

2. Research before being sent to scientific evaluators is subject to the quotation Turnitin program.

3. Research shall be accepted for publication after being judged by scientific evaluators and according to the rules.

4. The publication fee in the Journal is JD (75000) for the researcher from inside the Faculty of University Writers and (125000) JD for researchers from outside the college and (125 $) for the foreign researcher.

Second: To prepare research for publication, authors must follow the following procedures.

1.   The article:

The article needs to be typed on one side of A4 paper (Right margin =2.5 cm, left margin =2.5 cm and 2cm for the top and bottom) with 1.5 space and the pages must be numbered.

2.   The content organization:

MS Word to be used as follows: "Simplified Arabic" font for the Arabic paper, and "Times New Roman" for the English articles. The Size of the title is 18 bold. The name of the authors will be typed in 11 bold in Arabic and 11 bold in English. Abbreviations, key words, the main headings and the reference, and the acknowledgment will be typed in 14 bold. Subheadings will be in 12 bold. The abstract will be in size 12. The body of the article/paper in size 12. The order of the content of the paper will be as follows:

The article heading, the names of authors and their addresses, the abstract (Both in Arabic and English).

3.   Research paper title: The title must be as short as possible and indicates the contents of the subject together with the name (names) of the authors. The names of the authors to who correspondence to be made should be indicated with (*) and showing his / her email.

4.   The size: The paper should contain no more than 15 pages of the journal pages including charts and diagrams. Extra pages will be charged at 5000 ID (3$) each.

5.   Abstract: The abstract should include the purpose and the means of the founding results and the conclusions. It should also contain the knowledge values of the subject of research. It is meant to be no more than 250 words. It should also emphasis on the content of the subject and includes the keywords used throughout the paper.

6.   Diagrams: Figures and diagrams must be given following the explanation referring to the diagram. Each diagram must contain its title below the diagram at the first size of 12. The diagram should be editable in terms of enlargement or reduction within the margins of the paper size. The parts of each diagram must be grouped drawing parts.

7.   Tables: The tables should follow the parts of main body and should be located below of the indicated part of the text. Tables must have titles with a text size 12. The text used inside the tables should be of size 12 keeping with in the cells of the table.

8.   References: The references used in the paper must be given in order and their numbers given inside square bracken [ ]. The following instructions are to be followed:

If the reference is a book, the First name of the reference must be given first followed by the other names. Then the title (bold and Italic) of the book, edition, year of publication, the publisher, place of publication (year of publication).

Example: [1] P. Ring and P. Schuck, "**The Nuclear Many-Body Problem**", First Edition, Springer-Varlag, New York (1980).

(b) If the reference is a research paper or an article in a journal: The name of the author must be given first, the title of the article, the name of journal, the volume (issue), page (Year).

Example: [1] Ali H. Taqi, R. A. Radhi, and Adil M. Hussein, **"Electroexitation of Low-Lying Particle-Hole RPA States of ^{16}O with WBP Interaction"**, Communication Theoretical Physics, 62(6), 839 (2014).

c) If the reference is an M.Sc or Ph.D thesis, the name of the anther must be written with the first name first followed by the surname, title of thesis, the name of the university, Country (Year).

Example: [1] R. A. Radhi, **"Calculations of Elastic and Inelastic Electron Scattering in Light Nuclei with Shell-Model Wave Functions**", PhD Thesis, Michigan state University, USA (1983).

(d) If the reference is from conference. Authors Name, "**Paper Title**", Conference, Country, Publisher, volume, page (Year).

Example: [1] Ali H. Taqi and Sarah S. Darwesh, **"Charge-Changing Particle-Hole Excitation of ^{16}N and ^{16}F Nuclei"**, 3rdInternational Advances in Applied Physics and Materials Science Congress, Turkey, AIP Conf. Proc., 1569, 27 (2013)

1.   The editor of the journal has the right in changing any statement or phrase the research content he may find it necessary in order of expressing the work suitable to the general style of the journal.

2.   After publishing the paper and its presentation in the journal page, the editors' team will destroy all the scrap papers. The author has no right asking for them in any case.

Proofreading
Assist. Prof. Abbas Jawdat Raheem
English Auditing

Assist. Prof. Ibraheem Ahmad Al-Umairi
Arabic Auditing

Technical Supervision
Omar Adil M. Ali
Muhammed Numan Murad
Marwan Hazim Ahmad ali
Ammer Saad Salih

Letter from the Editor In Chief

The progress and prosperity of the nations is a foundation that builds up the science and the continuity of a country that is more than 6,000 years old. The University College is struggling to fulfill its scientific responsibility, like other governmental and non-governmental academic institutions, scientific and scientific researchers in our academic and scientific premises, academic institutions and other academic scientific centers to be embedded in the broad knowledge.

Al-Kitab Journal for Pure Sciences welcomes the research and scientific studies of professors and researchers from universities, academic institutions and research and scientific centers from inside and outside Iraq. Our Journal aims to evaluate and publish research by academics and researchers as well as graduate students' research. In view of the many disciplines in the disciplines of pure science, the editorial board has approved that this Journal should publish its products and scientific research in the specialties of the medical, engineering and biomedical sciences and all related fields.

The task of the editorial board is to receive the research from the researchers and check it in terms of conformity with the conditions of publication and registration of research and give it a special number and identify the reviewers in the field of competence and the editorial board to send research to the reviewers and follow-up. And the receipt of research returns from the evaluation and delivery to the researcher for the purpose of making amendments approved by the evaluators and then provide them with the acceptance of publication after making the required amendments and the publication of research in the preparation of the journal each according to the allocation and sequence.

Prof. Dr. Ayad Ghany Ismaeel
Dean of Al-Kitab University
College
Editor In Chief

Table of Contents

Speed Control of Three-Phase Induction Motor Based on V/F Technique

Ahmed M.T. Ibraheem AL-Naib,
Lecturer
Dep. of Electrical Power Technology Eng., Technical Eng. College/ Mosul, Northern Technical University, Iraq
ahmed_alnaib85@yahoo.com

Abstract :
This paper presents the design of a Xilinx Field Programmable Gate Array (FPGA) based Sinusoidal Pulse Width Modulation (SPWM) for a three-phase Voltage Source Inverter (VSI) with Variable Voltage Variable Frequency (VVVF) for controlling the speed of a three-phase Induction Motor (IM) by using V/F control strategy in open loop mode. In the present work a Xilinx FPGA SPARTAN 3E card is used as a PWM generator to generate appropriate signals to the inverter switches. The FPGA is programmed by using the Hardware Description Language VHDL. Using Xilinx FPGA to generate PWM provides flexibility to modify the designed circuit without altering the hardware part, easy and fast circuit modification, comparatively low cost for a complex circuitry and rapid prototyping.
Keywords: Inverter, SPWM, V/F control strategy, IM, FPGA.

Introduction

The IMs are called the workhorse of the motion industry because they are the most widely used motors for appliances, industrial control, and automation. They are robust, reliable, simple, cheap and available in all power ratings. The squirrel cage types of IMs are very popular in variable-speed drives. When AC power is supplied to an IM at certain specifications, it runs at its rated speed. However, many applications need variable speed operations. Due to the progress in the field of semiconductor devices i.e. power electronics and integrated circuit, enabled the application of IMs for high-performance s speed, but can 'drives. These power electronics means not only control the motor s dynamic and steady state characteristics [1]. Advances in the power 'improve the motor electronics has led to an increased interest in three-phase VSIs with PWM control [2]. There are various kinds of PWM techniques available such as SPWM, third-harmonic injection PWM, current tracking PWM, space vector PWM, and others [3]. All these techniques aim to generating a sinusoidal inverter output voltage without low-order harmonics. The most widely used industrial applications are the SPWM and space vector PWM [2]. Most PWM techniques are carried out using analog circuits or modern digital control circuits, such as microprocessors, microcontrollers, Digital Signal Processors (DSPs), or Application Specific Integrated Circuits (ASICs) [4, 2, 3]. The development of FPGA with several thousands of logic gates and high logic density forms the future digital platform for control. In recent years motor control and power conversion employing FPGA technology are receiving increased attention because of their ability to meet the need for complex modulation schemes and high speed switching requirement [5]. For this reason, the FPGA kit is used in this work as a SPWM generator for signals driving the three-phase VSI. A three-phase VSI based on SPWM make it possible to control both the frequency and magnitude of the voltage applied to a motor with constant V/F control method in open loop mode. This form of control is relatively inexpensive and easy to implement. Feedback from the rotor is not utilized and the rotor is assumed to

follow the rotating flux generated in the stator. Examples of these applications include heating, air conditioning, fans and blowers [4].

2 Three-Phase Sinusoidal PWM VSI

Voltage source inverters, as the name indicates, receive DC voltage at one side and convert it to AC voltage on the other side. The AC voltage and frequency may be variable or constant depending on the application. Three-phase bridge inverters are widely used for AC motor drives and general-purpose AC supplies. Fig. 1 shows the inverter circuit. The circuit consists of three half-bridge, which are mutually phase-shifted by $2\pi/3$ angle to generate three-phase voltage waves. The input DC supply V_{DC} is usually obtained from a single-phase or three-phase utility power supply through a diode bridge rectifier and LC or C filter [6]
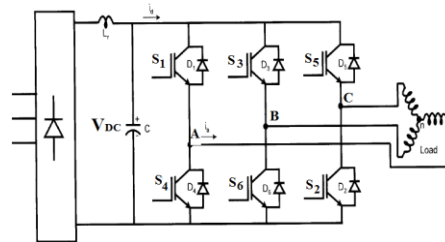
Fig(1): Three-phase bridge inverter

The SPWM technique is very popular for industrial converters. The generation of gating signals with SPWM is shown in Fig. 2. There are three sinusoidal reference waves (Vra, Vrb, and Vrc) each shifted by (120°). A triangular carrier wave (Vcr) is compared with the reference signal corresponding to a phase to generate the gating signals for that phase. Comparing the carrier signal (Vcr) with the reference phases (Vra, Vrb, and Vrc) produces (g1, g3, and g5) respectively these are applied to switches (S1, S3, and S5) respectively. Each of these gating signals are negated to produce gating signals (g4, g6, and g2) which are applied to the lower switches (S4, S6, and S2) [7]. The instantaneous 3-phase line-to-line output voltage can be expressed as:

$V_{ab} = V_{DC} (g1 - g3)$ …………….. (1)

$V_{bc} = V_{DC}(g3 - g5)$ ……………(2)

$V_{ca} = V_{DC} (g5 - g1)$ …………… (3)
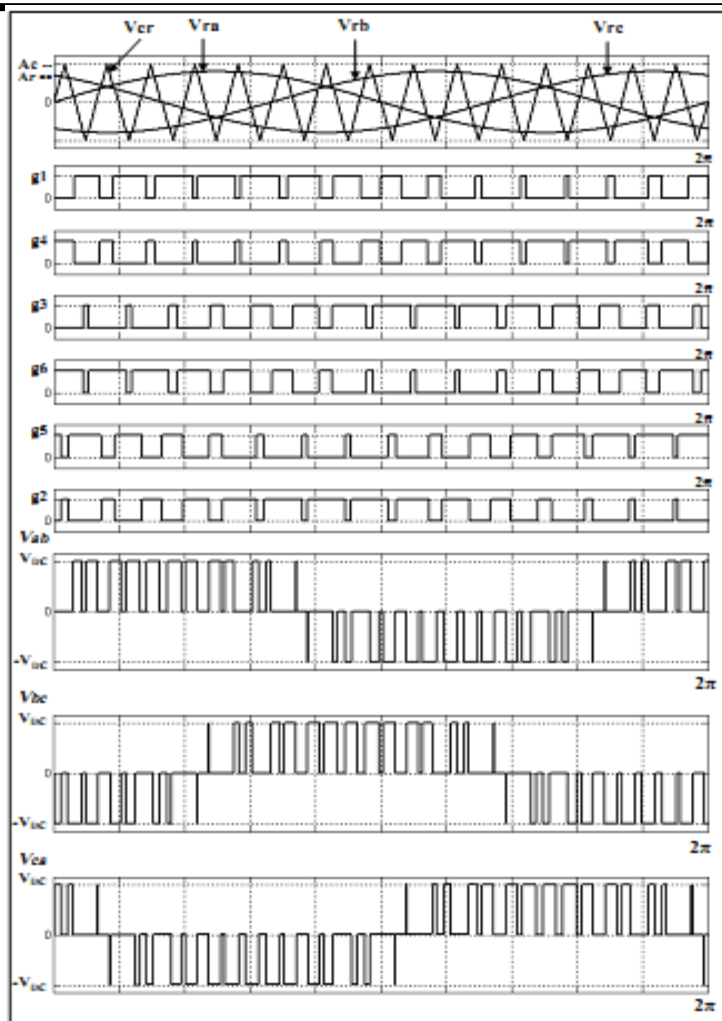
Fig(2): SPWM for three-phase inverter

The peak amplitude of the fundamental AC output line voltage can be given as [7:[

$$V_{ab1} = m_i * \sqrt{3} * \frac{V_{DC}}{2} \quad \text{for } 0<\text{m.}<1 \ldots \ldots (4)$$

Where $:m_i$ is the modulation index ratio, defined as the ratio of the amplitude of the sine reference wave) A_r (and triangular carrier wave) A_c (and is given by

$$m_i = \frac{A_r}{A_c} \quad \ldots \ldots \ldots \ldots .... \ldots \ldots (5)$$

Ideally ,m_i can be varied between 0 and 1 to give linear relation between the modulating signal and output voltage [6]

- V/F Speed Control Strategy :

The torque developed by the motor is directly proportional to the magnetic field produced by the stator. So, the voltage applied to the stator is directly proportional to the product of stator flux and angular velocity. This makes the flux produced by the stator proportional to the ratio of applied voltage and frequency of supply [8]

$stator\ voltage\ (V_s) = [stator\ flux\ (\phi)] * [angular\ velocity (w)]$

$$\phi = \frac{V_s}{w} = \frac{V_s}{2\pi f}$$

$$\phi \propto V_s / f$$

…………………………(6)

At rated voltage and rated frequency, the flux has rated value [7]. If the voltage is maintained fixed at its rated value while the frequency is reduced below its rated value, the flux increases. This will saturate the motor [9]. If the frequency is increased above its rated value, the flux and torque will decrease [7]. Variable frequency control below the rated frequency is generally carried out by reducing the machine phase voltage, along with the frequency (varying the voltage and frequency at the same ratio), in such a manner flux and hence, the torque can be kept constant throughout the speed range [8]

Block Diagram of the Proposed System

The basic block diagram of the AC drive system is shown in Fig. 3. This system is divided into five stages. The first stage represents generating the PWM signals via FPGA. The second stage represents gate drive circuit to isolate and buffer the FPGA from the three-phase bridge inverter circuit to protect the FPGA from being overloaded by excessive currents and to isolate it from the high voltages appearing on the power switches terminals. The third stage represents the three-phase bridge inverter circuit. Metal-Oxide Semiconductor Field-Effect Transistors (MOSFETs) are employed as the main switching devices. The fourth stage represents the three-phase step up transformer (for stepping up the output voltage of the three-phase inverter to feed the IM). Last stage represents the three-phase squirrel cage IM. The IM used in the study is a three-phase 380V, 1.7 A, 0.55 kW, 50 Hz with 4 poles.
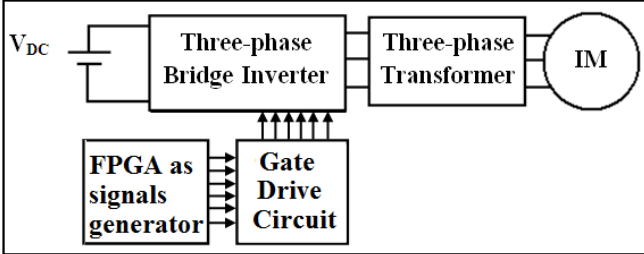
Fig(3): Block diagram of the proposed practical AC drive system

5 FPGA Based SPWM Control Scheme for VVVF Using V/F Control Strategy:

The overall block diagram of the proposed three-phase SPWM generator with V/F control strategy is shown in Fig. 4. The control system is divided into five major modules: three-phase sine wave generator module, triangular wave generator module, three-digital comparators module, dead time module, and V/F control module. This scheme (architectural control) gives the ability to adjust the speed of the IM by controlling the frequency and amplitude of the stator voltage, the ratio of stator voltage to frequency should be kept constant. VHDL code is used to model the entire system of the proposed architectural control .Xilinx-ISE 9.2i synthesis software is used as a developing environment. XILINX SPARTAN 3E XC3S500 FPGA Kit is used to downloaded VHDL code of the proposed architecture control.
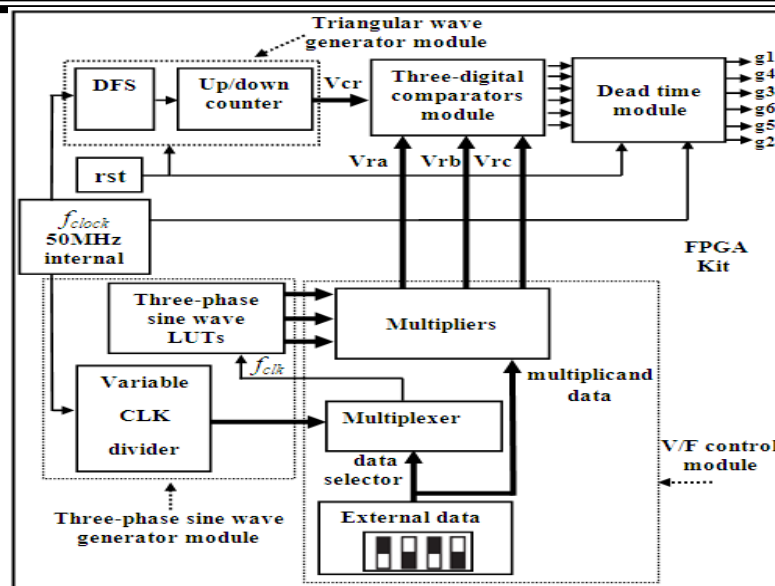
Fig(4): FPGA based SPWM control scheme for VVVF control

A. Three-Phase Sine Wave Generator Module

The sine wave generation is implemented via Sine/Cosine Look-Up Table (LUT) v5.0 which exists in the Xilinx Core Generator [10]

To generate three-phase sine reference waves, three separate sine LUTs are used with (120°) phase shift between each other. The Sine LUT module accepts an unsigned input value THETA and produces two's complement outputs of SINE (THETA). The values for the sine wave are stored in an internal ROM. Equation (5) defines the relationship between the integer input angle theta (THETA) supplied to the LUT (refer to Fig. 5) and the actual radian angle (θ).[10]

$$\theta = THETA * \frac{2\pi}{2^m} \text{ radians} \dots \dots \dots \dots \dots \dots \dots (7) \quad .$$

Where :m is THETA width in bits
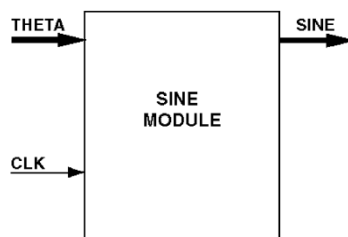
Fig(5) :Sine schematic symbol

In order to adjust the three sine waves reference frequency) $f_{reference}$ (conveniently, a clock divider is used to divide the main system frequency) f_{clock} (which equals to 50 MHz (coming from an oscillator existing on the FPGA board) to clock frequency) f_{clk} (which is used here.

The reference frequency ($f_{reference}$) has a relationship with the clock frequency (f_{clk}) and the THETA width (m), could be expressed as:

$$f_{reference} = \frac{f_{clk}}{2^m} \qquad \dots \dots \dots \dots \dots \dots \dots \dots \dots .(8)$$

If a variable frequency sine reference wave generator is required then clock frequency) f_{clk} (should also be made variable. A variable clock divider (clock divider gives different values of clock frequency suitable for adjusting the reference frequency) is used to adjust the reference frequency at different values with range of ($0 > f_{reference}$ $50 \geq$ Hz) (instead of using a single clock divider that adjusts the reference frequency at 50 Hz only) at a fixed THETA width) m (according equation (6.(

B. Triangular Carrier Wave Generation Module

The triangular carrier signal is generated using an up/down counter of n bits, which is incremented and decremented until the maximum and the minimum value of the triangular wave is reached respectively.

The carrier frequency) $f_{carrier}$ (has a relationship with the clock frequency and the up/down counter that could be expressed as:

$$f_{carrier} = \frac{f_{clock-dcm}}{2^{(n-1)} + 1} \quad \dots\dots\dots\dots\dots\dots\dots\dots (9)$$

Where $;f_{clock-dcm}$ is the clock frequency obtained from Digital Clock Manager (DCM) unit.

The DCM is used to multiply the main clock frequency (50 MHz) by a ratio of (23/9 (239via a Digital Frequency Synthesizer unit (DFS) to generate) $f_{clock-dcm}$ (equal to (127.7777MHz). The carrier frequency) $f_{carrier}$ (had been decided to operate at (1949.704408 Hz) which is the nearest value to the wanted frequency value of (1950 Hz), and the bit size of the up/down counter is) n-15=bit)[11.[

C. V/F Control Module

External data (4-bits) (as a multiplicand data) are used to multiply with the values of the three sine reference waves that are stored in the internal block ROM via using three multipliers to get a variation in the amplitude of the sine reference waves resulting in a variation of the modulation index with range of ($0 > m_i$) ($1 \geq$ for controlling the output voltage of the three-phase voltage source inverter which is an input supply to the IM). At the same time, these external data are used as a data selector for a multiplexer which is used to supply the three Sine modules with the clock frequency)f_{clk} (from the variable clock divider (adjust the clock frequency) f_{clk} (for the three Sine modules). The multiplexer works as follows:

For example

if   (external data = "1111")   then f_{clk} = 409.836 KHz;

(m_i =1)   ($f_{reference}$ = 50 Hz)

elsif (external data = "1110")   then f_{clk} = 358.4 KHz;

(m_i =0.875)   ($f_{reference}$ = 43.75 Hz)

elsif (external data = "1101")   then f_{clk} = 332.8 KHz;

(m_i =0.8125)   ($f_{reference}$ = 40.625 Hz)

By this manner the inverter output voltage over the inverter reference frequency will be constant. The value of the external data (ratio V/F) can be adjusted by using the four slide switches which already exist on the FPGA kit.

D. Comparator Module

The triangular carrier wave (Vcr) is to be compared with the sine reference waves (Vra, Vrb, and Vrc) (output data from the multipliers) by using three digital comparators. The digital comparator output is logic '1' if the value of the sine reference wave is greater than the value of the triangular carrier wave; otherwise its output is logic '0'. Each of the comparators outputs (g1, g3, and g5) are negated to produce the complement signals (g4, g6, and g2) which are needed to trigger the lower power switches of the three-phase inverter.

E. Dead Time Module

An important factor in the design of the PWM generator is the dead time control of the three legs of the inverter. This is required to avoid the top power switch (MOSFET) in each leg and the bottom to close at the same time, therefore a short circuit across the power supply will occur at that leg [2]. The dead time is programmed to be 4 μsec.[11]

6. Simulation via MATLAB/SIMULINK

To verify the experimental results, the simulation of sinusoidal PWM three-phase inverter feeding IM was made using MATLAB/SIMULINK and simpower system toolbox .The scheme of the system is shown in Fig. 6. It consists of three major parts (three-phase bridge inverter circuit, PWM generator, and three-phase induction motor). The three-phase sine reference waves (sinwave (A), sinwave (B), and sinwave (C)) are comparing with the triangular carrier wave by using three relational operator and the intersection of these waves generates the gating signals (g1, g3, and g5 (that applied to the upper switches (S1, S3, and S5), each of these gating signals are negated by using three logical operator (NOT) to produce a gating signals (g4, g6, and g2) are applied to the lower switches (S4, S6, and S2) of the three-phase bridge inverter to generate three-phase AC output voltage waveform to feed the induction motor .
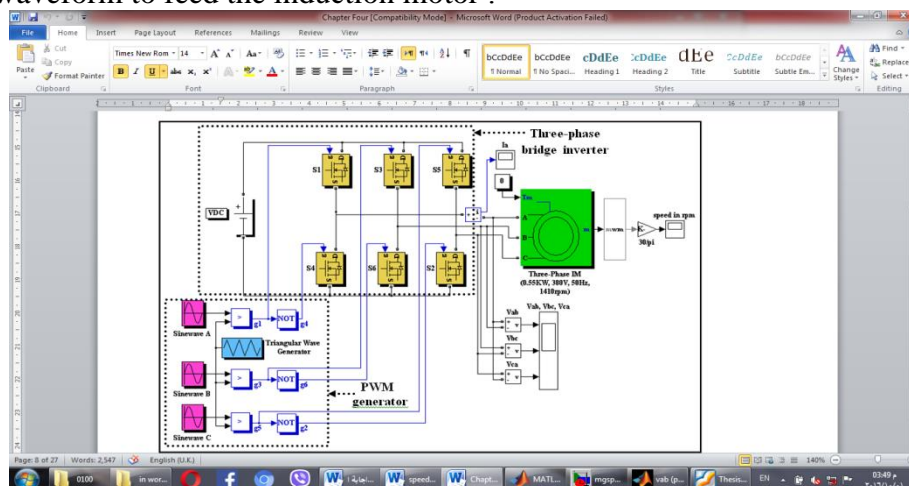
Fig(6): MATLAB Simulation of the SPWM three-phase VSI fed IM

7.   Experimental and Simulation Results

Fig. 7 shows the results of the line-to-line output voltage waveforms of the inverter circuit for VVVF using V/F control. Table 1 shows the actual speed of the IM with VVVF controller in open loop.
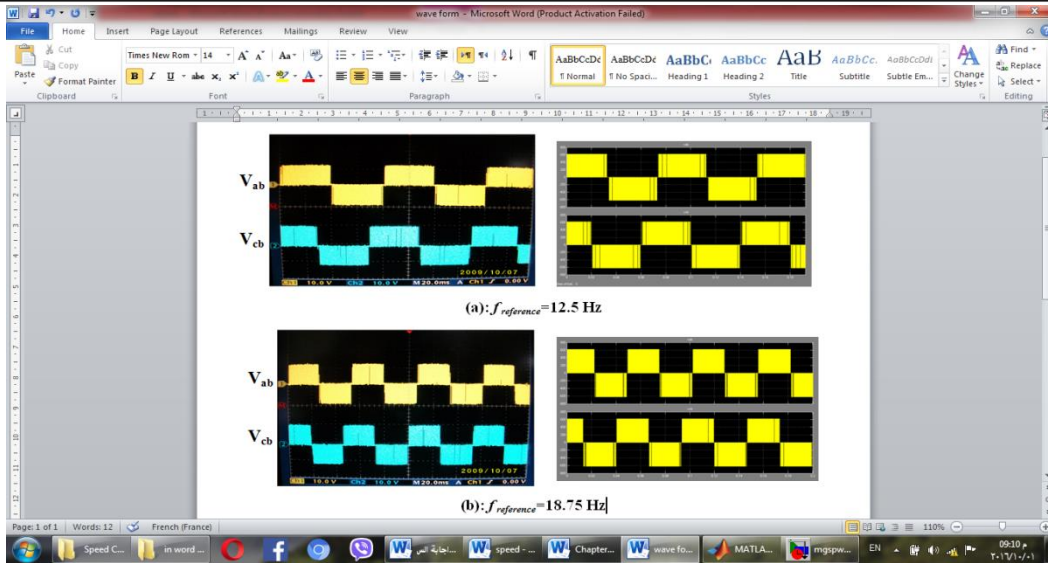
Fig(7): Experimental and simulation results of the line output voltage waveform of the inverter using V/F control

Table (1) :Results of the open loop V/F control of the IM

DC supply V_{DC} (V)	Supply Frequency (Hz)	Modulation index (m_i)	Stator Voltage (V)	Synchronous Speed (rpm) (as calculated)	Actual Speed (rpm) (as measured)
220	6.25	0.125	47.5	187.5	185
220	12.5	0.25	95	375	373
220	18.75	0.375	142.5	562.5	558.4
220	25	0.5	190	750	746.4
220	50	1	380	1500	1487

The relation between the stator voltage and the measured speed is shown in Fig(8).
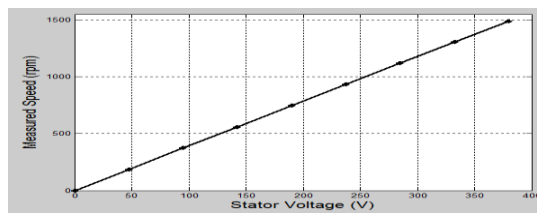
Fig(8): Relation between the stator voltage and the measured speed

The experimental setup of the three-phase inverter with the FPGA control is shown in Fig. 9.
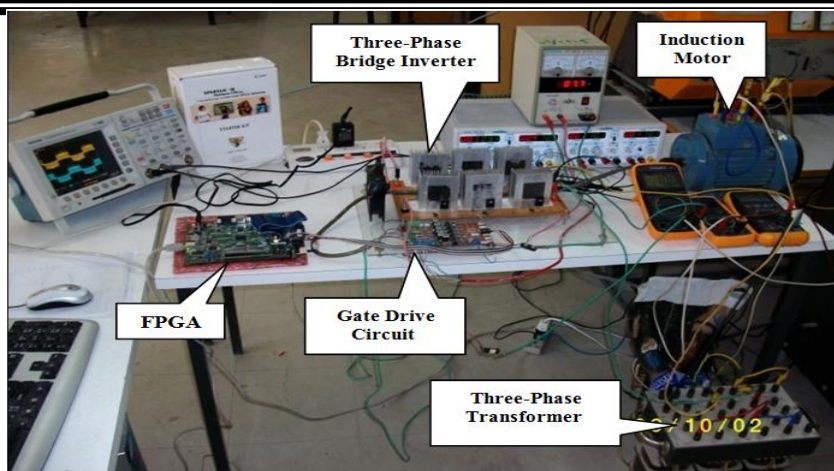
Fig(9): Experimental setup

7:Conclusion

The use of FPGA technology to generate PWM pulses for a three-phase inverter using VHDL programming language has been successfully implemented. The output fundamental frequency in the V/F speed control strategy can be varied from 6.25 Hz to 50 Hz (with step size of 6.25Hz); at the same time the modulation index can be varied from 0 to 1(with step size of 0.125). Then the speed of the IM can be adjusted in range 187.5-1500 rpm. The measured speed has a linear variation with the stator voltage as shown in Fig. 7.

References:

[1] Nalin Kant Mohanty, and Ranganath Muthu, "A Novel Implementation of Xilinx FPGA Based Four Switch Three Phase IGBT Inverter Fed IM Drive Using PWM", European Journal of Scientific Research, © Euro Journals Publishing, Inc. 2011, Vol. 48 No.3 (2011), pp.424-433.

[2] Dan Deng, Su Chen, and Geza Joos "FPGA Implementation of PWM Pattern Generator", Conference of IEEE on Electrical and Computer Engineering, 2001, VOL.1, pp. 1279-1284.

[3] M. S. N. Romli, Z. Idris, A. Saparon, and M. K. Hamzah, "An Area-Efficient SPWM Technique for Single Phase Matrix Converter (SPMC)", 3rd Conference of IEEE on Industrial Electronics and Applications, 2008, pp.1163-1168.

[4] Padmaraja Yedamale, "Speed Control of 3-Phase IM Using PIC18 Microcontrollers", Microchip Technology Inc.

[5] Kariyappa B. S, and Dr. M. Uttara Kumari, "FPGA Based Speed Control of AC Servomotor Using Sinusoidal PWM", International Journal of Computer Science and Network Security, October 2008, VOL.8 No.10, pp. 346-350.

[6] Bimal k. Bose, "Modern Power Electronic and AC Drives", Prentice Hall, Inc., 2002, ISBN 0-13-016743-6.

[7] Muhammad H. Rashed, "Power Electronics Circuits, Drives, and Applications", Prentice-Hall Inc., Third Edition 2004, ISBN 0-13- 122815-3.

[8] Moayed N. EL Mobaied, "Fuzzy Logic Speed Controllers Using FPGA Technique for Three-Phase Induction Motor Drives", Master thesis, Islamic University-Gaza, 2008.

[9] Thida Win, Nang Sabai, and Hnin Nandar Maung, "Analysis of Variable Frequency Three-Phase IM Drive", World Academy of Science, Engineering and Technology, Vol. 32, August 2008.

[10] "Sine/Cosine Look-Up Table v5.0" May 21, 2004 Xilinx Inc. URL: www.xilinx.com/ipcenter.

[11]   Ahmed M. T. Ibraheem, " FPGA Based Three-Phase Sinusoidal PWM Control for Voltage Source Inverter Fed IM ", Master thesis, Technical College / Mosul, 2010.

Enhanced Artificial Intelligent Method for Representing the Photonic Crystal Fiber Profile Index

Mahmood Sh. Majeed
Northern Technical University,
Al-Mosul Tech. Institute,

Raid W. Daoud*
Northern Technical University
Al-Hawija Tech. Inst.

raid.daoud@gmail.com

ABSTRACT:

A new method proposed in this paper to compute the fitness in Genetic Algorithms (GAs). In this new method the number of regions, which assigned for the population, divides the time. The fitness computation here differ from the previous methods, by compute it for each portion of the population as first pass, then the second pass begin to compute the fitness for population that lye in the portion which have bigger fitness value. The crossover and mutation and other GAs operator will do its work only for biggest fitness portion of the population. In this method, we can get a suitable and accurate group of proper solution for indexed profile of the photonic crystal fiber (PCF).

Key words: Genetic Algorithms (GAs), Fitness, Fiber Optics and Photonic Crystal Fiber (PCF).

1.INTRODUCTION:

Photonic Crystal Fibers (PCF), which are optical fibers with a cross-sectional microstructure of air holes and/or doped sections, have in recent years attracted much scientific and technological interest. PCFs offer a number of novel design options, such as very large or very small mode areas, high numerical aperture, guidance of light in air, and novel dispersion properties [1].

Based on pure silica glass, the invention of single material photonic crystal fiber also known as holy fibers (HFs) or microstructure fibers has attracted wide interest over the past few years. The air-filled holey cladding leads to unique guidance properties such as photonic band-gaps at optical wavelengths, very large core with endless single mode guidance and soliton effects, polarization maintenance and high birefringence and dispersion management arise and promise various novel applications [2].

In conventional optical fibers, electromagnetic modes guided by total internal reflection in a core region whose refractive index is raised by doping of the base material. In PCFs, two distinct guiding mechanisms are possible: the guided modes may be trapped in a core with a higher average index than the cladding region by an affect similar to total internal reflection (often termed modified internal reflection, or just index-guiding), or they can be trapped in a core of lower average index by a photonic band-gap (PBG) effect.

For instance, it is possible to produce PCF with very high birefringence, to get a single-mode fiber with anomalous dispersion regime in the visible wavelength domain, or to obtain fibers with very flat near zero chromatic dispersion curves on a large wavelength range. All of these properties are related to the fiber design, namely, the pitch (Λ) of the periodic array, the holes diameter (d) and the number (N) of rings around the core as shown in the Figure (1). A truly unique possibility offered by PCFs, is the realization of fiber that can be single-mode regardless of wavelengths and hence has been named "endlessly single mode" PCF [3].

2.THEORY

The core of the PCF is made of solid silica and the cladding consists of multiple layers of air holes separated by narrow silica bridges. Figure (1) illustrates an example of the cross-section of an index-guided photonic crystal fiber [4]. The idealized structure of the PCF have regular hexagonal array of perfectly circular air holes.

In recent years, photonic crystal fiber made of pure silica and air holes provided a new approach of dispersion compensation: large negative dispersion (D) can achieved in PCF due to high relative difference (Δ) between air and silica, and can tailored by the size and structure of air holes in the cladding. To determine the dispersion parameters in the conventional fiber the most important thing that must be fixed is the relation between the normalized propagation constant (B), and the V-number. [5] give the formula of the normalized propagation constant:
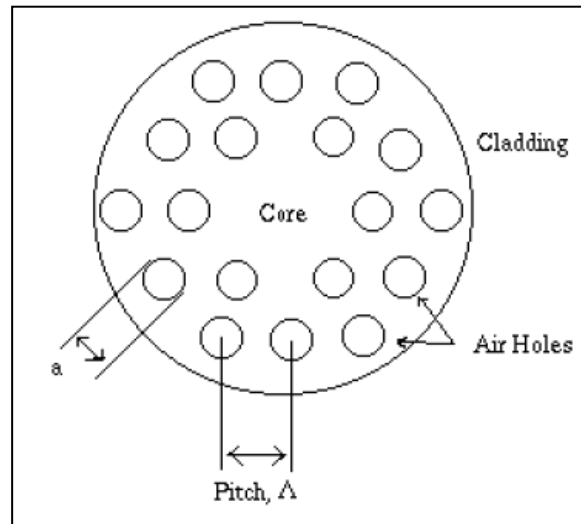
Fig(1): Cross section of a crystal "holey fiber".

$$B = \frac{(\beta/k)^2 - n_{cl}^2}{n_{co}^2 - n_{cl}^2} \qquad \dots (1)$$

where β is the propagation constant and must be within the range ($kn_{cl} \leq \beta \leq kn_{co}$), k is the wave number (k=2π/λ), λ is the wavelength while n_{co} and n_{cl} are the core and the cladding index, respectively.

Due to the high similarity between the n_{cl} and n_{eff} most researchers assume that they are the same. On the other hand, formulation of the V-parameter suggested to be based on an approximation with an equivalent step index (SIF). In the case of a SIF, the V-parameter, V_{SIF}, as function of wavelength, λ , is given by [6]:

$$V_{SIF}(\lambda) = \frac{2\pi}{\lambda} a\sqrt{n_{co}^2 - n_{cl}^2} \quad \ldots(2)$$

The refractive indices of the core and cladding, n_{co} and n_{cl}, respectively, are assumed to be wavelength independent and a denotes the core radius. One problem with using the step index approximation for describing the PCF is that the core region is not circular, complicating the definition of values for the refractive indices, is the problematic due to the strong wavelength dependency of the effective indices caused by the air-glass matrix. For these reasons, the V-parameter of the PCF, V_{PCF} instead of proposed to given as [7]:

$$V_{SIF}(\lambda) = \frac{2\pi}{\lambda} a\sqrt{n_{co}^2(\lambda) - n_{cl}^2(\lambda)} \quad \ldots(3)$$

The wavelength dependency of the effective refractive indices is taken into account by introducing the effective index of the fundamental mode, $n_{co}(\lambda)$, and of the first cladding mode, $n_{cl}(\lambda)$. Instead of an equivalent core radius it is suggested to use the characteristics length scale of the structure namely (Λ).

The effective index of the cladding, n_{eff}, is assumed a constant value for the microstructure cladding, and can be taken to be that of air, i.e. $n_{eff} = 1$, for PCFs with cladding consisted of large air holes. In PCFs where the air holes are not large enough for this assumption to be made, n_{eff} is approximated as [8]:

$$n_{eff} = n_{air} p_{air} + n_{silica} p_{silica} \quad \ldots(4)$$

where P_{air} and P_{silica} are the power fraction of air and silica that make up the microstructure cladding respectively, and nsilica is given by the Sellmeier formula.

Short optical pulses entering a dispersive channel such as an optical fiber are spread out into a much broader temporal distribution and hence dispersion problem will be arising. The total dispersion for the PCF can be determined by applying Equation (5), by taking second derivative of the (n_{eff}) given by equation (4) and then applying one of the curve fitting techniques [9].

$$D_T = -\frac{\lambda}{c} \frac{d^2 n_{eff}(\lambda)}{d\lambda^2} \quad \ldots(5)$$

where c is the speed of light.

Genetic algorithms (also known evolutionary algorithms) are a class of optimization algorithms that apply principles of natural evolution to optimize a given objective. In genetic optimization of a problem, different solutions to the problem are picked (usually randomly), and a measure of fitness is assigned to each solution [10]. The standard theory of genetic algorithm based on schema

analysis. Schema analysis operates in the representation (genotype) space and can be used provided that the chromosomes chosen are linear strings made up of a fixed number of genes (positions) each of which has a well-defined set of possible alleles (values) and also any combination of alleles is permitted (so that all strings are legal) [11].

On a given generation of the design, a set of operations, analogous to mutation and reproduction in natural selection, performed on these solutions, which should theoretically be "fitter" than their parents should. This process repeated until the algorithm terminates, typically after a predefined number of generations, or after a particularly "fit" solution found, or more generally, when a generation of solutions meets some pre-defined convergence criterion.

1. THE PROPOSED METHOD

Hence the goal of our work is to determine the propagation characteristics which is the normalized propagation constant (B), or the propagation constant (β) with respect to wavelength (λ) for the PCF.

To get more accurate results and to become more nearer to the exact solution, a new technique is proposed here by splitting the PCF cable cross section (almost circular) into more than one region (sectors) by taking many rays prolonged from the fiber center toward the cladding with different orientations as shown in figure (3). In order to study the dispersion effects, the selected possible profiles of all regions should take into account to find out the resultant value of propagation characteristics. Each region bounded between two rays; the first is the horizon (x-axis), while the second is the ray that makes a certain angle with the horizon; see Figure (2),Hence, the resultant propagation constant may be determined when all regional profiles are considered. The resultant value may simply calculated as the average of all individual propagation constants related to each region.
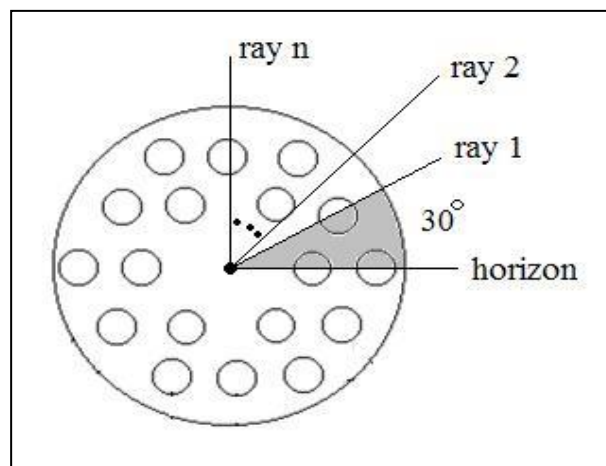
Fig(2): Splitting the PCF cross section into many sectors.

The clad region in the PCF consists of two materials (air and silica), as mentioned earlier, for this reason the n_{eff} may represent both materials, and in this work n_{eff} approximately depends on the PCF cross-section, see Figure (3).
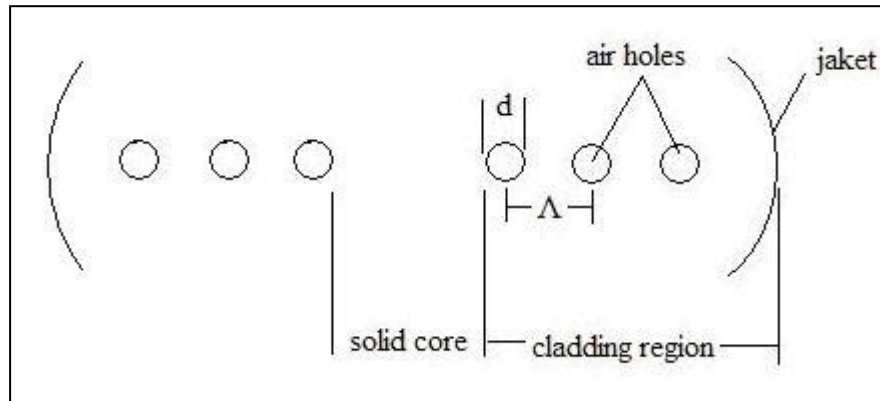
Fig(3): Simple section of PCF cross-section.

The most important two parameters that directly affect the total dispersion in such fibers are the number of air-hole layers (N) and the (Λ) value that is combined with (d) in (d /Λ) which is a relative function including the hole diameter (d) and hole-to-hole distance (Λ).

The fiber parameters taken into account during the computation were fixed as follows: (Λ =1.5µ, d/Λ =0.75 and N=5). The relative difference between n_{silica} and n_{eff} , is shown in Figure (4).
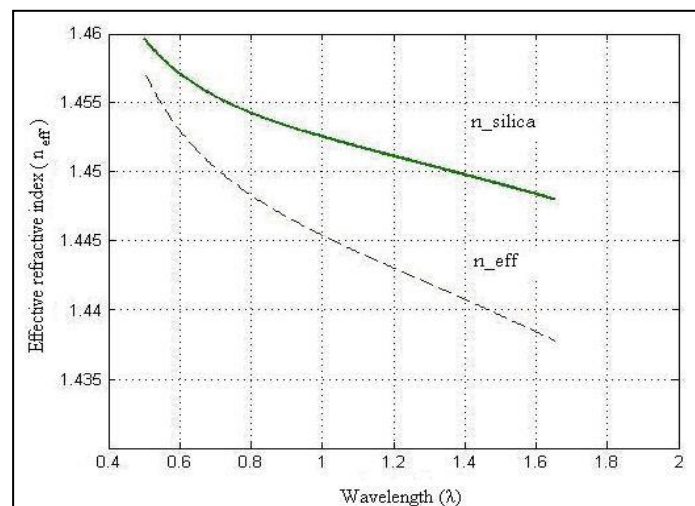
Fig(4): The relation between n_{silica} and n_{eff}.

Using the PCF structure of Figure (4), and after simple mathematical operations, Equation (4) may rewritten as (Shaker, Majeed and Daoud, 2011):

$$n_{eff}(\lambda) = n_{air}\frac{(d/\Lambda)N}{0.5\,d/\Lambda} + n_{silica}(\lambda)\frac{(1-d/\Lambda)N + 0.5\,d/\Lambda}{(0.5\,d/\Lambda)+N} \qquad \ldots (6)$$

Hence the parameters that directly affect the dispersion and should taken into consideration in the design are:

i. The profile shape of the PCF (the hexagonal is one of the most popular one).

ii. Number of air-hole layers (N).

iii. Distance between two adjacent air holes, (Λ).

iv. Diameter of air hole, d.

For given parameters, n_{eff} may calculated versus n_{silica} at some specific wavelength. The proposed method could applied to compute the propagation constant for different possible profiles when the following suggested orientation adopted 0°, 15°, 30°, 45°, 60°, 75° and 90°. Figure (5) gives the profile of (0° and 60°) orientations, as they are the same as well as the (30° and 90°) orientations, which are identical. On the other hand, Figure (6) represents the (15°, 45° and 75°) orientations.
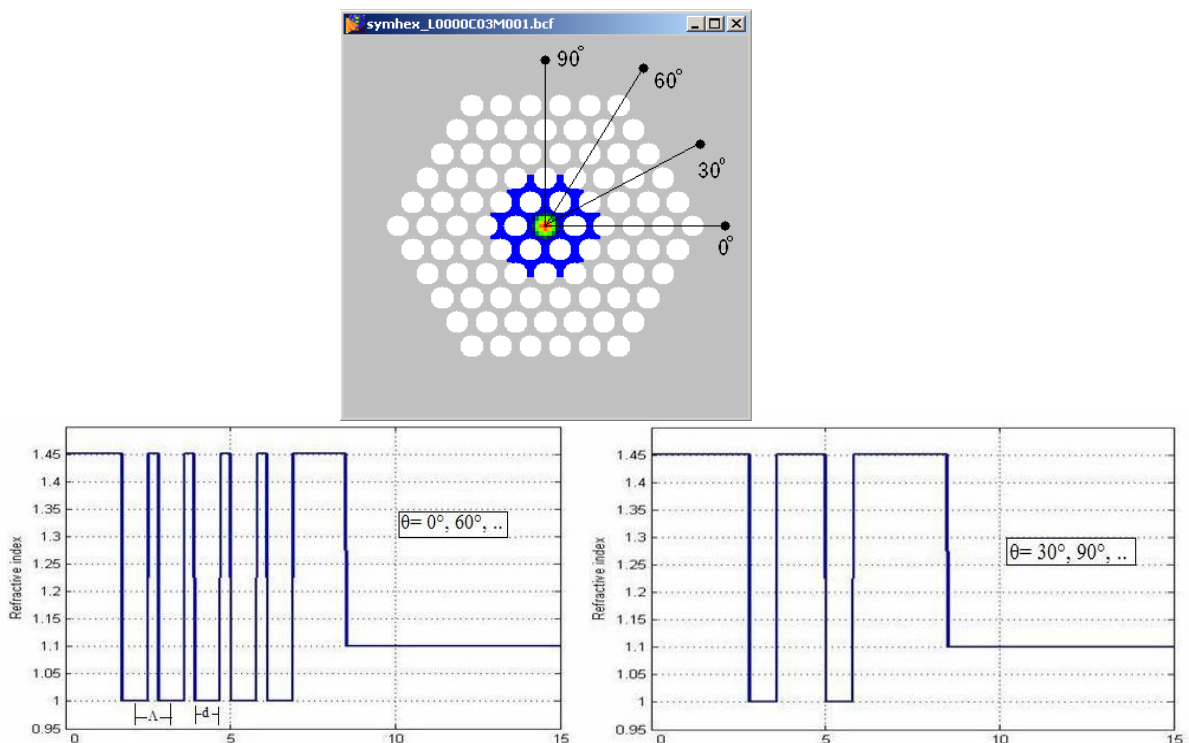
Fig(5): Refractive index profile for the PCF.
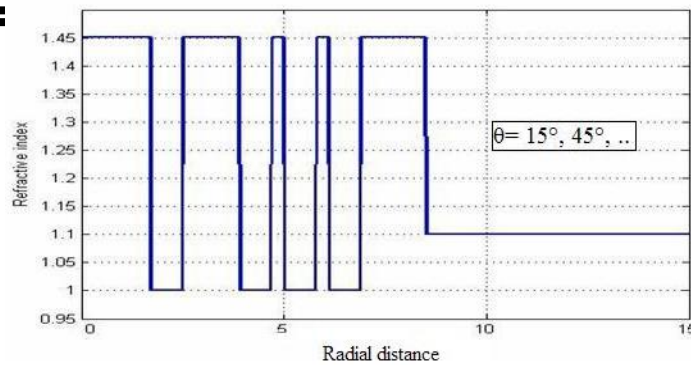
Fig(6): Refractive index profile for the PCF, the angles 15°, 45° and 75° are considered

2. RESULTS

To apply the proposed method, computation of PCF fiber with following parameters were adopted: hexagonal structure with N=5, Λ =1.5µ, and d/Λ =0.75, and for different orientation mentioned earlier. To demonstrate the validity of the GA and its usefulness, the effect of various profiles (at different orientations) were investigated. Figure (7) illustrates the relation between the normalized propagation constant, B, and the wavelength for the suggest PCF for two (0° and 30°) orientations.
It is apparent from this figure that there is a considerable difference which is increases toward higher wavelengths.

Figure (7) illustrates the relation between the normalized propagation constant, B, and the wavelength, λ, for the PCF whose parameters have been shown above but for two orientations, 0° and 30°, it is apparent from this figure that there is a considerable difference (about 0.12) and it increases toward higher wavelengths. Figure (8) shows the dispersion characteristics along some specific wavelength range for the same fiber and parameters given above and also for the two mentioned orientations. It is clear that the difference is small in 1.1µm to 1.6 µm range while below and above this range it is considerably higher.
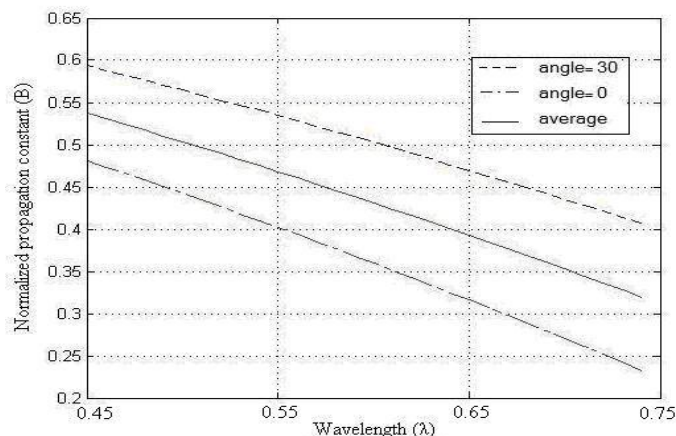
Fig(7): Normalized propagation constant versus wavelengths for the PCF profile with two orientations, (Λ =1.5µ, d/Λ =0.75 and N=5).

3. CONCLUSION

The following points can summarize the benefit of the proposed method:

i.   Time reduction in the propagation constant computation is the power of this way, five times or more less than from previous one.
ii. The crossover operation done for specific portion of the population not for all.
iii. This new Genetic Approaches can register a group of right solution.
iv. Finally, the ultra-flattened dispersion well sketched by this way for the PCF.
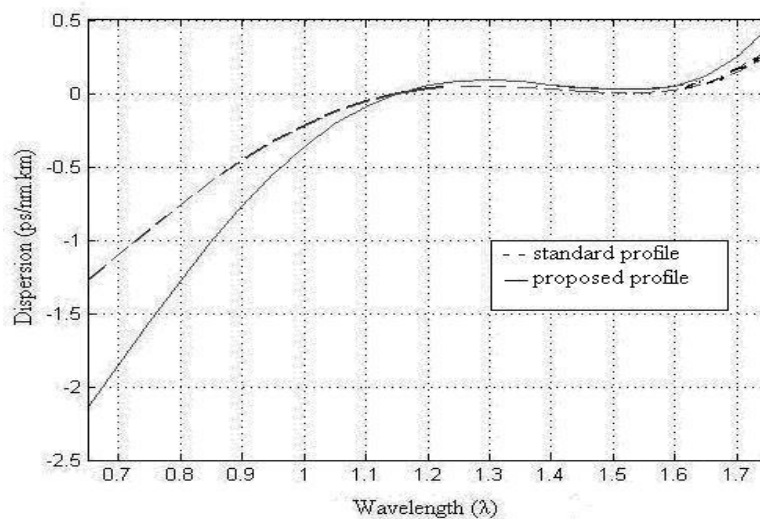
Fig(8): Dispersion along a wavelength range for the same fiber of Figure 7.

4. REFERENCES

[1] Feng X., Monro T., Petropoulos P., Fenazzi V. and Hewak D., (2003) *"Solid Microstructured Optical fiber"*. Optics express Vol. 11, No. 18,.

[2] Leagsgaard J., Barkou S., Hougaard K., Nielsen M., Jensen J. and Bjarklev A., (2004), *"Dispersion Properties of Photonic Crystal Fiber – Issues and Opportunities"*, Mat. Res. Soc. Symp. Proc, VOL. 797,.

[3] Maan M., Mahmood Sh. and Raid W., (2011), "A New Approach for Representing Photonic Crystal Fiber Index Profile to Determine their Optical Characteristics". Iraq J. Electrical and Electronic Engineering, Vol.7 No.1.

[4] Magnus C., (2003) *"Evolving Waveforms with Genetic Algorithms"*. Master of Science Thesis, University of California, San Diego.

[5] Mitchell M., (1996)*, "An Introduction to Genetic Algorithms"*. Massachusetts London, England.

[6] Ni Y., Zhang L., An L., Peng J. and Fan C., (2004), *"Dual-Core Photonic Crystal fibers for Dispersion Compensation"*. IEEE Photonic Technology Letter, VOL. 16, No. 6.

[7] Niemi T., (2002) *"Dispersion Measurements of Fiber Optic components and Application of a Novel Tunable Filter for Optical Communication"*. Master of Science Thesis, Helsinki University of Technology, Finland.

[8] Radcliffe N., (1994), *"The Algebra of Genetic Algorithms"*. Annals of Maths and Artificial Intelligence, VOL. 10, pp 339-384,.

[9] Saitoh K., Tsuchida Y., and Koshiba M., (2005), *"Endlessly Single-Mode Holy Fibers: the Influence of Core Design"*. Optics Express VOL. 13, No. 26.

[10] Ssu Yin Chen J., (2006), *"Optical Parametric Amplification in Photonic Crystal fibers"*. Master of Science thesis, University of Auckland, USA, 115.

Two-Phase Flow In Mini-Scale Complex Geometry

Raed Shakier; Hussam Muhammed ;Hussain Khathem ;Haider Abdul-Khathem
College of Engineering / OIL AND GAS Engineering Department
Thi-Qar University / Iraq
alraad461@gmail.com

Abstract:

Heat-transfer coefficients are reported for one surface, a plain surface, with 50 mm square base area. Parallel channel test piece has one mm by one mm, 25 channelsThe data were produced while boiling R113 at atmospheric pressure. For this surface, the mass flux range was 200 – 600 kg/m^{2}s and the heat flux range was 5 - 80 kW/m^2. The results obtained have been compared with standard correlations for tube bundles. The measured heat-transfer coefficients for the parallel micro-channel surface are slightly bigger for any plate channel surface. It is dependent on heat flux and reasonably independent of mass flux and vapor quality. Thus, heat transfer is probably dominated by nucleate boiling. The parallel channel heat transfer coefficients were typically bigger than other plate -channel values.

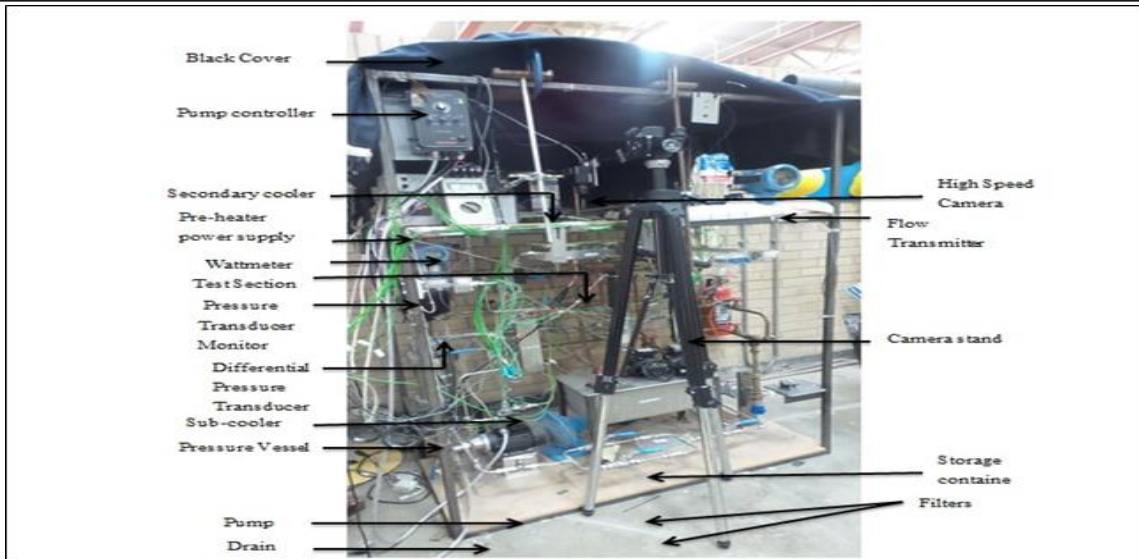*Keywords: - parallel channel; heat transfer coefficient*

1.Introduction

In recent years, electronic devices, such as micro-processors and lasers, have been growing in power and reducing in size. This has led to an increasing intensity in heat generation that needs to be removed during normal operation. Removing heat is becoming increasingly difficult. It therefore seems likely that new methods will be needed in the not too distant future. One possibility is to use a boiling fluid as the coolant, as this would transfer significantly more heat than its single-phase equivalent. This has led to an abundance of research into boiling in small diameter channels.Lie et al [1] investigated flow boiling of FC-72 on plain and pin finned surfaces at atmospheric pressure. Two pin-fin surfaces were tested; one with fins 200 μm square and 70 μm high on a square in line arrangement with a 400 μm pitch, and one with fins 100 μm square and 70 μm high on a square in-line arrangement with a 200 μm pitch. The mass fluxes used were within the range 287-431 kg/m2s and the heat fluxes within 1-100 kW/m^2. Single-phase and flow boiling heat transfer coefficients were reported. The single-phase, heat-transfer coefficients were based on the mean-wall to fluid-inlet temperature difference and the base area of the heat-transfer surface. The boiling coefficients used the mean-wall to fluid-saturation temperature difference. The mass flux was found to have only a slight effect on the boiling heat-transfer coefficient. The temperature at the onset of nucleate boiling was found to increase with increasing mass flux and, for the same temperature difference, the largest heat transfer occurred with the 100 μm fins. Cross-flow between channels was evident. The degree of wall superheat required for the onset of boiling was lower for the finned surfaces, with increased nucleation sites being evident in the corners of the fins. Bubbles grew to many times the size of the fins and became elongated and distorted. The bubble departure diameter reduced with increasing mass flux and with the addition of fins. The departure frequency increased with mass flux and the addition of fins. Correlations of the heat-transfer coefficients were produced by assuming that a convective and boiling component of heat flux existed.Work on multiple parallel micro-channels has revealed the importance of instabilities that result in flows with different flow patterns appearing in different tubes simultaneously, Hestroni et al [2]. Qu and Mudawar [3] concluded that existing correlations for boiling in single micro-channels were not applicable to multi-channel arrangements. Several instabilities have been identified. Xu et al [4] , working with water and methanol in 26 parallel rectangular channels 0.3 mm x 0.8 mm x 50 mm long, classified

the instabilities in terms of duration. Large amplitude/long period oscillations, occurring at 117 s intervals, resulted in large pressure pulses, with smaller oscillations occurring at periods of the order of a 10 s.Ma et al [5] investigated flow boiling of FC-72 at atmospheric pressure on square pin finned arrays. The fins were 30 μm wide and arranged on a square in-line configuration with a pitch of 60 μm. Two fin heights of 60 μm and 120 μm were tested. Both were compared to an open channel, or smooth, flow. The test pieces were 10 mm square and 0.5 mm high and were placed in a flow channel 30 mm wide and 5 mm high. The test piece location was 300 mm from the flow inlet. The downstream flow length was longer

2.Experimental setup

In the Figure 1 Schematically, the flow loop is presented. Before to running each single phase flow exam series, the working fluid was degassed by vigorous boiling for closely three hours to force any dissolved gases to run away from the system to the ambient. During this interval the vent valve above the condenser was periodically opened to permit dissolved gases goes to elopement to the atmosphere. This furthermore set the test pressure to close atmospheric. After degassing the liquid, as it was observed that no gas or air bubble coming out of the liquid inside the test piece before to boiling, flow boiling exams were executed. Exams were conducted by setting the wanted liquid mass flow rate and inlet temperature. Mass flow rate was adjusting by the by-pass valve and modify by the throttling valve located before the filters. The pre-heater was linked to a controller. With respect to the exam's mass flow rate, the controller was adjusting to the wanted applied heat to the fluid flow which was passing the pre-heater, to supply the required inlet temperature. Simultaneously the test section heater was adjusting to the required heat flux to the test piece. The liquid was distributed through the flow loop until the wanted entry temperature was obtained. This took three hours approximately. Steady state conditions were obtained when the fluid outlet, heater and the aluminum housing temperatures were seen to be stable. This took half an hour approximately. All of the wanted readings were achieved before the heat flux was re-set to the next required value and the process iterated. During the exams to maintain the system pressure close the atmospheric pressure, the vent valve above the condenser was periodically open and a balloon was connected to it to block the vapor to elopement from the system. High speed videos were taken of the boiling occurring on the test piece by a Kodak micro motion 1000 camera. The camera was set to 240 frames /s at a resolution of 720 by 480 pixels.

Fig(1). Schematic of flow loop[6].

Fig.(2) .the aluminum test section is shown. Liquid entered the inlet plenum of the test-section through the two inlet ports, set at 90ᵉ to the direction of stream in the aluminum test piece. The plenum chamber dimensions were set to reduce the liquid velocity to close to zero before it.
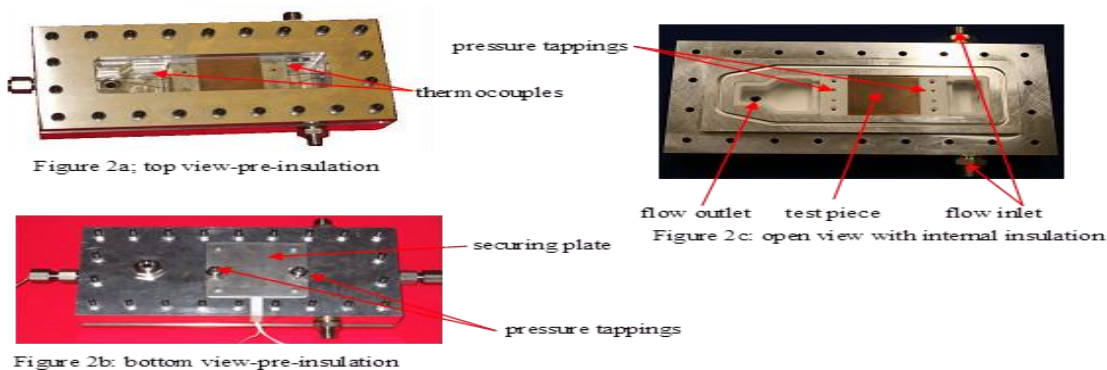
Fig(2). Test section construction .[7]

The parallel micro-channel test piece is shown in Fig. 3.The plain-channel was constructed from a piece of copper, 50 mm wide by 50 mm long and 6 mm high. Three holes, 0.6 mm in diameter by 12.5 mm long, were drilled into the test piece at the inlet and outlet ends. The holes were located 2.5 mm from the top of the boiling surface and 11, 25 and 39 mm from an edge. These holes allowed six sheathed K-type thermocouples, 0.5 mm in diameter, to be located below the boiling surface. All thermocouples were calibrated in a water bath and were accurate to ±0.15 K
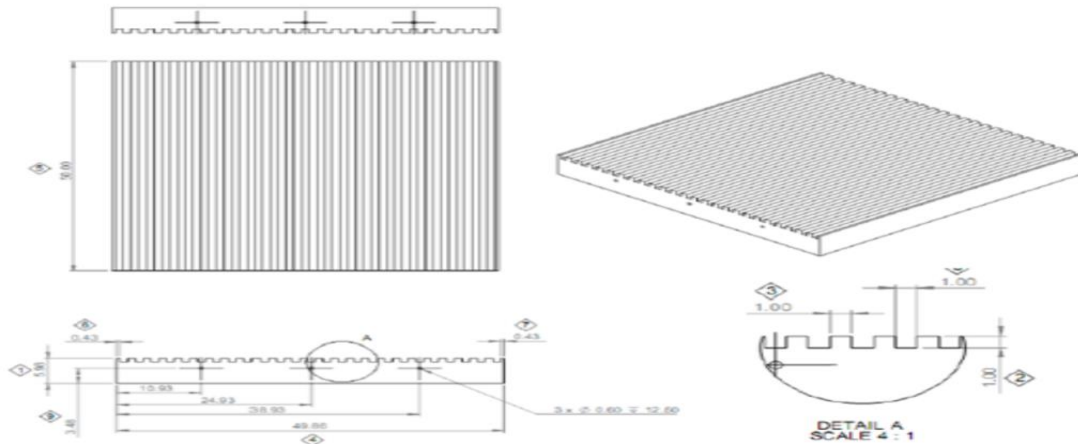
Fig(3): Test section top view showing thermocouples. [3]

3.Mathematical models

   The design of the test section comprises two plates placed in between a ceramic heater and R113 fluid.one plate is made of copper and one is aluminum. Each is 50 mm width and 50 mm length and 5 mm in thickness.The average base heat flux, q_p, was determined from the ratio of the increase in sensible heat of the liquid to the base area of the test-piece, and was correlated by

$$q_p = 2.3 (T_h - T_w) - 0.9 \qquad \ldots\ldots (1)$$

This permitted the local outlet and inlet heat-transfer coefficients to be got from a one-dimensional heat balance through a small flow length (Δz) at the base of the channel gave:

$$q_p (W_{ch} + W_w) \Delta z = h_{tp} (T_w - T_{sat}) \Delta z [W_{ch} + 2\eta H_{ch}] \qquad \ldots\ldots(2)$$

The size of the heights and widths in Equation (2) are given in Table (1). The fin efficiency was determined by considering that the fins could be processed as rectangular fins with adiabatic tips, i.e

$$\eta = \tanh(\lambda H_{ch}) \lambda H_{ch} \qquad \ldots\ldots(3)$$

In which λ was the fin parameter, given by

$$\lambda = 2\alpha k_c W_w \qquad \ldots (4)$$

An initial analysis revealed that the fin efficiency was always near to unity. It was subsequently got as one. The copper test piece has three thermocouples 12.5 mm from the inlet was set inside and also three thermocouples 12.5 mm from the outlet was set inside the copper test piece. In total, there are six thermocouples in the copper test piece, hereafter indicated to as the inlet and outlet locations. The alteration in the measured outlet and inlet wall temperatures was normally less than 0.6 °C, but could, on occasion, be as large as 1.6 °C. The local wall temperature was therefore got by averaging the data from the three relevant thermocouples to get T_{tc} , which was then corrected for depth from the plate surface, H_{tc} , through the one dimensional heat conduction equation, i.e.

$$T_w = T_{tc} - q_p H_{tc} k \qquad \ldots\ldots (5)$$

The local of the single-phase heat transfer coefficients was obtained by separating the flow filed into cells. A typical two-dimensional unit cell at the location of a thermocouple situated inside the copper test piece for the parallel test pieces is seen in the table below.

Table(1): Dimension for channel heat transfer analysis[3]

Parallel channel test piece									
Ww	Wch	Wcell	Lcell	Hw1	Hw2	Hw3	Hch	Htc	Hcell
mm	mm	mm	mm	mm	mm	mm	mm	mm	mm
1.0	1.0	2.0	2.0	10.0	5.0	5.0	1.0	1.5	21.0

The local pressure, p, was estimated from an assumed linear pressure distribution across the test piece. This was determined from the measured inlet pressure, pin, and the measured pressure drop, Δp. Thus,

$$p=p_{in}-\Delta p \ zL \qquad\qquad ……(6)$$

A specific heat capacity for a R113 working fluid with of ($C_{p,f}$), the liquid temperature was found from

$$T_l=T_{in}+\frac{W}{MC_{p,f}}\int_0^z q_s p \, dz \qquad\qquad …….. (7)$$

Also the equation of the hydraulic diameter to the copper channel in the existence of the heat-transfer procedures, calculated by

$$D_h=\frac{4 \ H_{ch}W_{ch}}{2(W_{ch}+H_{ch})} \qquad\qquad …………(8)$$

Where Prf and Ref are the liquid Prandtl number and Reynolds number relied on local flow, i.e

$$Pr_f=\frac{C_{p,f} \ \mu_f}{k_f} \qquad\qquad …………. (9)$$
9)

$$Re_f=\frac{G \ D_h}{\mu_f} \qquad\qquad ……………(10)$$

4.Experimental Results and Discussion

Two-phase analyses and Single-phase analyses, heat transfer coefficients measurements which were given are analyzed in this journal. For the parallel channel surface, several popular macro- and micro-channel methods for the heat transfer coefficient were compared with the empirical data. The data were compared to tube bundle standard correlations for the heat transfer coefficient.

1. Wall Temperature Distribution

Figure 7 . Shows variation of parallel channel distance from plate inlet with wall temperature for mass fluxe.as it is shown*,* the wall temperature is decreased with increasing plate position from plate inlet
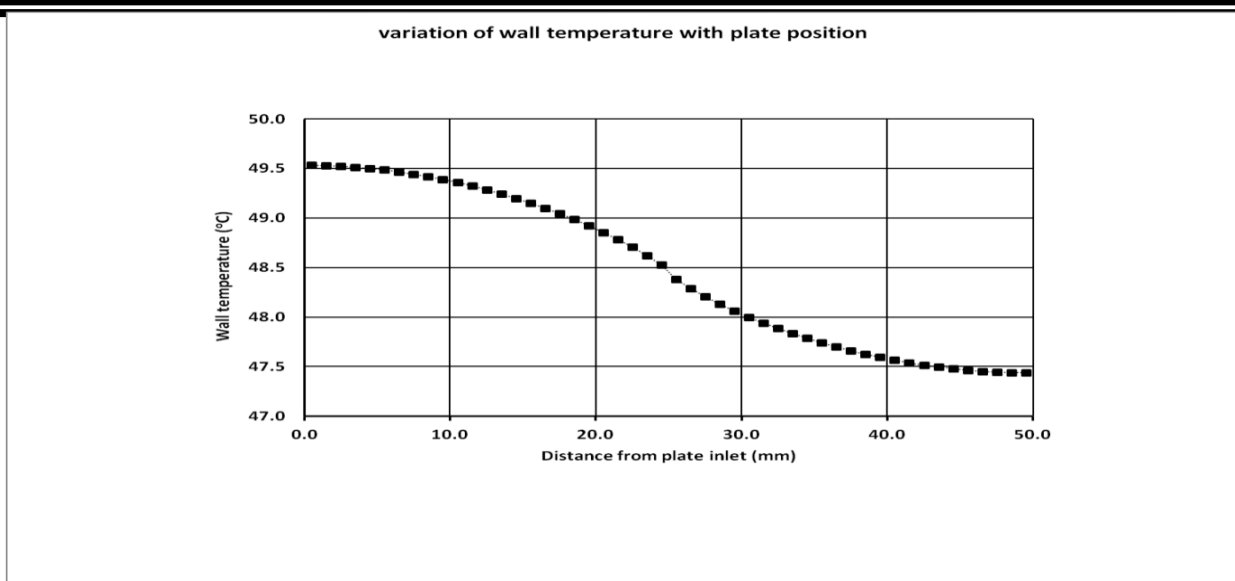
Fig(7): Variation of wall temperature with plate position.

2.Boiling Heat Transfer Coefficient Distribution

The heat flux at the inlet and outlet position of the channel are shown; the heat flux has small values at the channel inlet till **27.6** kW/m²2.755 kWm2 then jump up rapidly then decreasing slowly to the channel outlet. The wall temperature distributions are shown in Figure 8; they have high values at the channel inlet after that continues decreasing till the channel outlet.
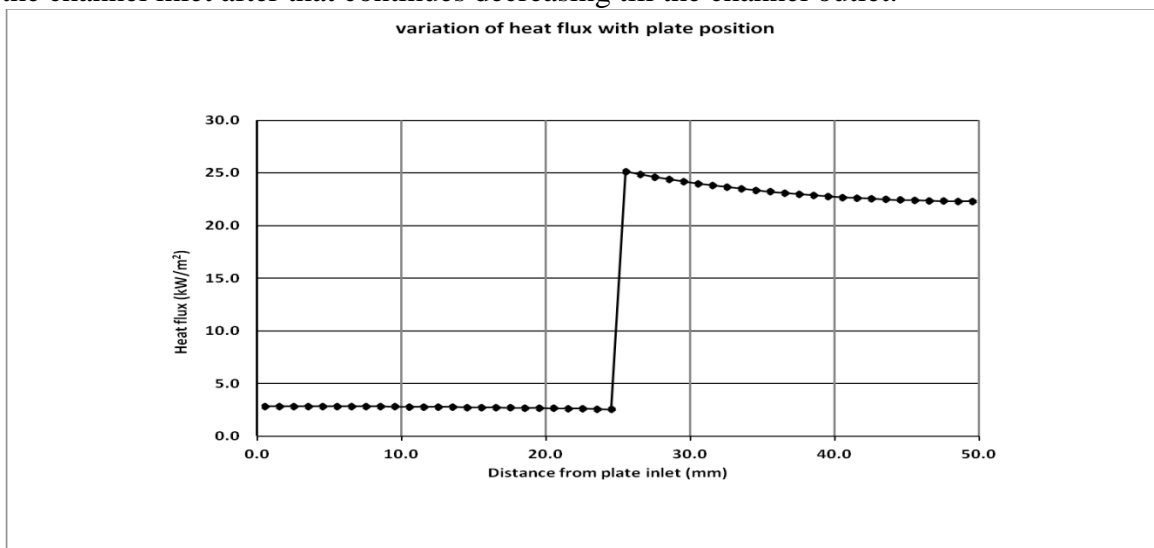
Fig(8): Variation of heat transfer coefficient with plate position.

5. Conclusion

To demonstrate the difference of heat flux, wall temperature and heat transfer coefficient with plate status to know the relation between them. Heat-transfer data has been gained for a 25 parallel channel copper test piece boiling R113 at atmospheric pressure. The channels were 1 mm square by 50 mm long and were heated from below by a constant heat flux. Heat-transfer coefficient data was

gained for single-phase liquids and sub cooled and saturated boiling flows. The analysis in this paper explains that the conventional depiction of boundary conditions as constant temperature or constant wall heat flux is unsuitable when dealing with a flow in small scale channels under conditions which lead to changing spatially heat transfer mechanisms. Deformation in the heat-flux distribution has two causes. The first is due to end effects and the second is due to the variation in heat transfer coefficient and liquid temperature. To explain the first cause, suppose the channel contained a flow that was subjected to a uniform heat flux, Equations. (2) and (7) give

$$Twall=Tinlet +qpWw ZM Cp+qpA+ hSP \qquad \ldots\ldots\ldots\ldots.. (11)$$

Finally we recommendation that the heat comes to the test piece by to type of heat transfer there are conduction and convection heat transfer. Also can saying the heat transfer coefficients inlet and outlet locations are not constant on the top test piece surface in this flow boiling tests.

Reference

[1]   Y. M. Lie, J. H. Ke, W. R. Chang, T. C. Cheng, and T. F. Lin, "Saturated flow boiling heat transfer and associated bubble characteristics of FC-72 on a heated micro-pin-finned silicon chip," *International Journal of Heat and Mass Transfer,* vol. 50, pp. 3862-3876, 2007/09/01/ 2007.

[2]   G. Hetsroni, A. Mosyak, Z. Segal, and E. Pogrebnyak, "Two-phase flow patterns in parallel micro-channels," *International Journal of Multiphase Flow,* vol. 29, pp. 341-360, 2003.

[3]   W. Qu and I. Mudawar, "Flow boiling heat transfer in two-phase micro-channel heat sinks––I. Experimental investigation and assessment of correlation methods," *International Journal of Heat and Mass Transfer,* vol. 46, pp. 2755-2771, 2003.

[4]   J. Xu, J. Zhou, and Y. Gan, "Static and dynamic flow instability of a parallel microchannel heat sink at high heat fluxes," *Energy Conversion and Management,* vol. 46, pp. 313-334, 2005.

[5]   A. Ma, J. Wei, M. Yuan, and J. Fang, "Enhanced flow boiling heat transfer of FC-72 on micro-pin-finned surfaces," *International Journal of Heat and Mass Transfer,* vol. 52, pp. 2925-2931, 2009/06/01/ 2009.

[6]   D. McNeil, A. Raeisi, P. Kew, and P. Bobbili, "A comparison of flow boiling heat-transfer in in-line mini pin fin and plane channel flows," *Applied thermal engineering,* vol. 30, pp. 2412-2425, 2010.

[7]   D. McNeil, A. Raeisi, P. Kew, and R. Hamed, "Flow boiling heat-transfer in micro to macro transition flows," *International Journal of Heat and Mass Transfer,* vol. 65, pp. 289-307, 2013.

Single-phase and two-phase Flow into In-Line pin-fin micro-channel heat Sink

Raed Shakier

College of Engineering / Oli and Gas Engineering Department
Thi-Qar University / Iraq / E-mail:- alraad461@gmail.com

ABSTRACT

Heat-transfer coefficients are reported for one surface, a pin-fin surface with 50 mm square base area. The In Line pin-fin surface comprised of 1 mm square pin fins that were 1 mm high and located on a 2 mm square pitch array it that covering the base. The channel was 1 mm high and had a glass top plate. The data were produced while boiling R113 at atmospheric pressure. For this surface, the mass flux range was 50 - 250 kW/m^{2}s and the heat flux range was 5 - 140 kW/m^2. The results obtained have been compared with standard correlations for tube bundles. The measured heat-transfer coefficients for the pin-fin surface are slightly higher any surface. It is dependent on heat flux and reasonably independent of mass flux and vapor quality. Thus, heat transfer is probably dominated by nucleate boiling and is increased by the pin fins due to increasing in area and heat-transfer coefficient, the pin-fin pressure drops were typically larger than other values.
KEY WORDS: Single-phase; Two-phase; In-Line pin-fine.

1. INTRUCTION

Flow boiling in mini- and micro-flow passages can be used for cooling many high power density devices such as Micro Electro Mechanical Systems (MEMS), microprocessors, laser diode arrays and Light Emitting Diodes (LEDs). This has led to an abundance of research into flow boiling in small-scale flow passages. Many researchers have investigated flow boiling heat transfer phenomena with the objective of developing reliable design models for

mini and micro-flow passages. Nevertheless, there is still a lack of understanding of the phenomena involved. Hence there is some doubt about the reliability of the new models and when they should be applied.
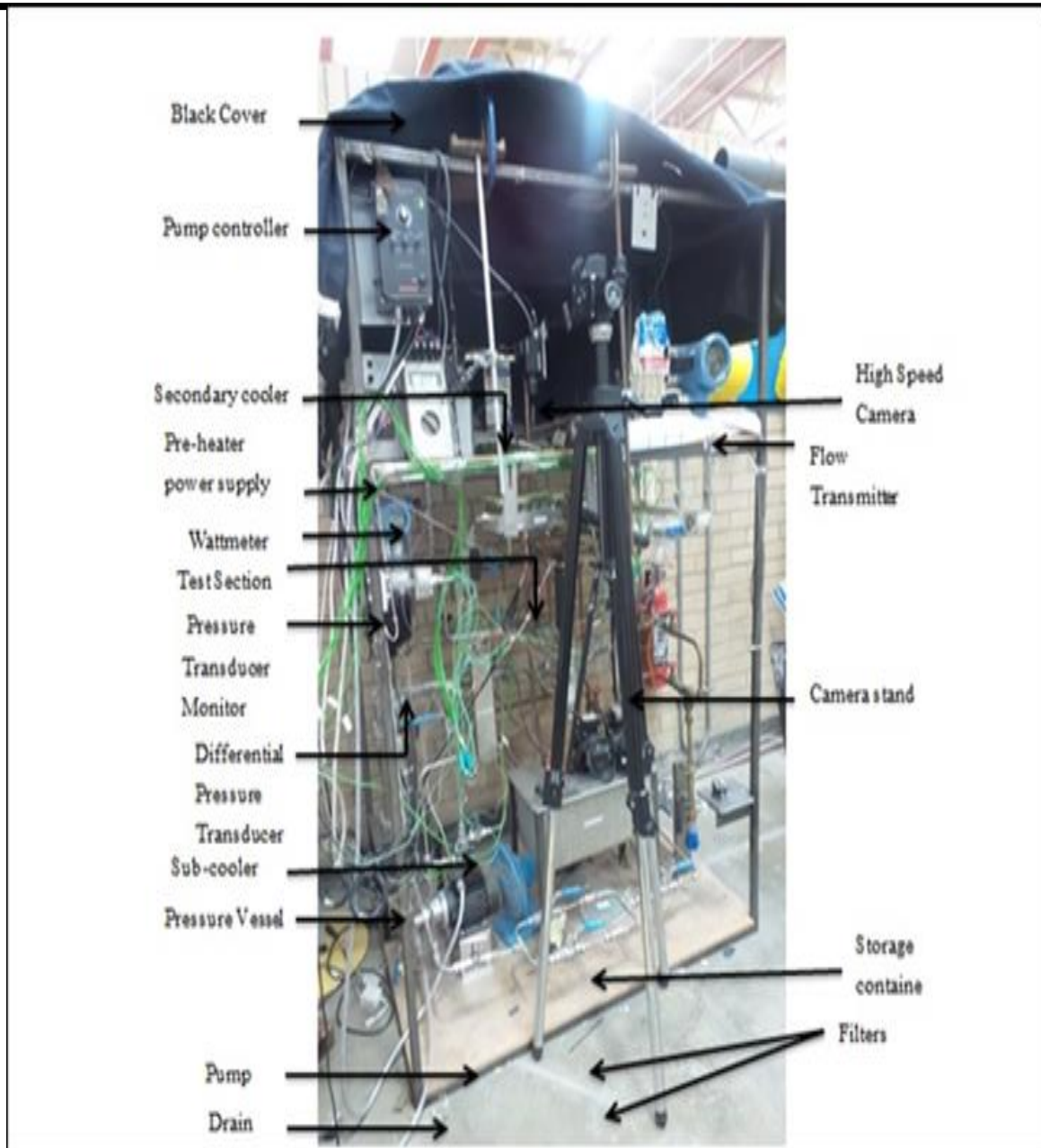
Boiling studies of complex geometries have been undertaken at the macro-scale, for example Ishihara et al. [1] , Schrage et al. [2] , Dowlati et al. [3] , Dowlati et al. [4] and Feenstra et al. [5]. These studies have investigated flow patterns, heat transfer, pressure drop, and void fraction characteristics for flow across a bank of conventional size tubes. A state-of-the-art review of research on two-phase flow and flow boiling across conventional horizontal and small tube bundles has been investigated by Ribatski and Thome [6] . Lie et al. [7] reported flow boiling of FC-72 on plain and pin finned surfaces at atmospheric pressure. Two pin–fin surfaces were examined; one with fins 200 μm square and 70 μm high on a square in-line configuration with a 400 μm pitch, and one with fins 100 μm square and 70 μm high on a square in-line configuration with a 200 μm pitch. The mass fluxes used were within the range 287–431 kg/m^2 s and the heat fluxes within 1–100 kW/m^2. Single phase and flow boiling heat-transfer coefficients were investigated. The mass flux was found to have only a slight effect on the boiling heat-transfer coefficient. The temperature at the onset of nucleate boiling was found to increase with increasing mass flux and, for the same wall-to-fluid temperature difference, the largest heat transfer occurred with the 100 μm fins. Krishnamurthy and Peles reported water [8] and Krishnamurthy and Peles [9] investigated nitrogen-ethanol flows across an array of circular pin fins, 10 μm diameter and10 μm high. The fins were arranged in a staggered array with a longitudinal and transverse pitch of 150 μm on a surface of 1.5

mm wide and 10 mm long. Surface tension effects were deduced by comparing the results of two studies. Water has a similar density and viscosity to ethanol but a much higher surface tension. The flow pattern transition boundaries were found to depend on surface tension. The pressure drop was also affected because of its flow map dependence. Except for a small range of gas-mass fractions, the void fraction was found to be reasonably independent of surface tension.

2. EXPERIMENTAL SETUP

In the Figure 1 Schematically, the flow loop is presented. Before to running each single phase flow exam series, the working fluid was degassed by vigorous boiling for closely three hours to force any dissolved gases to run away from the system to the ambient. During this interval the vent valve above the condenser was periodically opened to permit dissolved gases goes to elopement to the atmosphere. This furthermore set the test pressure to close atmospheric. After degassing the liquid, as it was observed that no gas or air bubble coming out of the liquid inside the test piece before to boiling, flow boiling exams were executed. Exams were conducted by setting the wanted liquid mass flow rate and inlet temperature. Mass flow rate was adjusting by the by-pass valve and modify by the throttling valve located before the filters. The pre-heater was linked to a controller. With respect to the exam's mass flow rate, the controller was adjusting to the wanted applied heat to the fluid flow which was passing the pre-heater, to supply the required inlet temperature. Simultaneously the test section heater was adjusting to the required heat flux to the test piece. The liquid was distributed through the flow loop until the wanted entry temperature was obtained. This took three hours approximately. Steady state conditions were obtained when the fluid outlet, heater and the aluminum housing temperatures were seen to be stable. This took half an hour approximately. All of the wanted readings were achieved before the heat flux was re-set to the next required value and the process iterated. During the exams to maintain the system pressure close the atmospheric pressure, the vent valve above the condenser was periodically open and a balloon was connected to it to block the vapor to elopement from the system. High speed videos were taken of the boiling occurring on the test piece by a Kodak micro motion 1000 camera. The camera was set to 240 frames /s at a resolution of 720 by 480 pixels.

Fig(1): Schematic of flow loop[10]

Fig(2 .the aluminum test section is shown. Liquid entered the inlet plenum of the test-section through the two inlet ports, set at 90ᵉ to the direction of stream in the aluminum test piece. The plenum chamber dimensions were set to reduce the liquid velocity to close to zero before it.
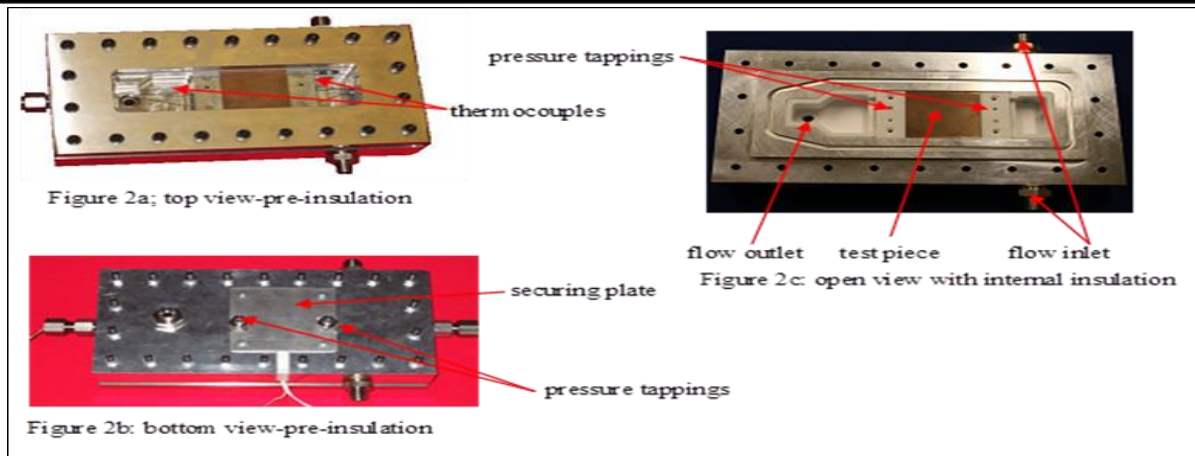
Fig(2): Test section[10]

The In-Line pin-fin micro-channel test piece is shown in Fig. 3.The In-Line pin-fin micro-channel was constructed from a piece of copper, 50 mm wide by 50 mm long and 6 mm high. The channels were formed by cutting slots 1 mm wide and 1 mm deep in the longitudinal direction. The slots were 1 mm apart. Three holes, 0.6 mm in diameter by 12.5 mm long, were drilled into the test piece at the inlet and outlet ends. The holes were located 2.5 mm from the top of the boiling surface and 11, 25 and 39 mm from an edge. These holes allowed six sheathed K-type thermocouples, 0.5 mm in diameter, to be located below the boiling surface. All thermocouples were calibrated in a water bath and were accurate to ±0.15 K.
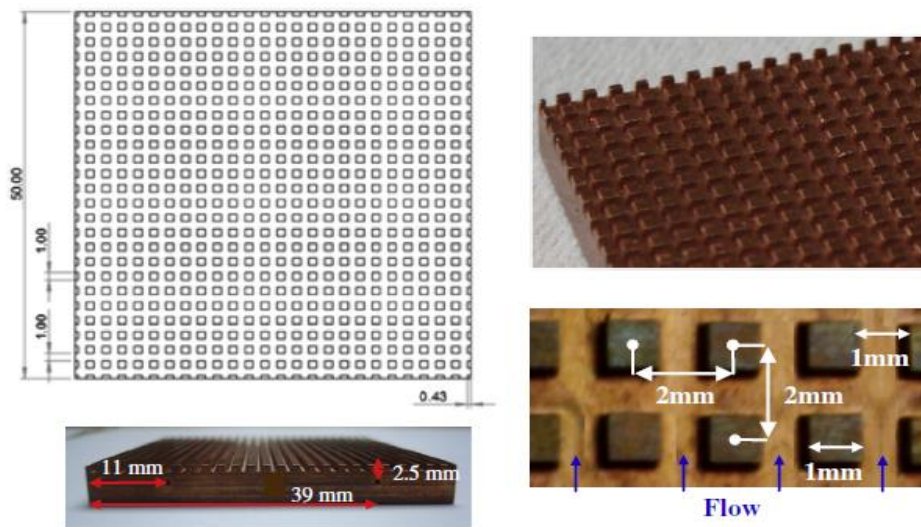
Fig(3).The test piece[10]

3. MATHEMATICAL MODELS

The heat flow from the heater to the test piece is proportional to the difference between the heater temperature, T_h, and the test piece surface temperature, T_w. Data taken when the liquid outlet temperature was below the saturation temperature, deduced from the outlet fluid pressure, were used to establish this relationship. The effective heat flux, q_{eff}, was determined from the ratio of increase in sensible heat of the liquid to the base area of the test Piece, and was correlated by

$qE1 = 2.9 (Th- Tw) - 1.4$ ………(1)

The design of the test section comprises two plates placed in between a ceramic heater and R113 fluid. One plate is made from copper and one from aluminum. Each is 50 mm width and 50 mm length and 5 mm in thickness. During single-phase flow the sensible heat gain by the liquid is given by:

$qsp = M CP(Tout-Tin)$ ……………(2)

This permitted the local outlet and inlet single-phase heat-transfer coefficients to be got from a one-dimensional heat balance through a small flow length (Δz) at the base of the channel gave

$qp (Wch+Ww)2\Delta Z = \alpha sp \Delta TLMTD \Delta Z [(Wch+Ww)2+Ww2-4\eta WwHch]$ …..(3)

The log mean temperature difference (LMTD) represents the wall to fluid temperature difference [11] and Dimensions of heat-transfer unit cell [4]:-

$\Delta TLMTD = Tout-Tinln$ ……….(4)
$(Tw-TinTw-Tout)$

The fins could be processed as rectangular fins with adiabatic tips, i.e.

$\eta = tanh (\lambda Hch)\lambda Hch$ …...(5)

In which λ was the fin parameter, which is given by

$\lambda = 4\alpha kcWw$

Wall temperatures was normally less than 0.7 °C, but could, on occasion, be as large as 1.4 °C. The local wall temperature was therefore got by averaging the data from the three relevant thermocouples to get Ttc, which was then corrected for depth from the plate surface, Htc, through the one dimensional heat conduction equation, i.e.

$Tw = Ttc-qp Htck$ …….(6)

The local outlet and inlet two-phase heat-transfer coefficients to be got from two –phase heat transfer from:-

$qp (Wch+Ww)2\Delta Z = \alpha tp (TW-Tsat)\Delta Z [(Wch+Ww)2+Ww2-4\eta WwHch]$ ….(7)

For a liquid with a specific heat capacity of cp, the liquid temperature was obtained from

$TF = Tin+WMCP0zqp dz$ …….(8)

Where T_{in} is the liquid inlet temperature, M is the mass flow rate of fluid supplied and W is the width of the test piece.

The assessment of the single-phase, heat-transfer coefficients assumed that each channel contained a developing flow where the heat-transfer coefficient could be obtained from

$NU-p = 0.06(RePr)0.73$ ……(9)

In the first instance, a uniform heat flux was assumed for q_b. This allowed the local inlet and outlet heat-transfer coefficients to be obtained from Eq. (3) for each heat and mass flux setting tested. These heat-transfer coefficients were used in a least squares analysis to find values of 0.06 and 0.73 in Eq. (9). This heat-transfer coefficient was imposed on the wall conduction model and Eq. (8) was used to find the liquid temperature, which for these tests is the heat-transfer temperature. This allowed the heat flux distribution to be found and hence an update to the inlet and outlet heat-transfer coefficients. The process was repeated until 0.06 and 0.73 became reasonably constant. Where Prf and Ref are the liquid Prandtl number and Reynolds number relied on local flow, i.e

$$Prf = Cp, f\mu fkf \ldots\ldots\ldots\ldots\ldots\ldots(10)$$

$$Ref = GDh\mu f \ldots\ldots\ldots\ldots\ldots..(11)$$

All Nusselt numbers were defined as

$$NU\text{-}m = \propto DhKf \quad \ldots\ldots(12)$$

The equivalent diameter for a square pin was chosen to give the same circumference as an equivalent circular tube

$$Dh = 4 Ww\pi \ldots\ldots\ldots..(13)$$

A typical two-dimensional unit cell at the location of a thermocouple situated inside the copper test piece for the parallel test pieces is seen in the table below.

Table(1): Dimension for channel heat transfer analysis[10]

Pin-fin channel test piece									
Ww	Wch	Wcell	Lcell	Hw1	Hw2	Hw3	Hch	Htc	Hcell
mm	mm	mm	mm	mm	mm	mm	mm	mm	mm
0.5	1.0	2.0	2.0	10.0	5.0	5.0	1.0	1.5	21.0

the heat transfer unit cell for pin-fin micro-channel dimension in the secheme .
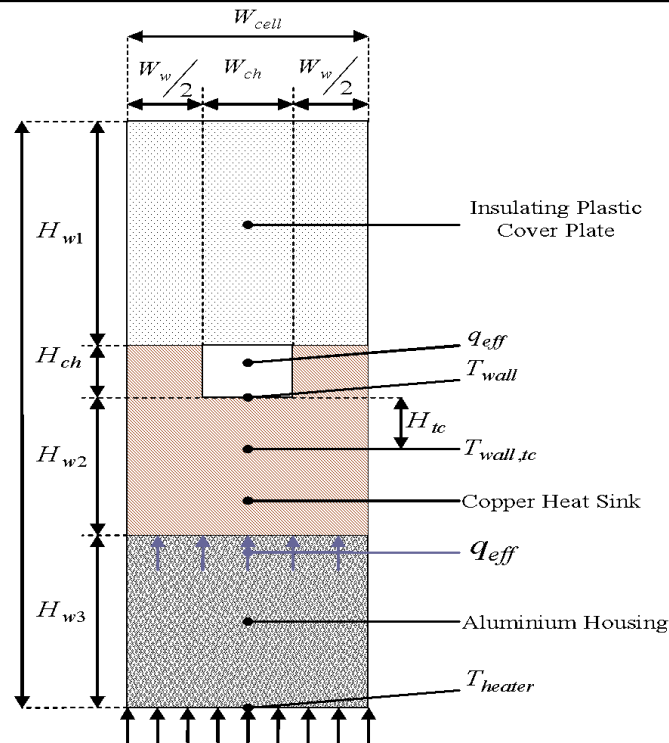
Fig(4): the heat transfer unit cell [10]

4. EXPERIMENTAL RESULTS FOR SINGLE-PHASE AND TWO-PHASE FLOWS

Heat-transfer coefficients and pressure were obtained for single-phase liquid R113 near atmospheric pressure and temperature. For the pin-fin surface, heat-transfer Coefficients were obtained for heat loads in the range 25 - 140 W. The heat load was chosen to give a rise in fluid temperature of at least 4 -5 K. This gave apparent heat fluxes in the range 5 - 50 kW/m2, based on the base area of the test plates. Five equally spaced mass flow rates between 2.5 g/s and 12.5 g/s were used. This gave mass fluxes in the range 50−250 kg/m2s, based on the unrestricted flow area in the test channels. Pressure drops were obtained under isothermal conditions for the same mass fluxes.Single-phase analysis, heat transfer coefficients measurements which were presented are analyzed in this paper. For the parallel channel surfaces, several popular macro- and micro-channel correlations for the empirical data were compared with the heat-transfer data. The variation of single phase heat transfer with heat flux is shown for the In Line Pin-Fin Channel surface as shown in Figure 5 .Heat flux is plotted in terms of Th , for all mass fluxes and the relevance was Linear relationship. The difference between channel base wall temperature, Tw , and heater temperature ,Th **.**
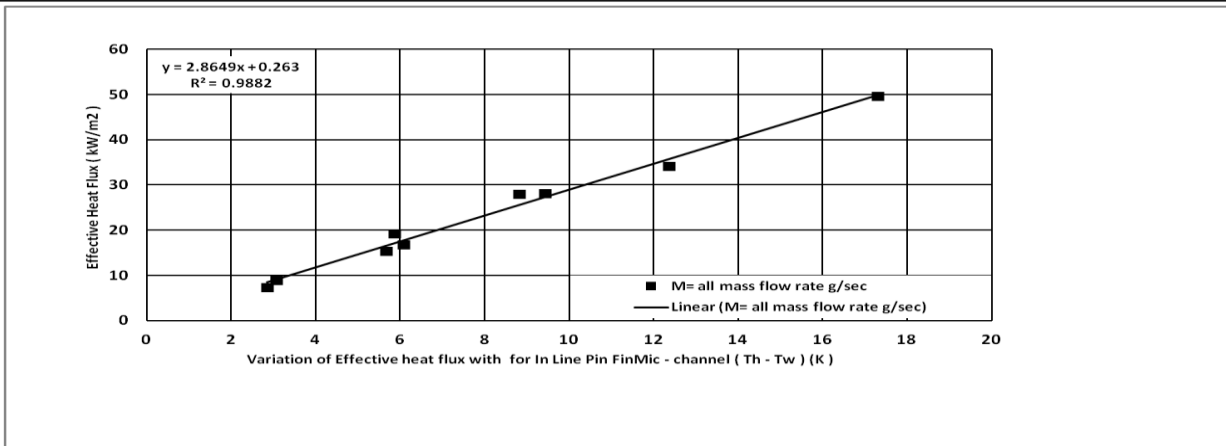
Fig(5): Variation of effective heat flux with (Th- Tw) for In Line Pin-Fin Channel
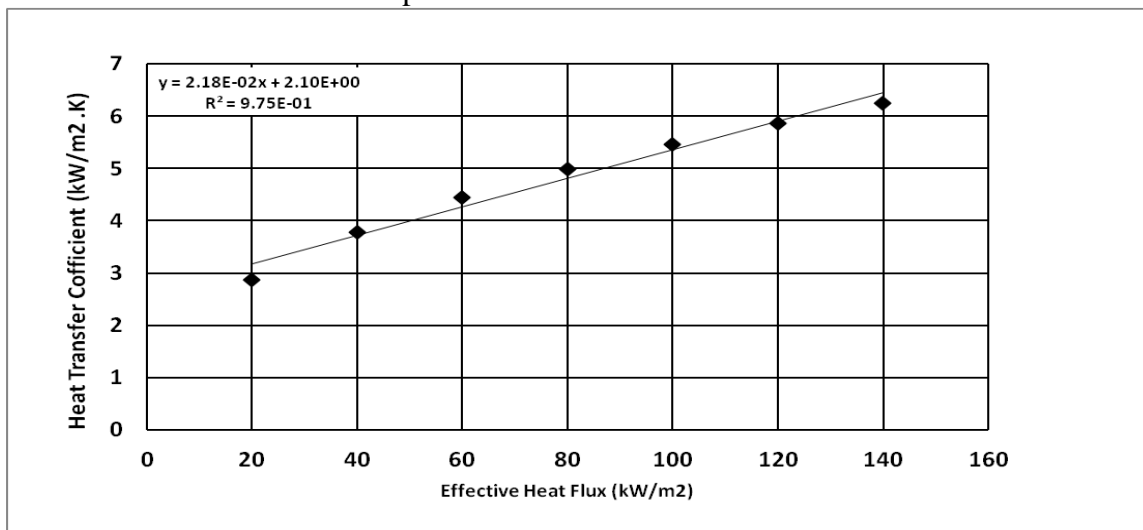
The single-phase heat-transfer coefficients are shown for the range of mass fluxes in Fig. 6. The estimated error in the heat transfer coefficient. The heat-transfer coefficients at the inlet and outlet positions of the pin-fin are shown to be similar in magnitude and to increase with increasing mass flux. The pin-fin inlet and outlet values are shown to be different in magnitude, with both following a Linear function of the mass flux, inlet and outlet positions of the pin-fin are shown to be similar in magnitude and to increase with increasing mass flux. The pin-fin inlet and outlet values are shown to be different in magnitude, with both following a Linear function of the mass flux.
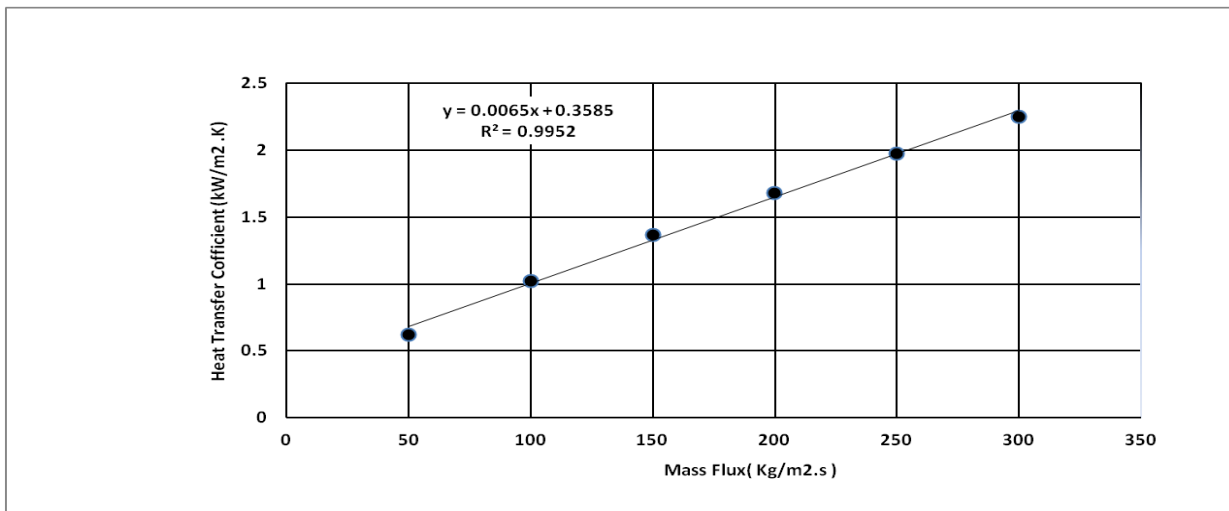
Fig(6) : Variation of Heat Transfer Coefficient with Mass Flux for In Line Pin-Fin Channel

The two-phase tests were performed by supplying liquid R113 near atmospheric pressure to the test section with 2-5 K of sub cooling. Heat-transfer and pressure drop data were obtained for heat loads in the range 25 - 400W. These were applied to each mass flow rate in steps of 25 W, with the 375 W load avoided. This gave apparent heat fluxes in the range 10-160 kW/m². The heat-transfer coefficients at the inlet and outlet positions of the pin-fin are shown to be similar in magnitude and to increase with increasing effective heat flux. The pin-fin inlet and outlet values are shown to be different in magnitude, with both following a Linear function of the mass flux. All of the saturated

boiling data identified in the pin-fin data, Fig(7). Are reasonably independent of location and mass flux and follow the linear relationship

Fig(7):Variation of Heat Transfer Coefficient with Effective Heat Flux

5. CONCLUSIONS

The experimental procedure for these tests led to the occurrence of three types of heat-transfer, single-phase, sub cooled boiling and saturated boiling. Single-phase heat-transfer was taken to have occurred when the fluid above the thermocouple was in a sub cooled State and the wall temperature was below the local saturation value. Sub cooled boiling heat-transfer was taken to have occurred when the fluid above the thermocouple was in a sub cooled state and the wall temperature was above the local saturation value. Saturated boiling heat-transfer was taken to have occurred when the fluid above the thermocouple was in a saturated state and the wall temperature was above the local saturation value. Heat-transfer and pressure drop data have been obtained for pin fin channel geometry. The two-phase heat-transfer coefficient for the pin-fin surface is had been investigated. However, the pin-fin surface area is larger and the heat-transfer coefficient is slightly larger, allowing a much lower surface temperature for the same heat flux compared with plate channel.The following conclusions can be drawn from this study:-
1. The heat flux distributions have deformities obtained from two causes. The first cause is because of end effects, and the second cause is because of the variation in liquid temperature, and heat transfers coefficient. To demonstrate the first cause, assume the channel contained a flow that was subjected to a uniform heat flux. To explain the

Importance of the second effect, the heat conduction model outlined was solved for single phase flows.

2.The In-Line pin-Fine Channel had a bigger heat transfer area than plate surface when compared it with a Literature Survey.

3.In-Line pin-fin surfaces improve the heat transfer by increasing the heat-transfer surface and the heat-transfer coefficient.

These data were obtained for R113 and are therefore likely to be applicable to more readily available fluids.

NOMENCLZTURE

D_h = hydraulic diameter (mm)
K_c=copper thermal conductivity (W/m^2.k)
K_f =fluid thermal conductivity (W/m^2.k)
Q =heat transfer (Watts)
Nu-$_m$= measure Nusselt number (-)
Nu-$_p$ = prediction Nusselt number (-)
Pr = Prandtl number (-)
Re= Reynods number (-)
T= temperature (^{o}C)

GREEK LETTERS

α = heat transfer coefficient (W/m2.k)
μ= dynamic viscosity (kg/m.s)
subsecript
c=copper
f=fluid
in =inside
out = outside
sat = saturated
sp = single-phase
tp =two-phase
w = micro-channel wall

REFERENCE

[1]   K. Ishihara, J. W. Palen, and J. Taborek, "Critical Review of Correlations for Predicting Two-Phase Flow Pressure Drop across Tube Banks," *Heat Transfer Engineering,* vol. 1, pp. 23-32, 1980/01/01 1980.

[2]   D. S. Schrage, J. T. Hsu, and M. K. Jensen, "Two-phase pressure drop in vertical crossflow across a horizontal tube bundle," *AIChE Journal,* vol. 34, pp. 107-115, 1988.

[3]   R. Dowlati, M. Kawaji, and A. M. C. Chan, "Pitch-to-diameter effect on two-phase flow across an in-line tube bundle," *AIChE Journal,* vol. 36, pp. 765-772, 1990.

[4]   R. Dowlati, A. M. C. Chan, and M. Kawaji, "Hydrodynamics of Two-Phase Flow Across Horizontal In-line and Staggered Rod Bundles," *Journal of Fluids Engineering,* vol. 114, pp. 450-456, 1992.

[5]   P. A. Feenstra, D. S. Weaver, and R. L. Judd, "An improved void fraction model for two-phase cross-flow in horizontal tube bundles," *International Journal of Multiphase Flow,* vol. 26, pp. 1851-1873, 2000/11/01/ 2000.

[6]   G. Ribatski and J. R. Thome, "Two-Phase Flow and Heat Transfer across Horizontal Tube Bundles-A Review," *Heat Transfer Engineering,* vol. 28, pp. 508-524, 2007/06/01 2007.

[7]   Y. M. Lie, J. H. Ke, W. R. Chang, T. C. Cheng, and T. F. Lin, "Saturated flow boiling heat transfer and associated bubble characteristics of FC-72 on a heated micro-pin-finned silicon chip," *International Journal of Heat and Mass Transfer,* vol. 50, pp. 3862-3876, 2007/09/01/ 2007.

[8]   S. Krishnamurthy and Y. Peles, "Gas-liquid two-phase flow across a bank of micropillars," *Physics of Fluids,* vol. 19, p. 043302, 2007.

[9]   S. Krishnamurthy and Y. Peles, "Surface tension effects on adiabatic gas–liquid flow across micro pillars," *International Journal of Multiphase Flow,* vol. 35, pp. 55-65, 2009/01/01/ 2009.

[10]   D. A. McNeil, A. H. Raeisi, P. A. Kew, and R. S. Hamed, "An investigation into flow boiling heat transfer and pressure drop in a pin–finned heat sink," *International Journal of Multiphase Flow,* vol. 67, pp. 65-84, 2014/12/01/ 2014.

[11]   T. Chen and S. V. Garimella, "Effects of dissolved air on subcooled flow boiling of a dielectric coolant in a microchannel heat sink," *Journal of Electronic packaging,* vol. 128, pp. 398-404, 2006.

"Voltage Profile Enhancement using fuzzy self-tuned STATCOM"

Dr. Abdelelah K. Mahmood [1]
Electrical Engineering Department
Mosul University

Dr. Inaam I.Ali [2]
Electrical Engineering Department
University of Technology

Ayad A. ALGailany [3]
Electrical Engineering Department
Mosul University

Abstract:

Recently, the demand on electrical energy is growing day by day as a result of rapid industrial development so that it is making the transmission lines more exhausted and affected especially the voltage stability. In order to overcome these problems, a FACTs device STATCOM of 12 pulse two levels is used to increase the capability of transmission lines and improving the voltage profile of the system. In this work, a new technique of fuzzy self-tuning is used in STATCOM's controller where the parameters of PI controller tuned online that is lead to improve the voltage profile when the power system exposed to the abnormal condition. The simulation results of STATCOM with tuned fuzzy-PI controller show an enhancement in voltage profile under many disturbances as compared with the system used STATCOM without this new technique. The results show a voltage profile using fuzzy-PI less over shoot and reach to steady state efficient than conventional PI. The results of total harmonic distortion (THD) show low values due to application of the Sinusoidal Pulse Width Modulation (SPWM) technique and assuming the loads are linear.

Keywords: FACTs, STATCOM, Voltage profile, fuzzy self-tuning PI

الملخص:

لوحظ في الآونة الاخير زيادة الطلب على الطاقة الكهربائية نتيجة التنمية الصناعية السريعة ومن المعروف ان ذلك يجعل خطوط النقل الكهربائية اكثر استهلاكاً وتأثراً لاستقرارية الفولتية. من اجل التغلب على تلك المشاكل, يتم استخدام المعوض التزامني الساكن ذو 12 نبضة وثنائي المستوى لزيادة قابلية خطوط النقل على نقل الطاقة وتحسين الفولتية عموما. احدى التقنيات الجديدة المستخدمة في هذا البحث هي تقنية التنغيم الذاتي لمعاملات المسيطر التناسبي التكاملي باستخدام المنطق المضبب حيث يتم تنغيم تلك المعاملات مباشرة ولحظة حدوث الاضطراب وذلك لتحسين الفولتية. اظهرت نتائج التمثيل تحسن لفولتية النظام المربوط عليه المعوض التزامني الساكن مع تقنية التنغيم الذاتي باستخدام المنطق المضبب عند حصول الاضطراب ومقارنته مع نتائج المعوض التزامني الساكن من دون تلك التقنية. وكذلك اظهرت نتائج تلك التقنية الحصول على اقل تجاوز للحد لموجة الفولتية لحظة حصول الاضطراب وكذلك الوصول للحالة المستقرة اسرع من الطريقة التقليدية. أظهرت نتائج تشوه التوافقيات الكلي (THD) لموجة الفولتية والتيار قيم جيدة وقليلة وضمن معايير IEEE بسبب استخدام تقنية تعديل عرض النبضة الجيبي SPWM وافتراض الاحمال المستخدمة خطية.

1. **Introduction**

 The Flexible AC Transmission Systems (FACTS) is static equipment used in ac transmission and distribution systems. It introduces a new power electronic technology into conventional AC power systems and improves the power system stability[1]. Power system stability is a significant remarkable aspect, it is substantial to reduce the load losses and to acquire a remarkable output from power system. As demand increased, the new power stations are increased and that rapid of transient and steady-state stability problems in power system [2]. The one favorable FACTS device for voltage profile enhancement is STATCOM. The most benefit of a STATCOM is to control and regulate the voltages at any busbar used to connect of it in power system as shown in figure(1).
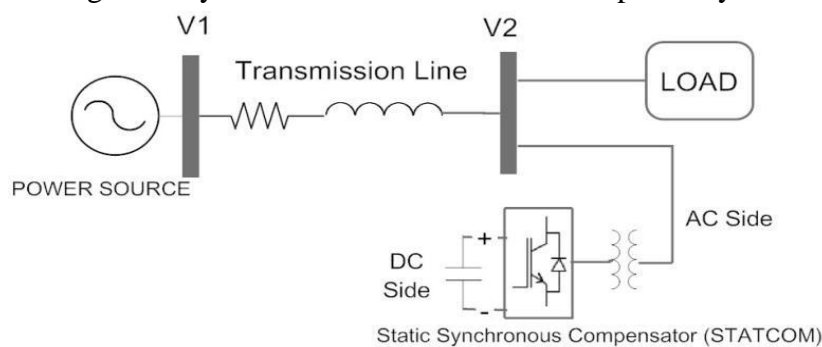
Fig(1): STATCOM equipped into single line diagram

The PI controller is used in many industrial processes for control issue also featured by robustness and simplicity so that it is used in STATCOM construction.

    In previous research, numerous of them were dealt with STATCOM for voltage profile and control strategy. In [3] Dhiya. Al-Nimma and Majed. Al-Hafid presented a STATCOM for voltage profile improvements in Mosul ring. A conventional PI controller was used for voltage control so that under some small disturbances, the results showed a good improve in voltage profile at weak Bus. In [4] Tao Huang was used fuzzy logic control for multi objective to the STATCOM controller. The utilized adaptation of fuzzy control multi objective enhanced the dynamic condition much better than traditional PI control under small and large disturbances. In [5] V. Ponananthi and B.R. Kumar presented STATCOM with PI controller and fuzzy logic controller for voltage regulation. They show that terminal voltage kept constant under unbalance loads. In [6] N. Goel et al used a genetic algorithm for tuning the parameters of PID controller in STATCOM. The results show the performance of STATCOM with G.A tuned is the best and make a voltage profile closest to 1pu under three kinds of disturbances.

    As used in this research, STATCOM is hold over of PI controller as well as an adaptation for locating the gains of Integral controller online through any disturbance take place by using fuzzy logic controller to enhance the process control and thereby the voltage stability.

2- Voltage Profile Improvements:

 When reactive power support did not attain to the desired value the voltage goes towards collapse and causing an effect of cascading on the near region [7]. Figure (2) shows the single line diagram

system with an inductive load at bus 2 (V2). In absence of any compensation device and from phasor diagram, the current (Ip) is concur with the vector of voltage (V2).

In compensation process, the reactive power is produced near to load by injecting/absorbing reactive current (IC), and that is reducing the currents flowing in the lines from main source so that lead to improve the voltage stability. The STATCOM also can provide the ultimate inductive and capacitive reactive power at minimum and maximum value of system voltage as far as lower system voltage as clarified in figure (3) [8].

a) Without Reactive compensation

b) Compensation with a Current Source
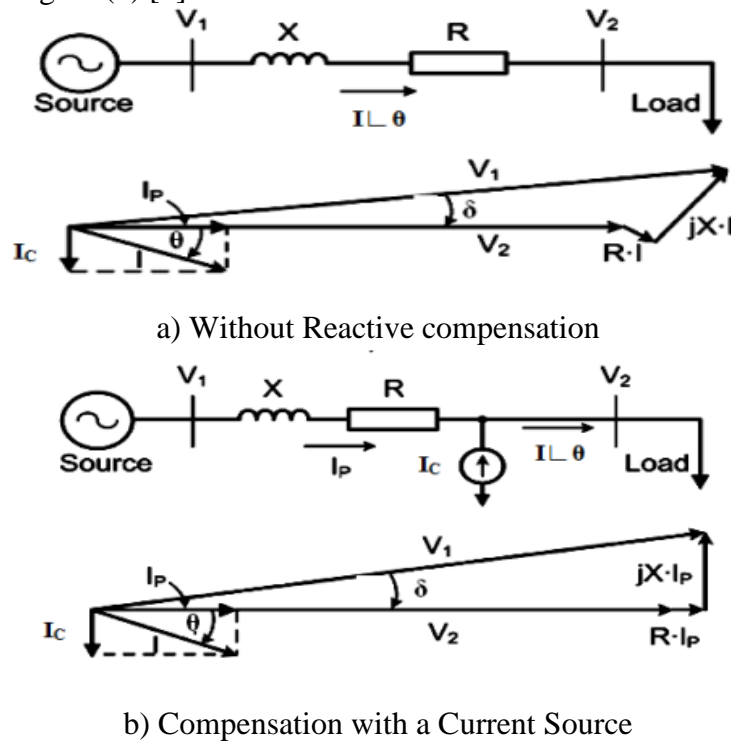
Fig(2): Principles of Shunt Compensation in AC system [8]
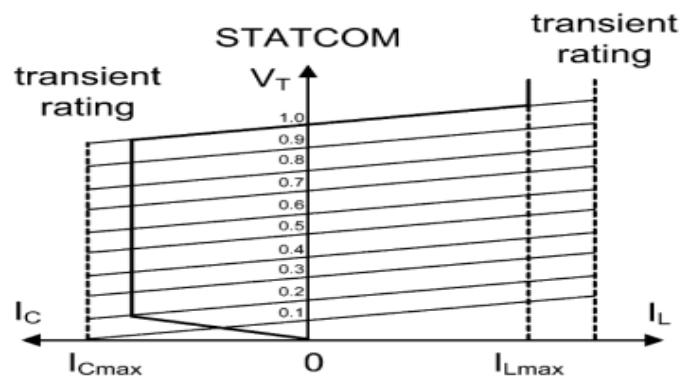

Fig(3): STATCOM V-I characteristics [1]

3- Mathematical Model of STATCOM

Generally, STATCOM is a shunt connected device with the power system through a coupling transformer and interface reactor. STATCOM's equivalent circuit clarified in figure (4) which

represents VSC that formed by self-commutated device such as GTO or IGBT, and a capacitor (*C*). The symbols of va, vb and vc indicate the 3- phase system voltages at the point of common coupling (PCC), ea, eb, and ec can be represented a 3- phase voltage at AC side of STATCOM's converter. The symbols ia, ib and ic represents the flowing currents between STATCOM and power system.

The resistance (*Rp*) connected in parallel with *(C)* represents both the switching and capacitor losses. To connect the STATCOM into AC power system required a magnetic coupling that is represented by leakage inductance (*Ls*) and resistance (*Rs*) [9].
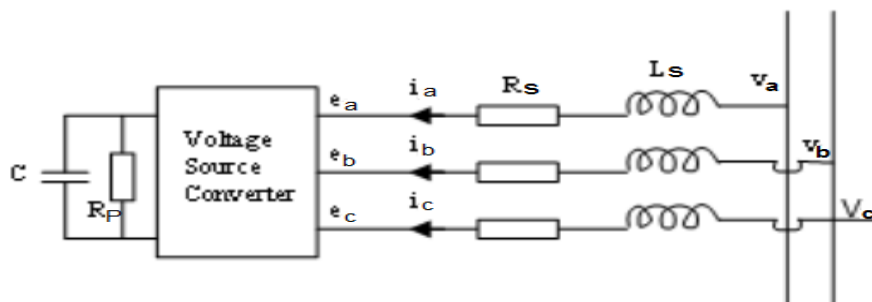
Fig(4): Schematic for equivalent circuit of STATCOM

The First order differential equations of STATCOM in AC side as introduce in figure (4) can be formed below:

$$Va - ea = Rs * ia + Ls * \frac{dia}{dt} \qquad \dots (1)$$
$$Vb - eb = Rs * ib + Ls * \frac{dib}{dt} \qquad \dots (2)$$
$$Vc - ec = Rs * ic + Ls * \frac{dic}{dt} \qquad \dots (3)$$

It can be transformed to the per-unit system and converted from ABC to dq rotation coordinate system as presented in equation (4).

$$\frac{d}{dt}[id'\ iq'] = [-Rs'\ \omega bLs'\ \omega\ -\omega\ -Rs'\ \omega bLs'][id'\ iq'] + \omega bLs'[ed' - |v'|\ eq'] \qquad \dots (4)$$

Also the DC-side can be analyzed mathematically as equation (5).

$$\frac{dvdc'}{dt} = -\omega b\ C'\ (idc' + \frac{vdc'}{Rp'}) \qquad \dots (5)$$

The final equation of STATCOM and after linearization, the decoupled term of iq' and id' can be written as:

$$\frac{d}{dt}[\Delta id'\ \Delta iq'] = [-Rs\ \omega bLs'\ 0\ 0\ -Rs\ \omega bLs'][\Delta id'\ \Delta iq'] + [C1\ C2] \qquad \dots (6)$$

Where C1 and C2 are defined the PI controller used in current regulator as written below:

$$[C1\ C2] = [(Kp1 + \frac{Ki1}{s})(id'* - id')\ (Kp2 + \frac{Ki2}{s})(iq'* - iq')] \qquad \dots (7)$$

Where id' * and iq' * are defined the reference value of dq currents drawn from power system.

The dq voltages are out from the controller and needed to introduce the parameters of modulation index (M) and angle (α). The symbol (M) means the modulation index that is related by a magnitude ratio between AC and DC side terminal voltage. The symbol (α) represents the angle of bus voltage lagging or leading of inverter voltage. These parameters are converted into control signal needed for PWM. The dq voltages can be introduced in the equations below.

e'd=M .vdc'cosα   … (8)

e'q=M .vdc'sinα   … (9)

The block diagram of single line diagram of power system with STATCOM has been introduced as shown in figure (5).
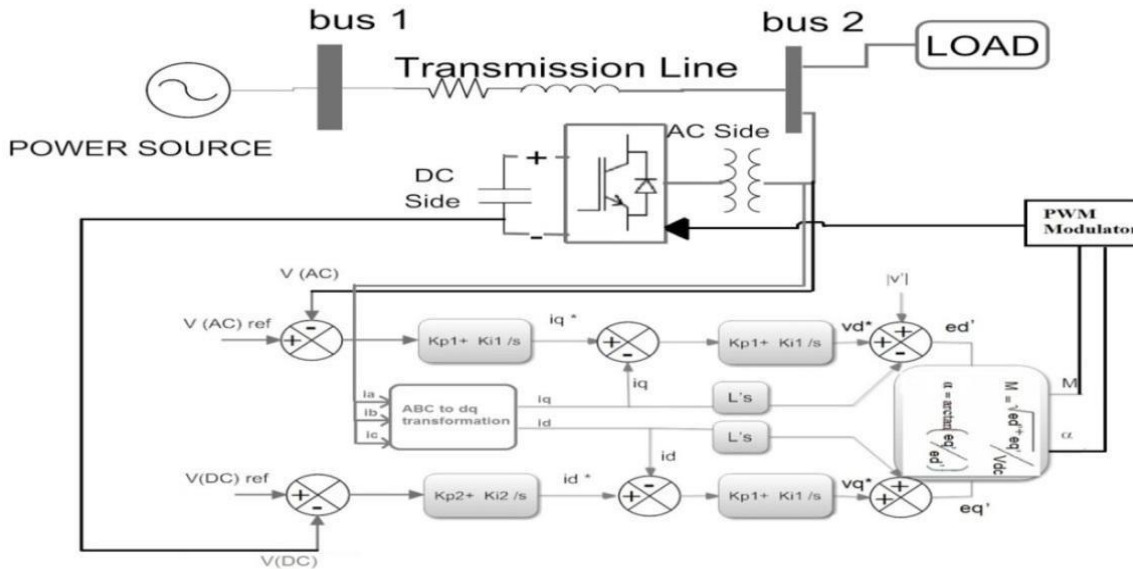
Fig(5): single line diagram with STATCOM's controller [10]

## 4- Power System and STATCOM Design

A simple power system proposed consisted of one Thevenin equivalent three-phase voltage source with capacity about 100MVA and 132 KV nominal voltage. The transmission line of 21 km connects the generation area with load area. A linear and constant load of (15MW, 8MVAR) has been used as inductive load connected at the end of system. The voltage source converter (VSC) of STATCOM is formed using two three-phase bridges (IGBT). The two sets of the triggering pulses are used to achieve the 2-level converter with SPWM. All of these components with power system proposed are simulated using MATLAB/SIMULINK /PSB as shown in figure (6).
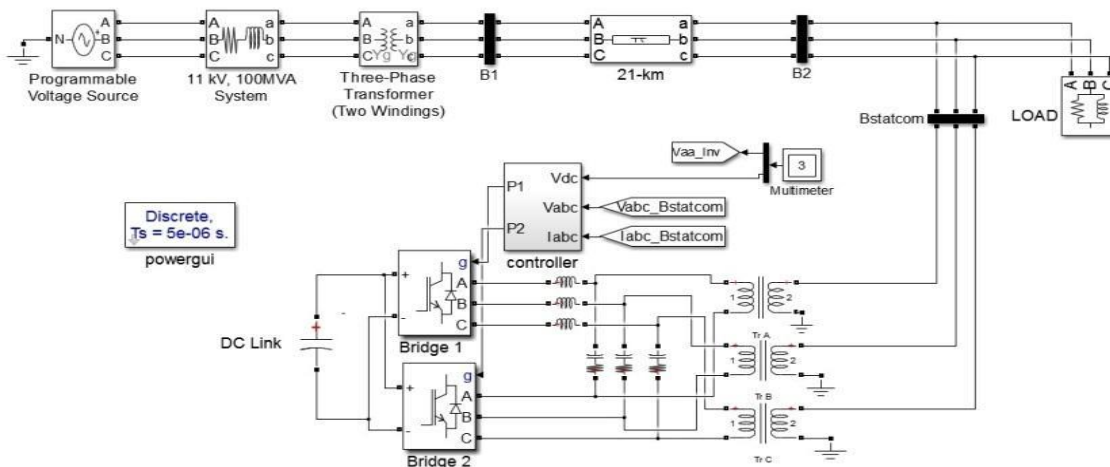
Fig(6): simple structure of power system modeled with STATCOM

5- Controller Design of STATCOM

Many controller strategies have been used for STATCOM such as phase shifting control, PQ theory and Synchronous Reference Frame (SRF) [11]. In this work, SRF has been used widely and preferable using for carrier based PWM control. Fig.(7) shows the controller block that contains three important regulators needed for finding the reference signals. A phase locked loop used to synchronize on the positive sequence components of bus terminal voltage by extract a time varying angle (ωt).
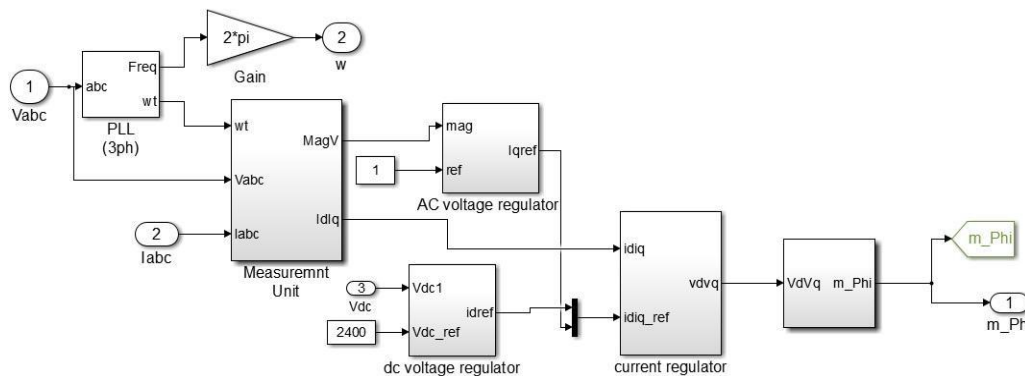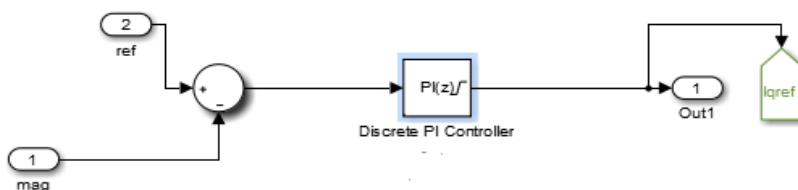

Fig(7): STATCOM's controller design using MATLAB/SIMULINK/PSB

6- AC Voltage Regulator

6.1 – Conventional PI Controller Design

The voltage magnitude resulting from equation (10) is comparing with reference voltage that always being 1 pu then error signal has been proceeded by PI controller to get the reference signal of reactive current as shown in fig.(8).

$$\left| V \right| = vd2 + vq2 \qquad \ldots (10)$$

Fig(8): AC voltage regulator modeled by MATLAB/SIMULINK

6.2 – Self-tuned PI Controller Design

PI controllers with fixed parameters in the industrial working environments are robust but voluntary. Therefore, tuning of the PID-parameters has been performed. Fuzzy logic is a way for decision action utilized for expert systems and process control. In this work, fuzzy-PI technique has been used to achieve tuning parameters. The outputs of PI controller are actions of proportional and integral summed together. These actions are controlled by gains parameter for each one when taking into account that outputs of controller which are limited to the range set for control output. Two inputs are presented; the first is error resulting from comparison between magnitude of

terminal voltage and its reference while the second is change of error. These values are mapping through a member ship function. The output is chosen to be a variation of integral gain (ΔKi) as shown in fig.(9).
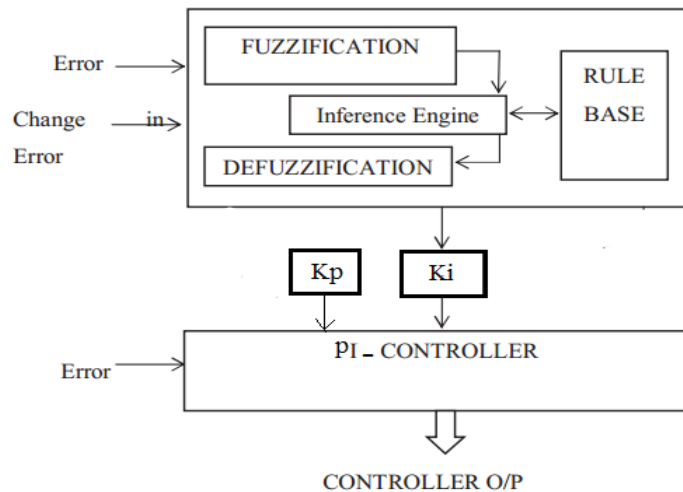

Fig(9): inputs and output formed by fuzzy logic [12]

This output is based on two inputs; error (e) and change of error (Δe). The variation value of integral gain (ΔKi) can be summed to a reference value of integral gain (Ki*) that came from conventional tuning like trial and error method as introduced in equation (11). Finally, the value of integral gain can be ready to use in the I-controller with fixed value of P-controller to form finally a PI controller as shown in fig(10).

$$Ki = Ki^* + \Delta Ki \qquad \qquad \dots (11)$$

For more comprehension about the control process, two cases are introduced below to show the action of fuzzy during disturbances:

a.When the error resulting from voltages comparison is out of range towards positive more than +0.024 and in negative less than -0.024, the output of fuzzy can be large value of "change of integral gain (ΔKi)" in order to make an enhancement in voltage profile under disturbances.

b.When the error is located in the range of (+0.024 and -0.024), the action of fuzzy must zero and led to get zero value of "change of integral gain (ΔKi)" so that the value of Ki is equal to the reference value (Ki*).
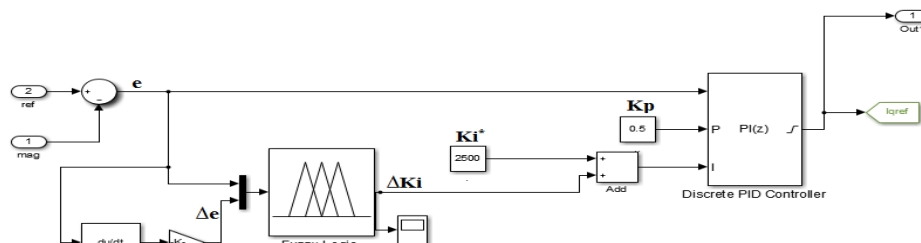
Fig(10): Model of Self-tuned PI Controller using Fuzzy Technique

Triangular membership function (Trimf) can be used for this process. Five sets of membership have been chosen for inputs categorized as error and change of error as shown in figure (11) and figure (12) and two sets of membership have been chosen for output. Every membership introduced must be named in the fuzzy logic toolbox and categorized by a Linguistic variable as presented in Table (1).

Table (1): Linguistic variable for input and output M.S function

Linguistic variable symbol	Linguistic variable
P B	Positive Big
P S	Positive Small
Z	ZERO
N S	Negative Small
N B	Negative Big
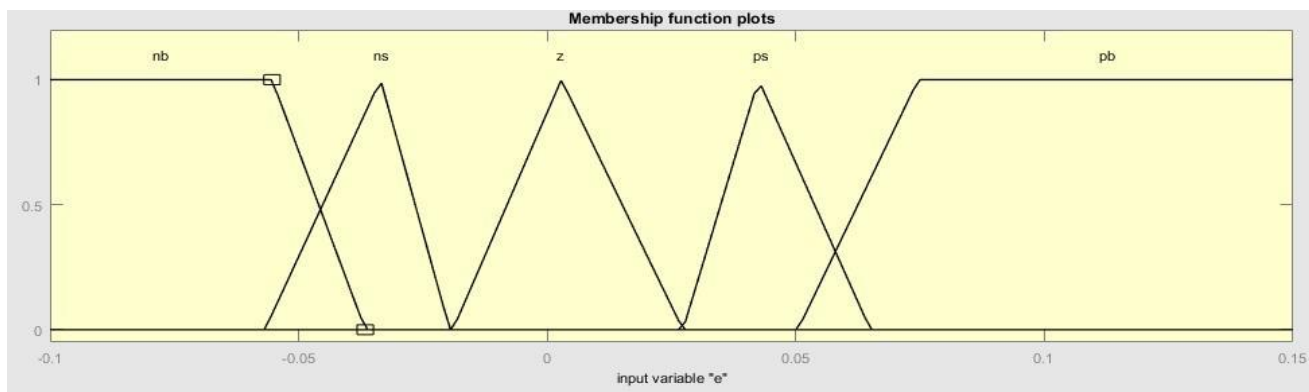
Fig(11): Error membership function
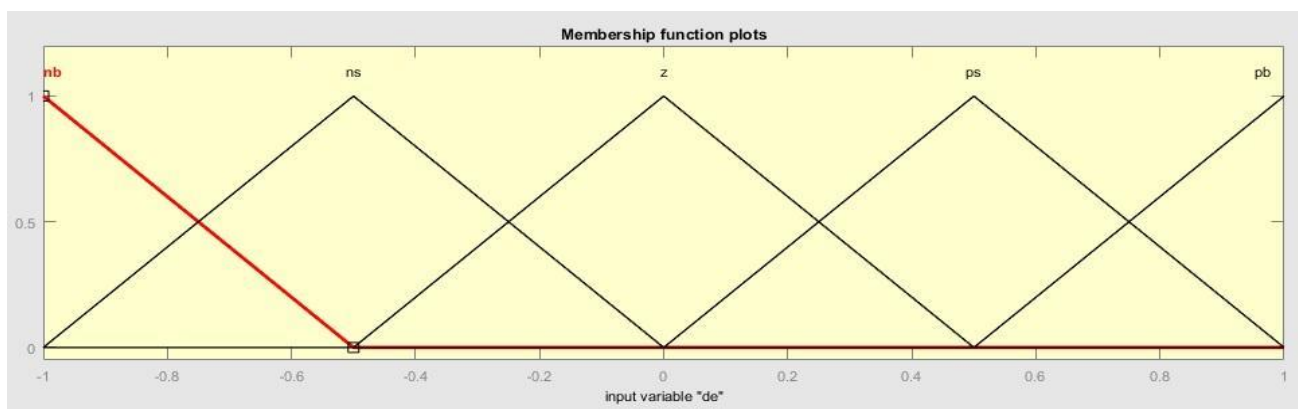
Fig(12): Change of error membership function

The rule base using for tuning of the integral parameters are listed in the table (2), and the surface viewer for these rules can be designed as shown in figure (13).

Table (2): adjusting fuzzy rules of (ΔKi)

Δe e	N B	N S	Z	P S	P B
N B	P B	PB	P B	P B	P B
N S	P B	PB	P B	P B	P B
Z	Z	Z	Z	Z	Z
P S	P B	P B	P B	P B	P B
P B	P B	P B	P B	P B	P B
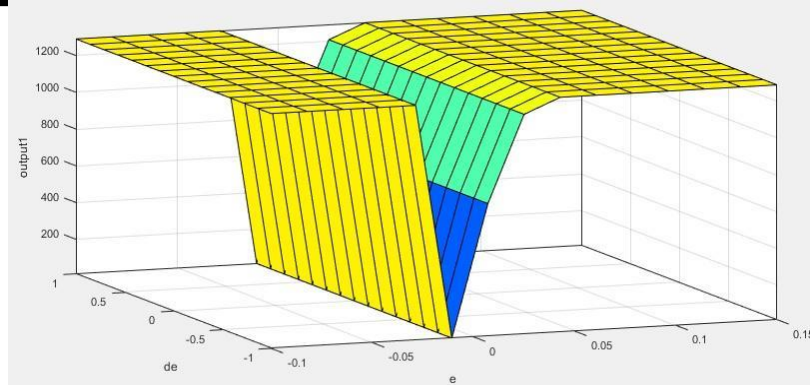
Fig(13): Surface viewer for the rule base

7- Simulation Results

Three cases are presented in this work to show the enhancement in voltage profile when accomplished the conventional PI controller or self-tuned controller.

Case1: The inductive load of (9 MW, 4 MVAr) is entered at bus 2 to increase the loading and test the system with STATCOM for how to deal with this case. Figure (14) shows an enhancement in voltage profile with disturbance due to load entered at 0.4second and outage at 0.6 second.
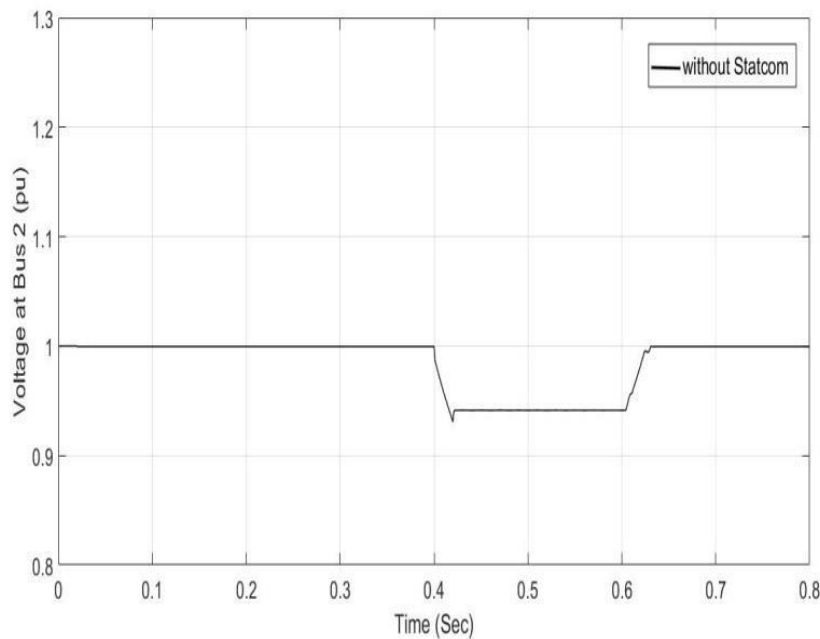
The modulation index has been increased from 0.75 to 0.98 and that is required to increase voltage magnitude to the value in stable state.

The percentage of THD for phase voltage and current by using Fast Fourier Transform (FFT) at receiving end is presented as shown in figure (15). The results where is 0.4% for voltage and 0.54% for current waveform while at sending end the results where is 0.45 for voltage and 0.34 for current waveform as shown in figure (16).These values are acceptable in IEEE standards [13].
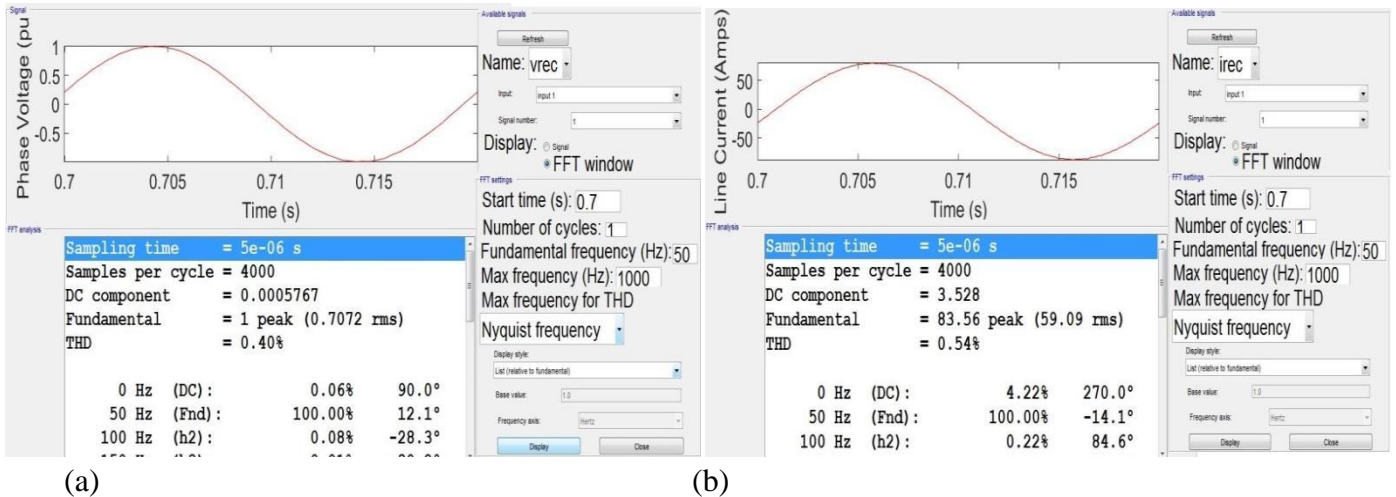
  (a)   (b)
Fig(15): the percentage of THD at receiving end for; a) phase voltage, b) line current

 (a)   (b)
Fig.(16) the percentage of THD at sending end for; a) phase voltage, b) line current
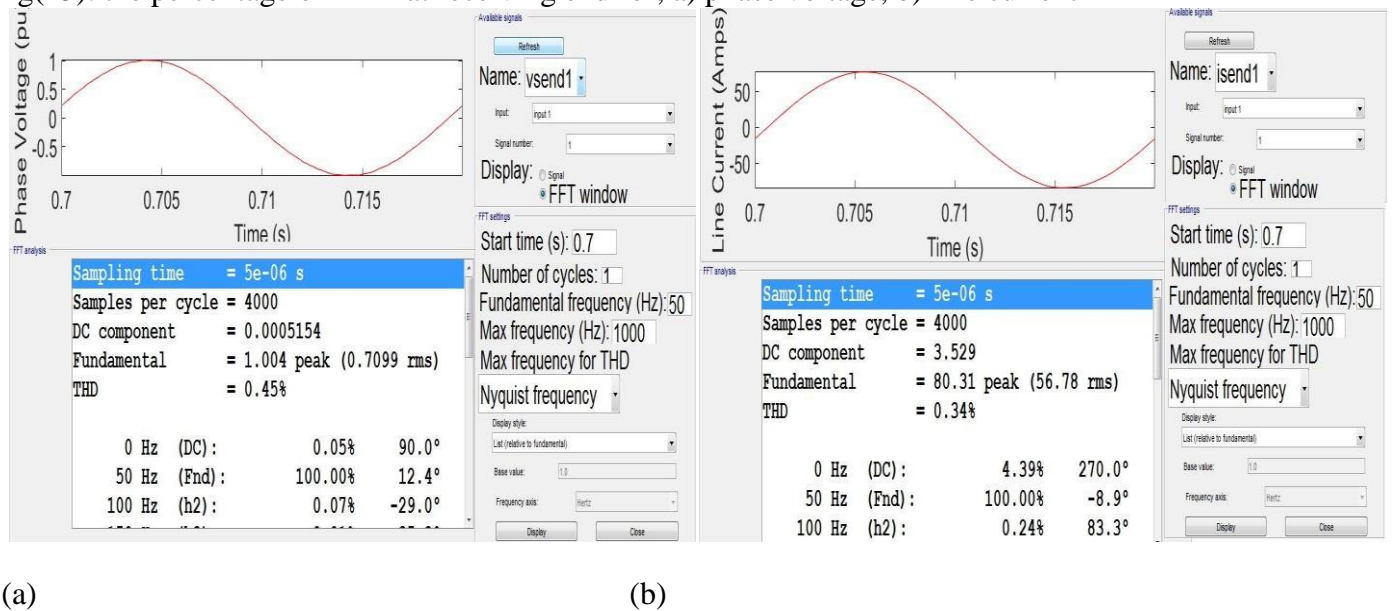
Case 2: When the three phase voltage source is raised or reduce and voltage fluctuated take place at load bus for any reason suddenly, the STATCOM must deal with this changing and enhancing the voltage profile as shown in fig.(17).
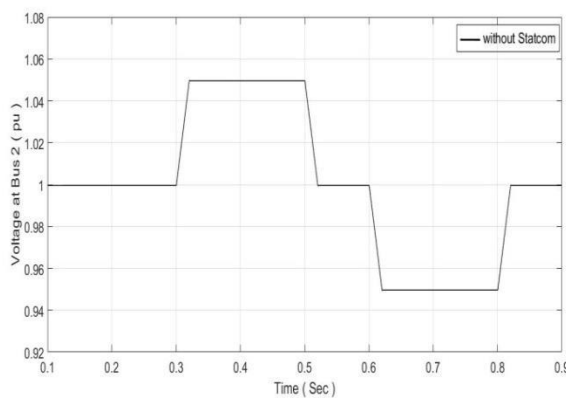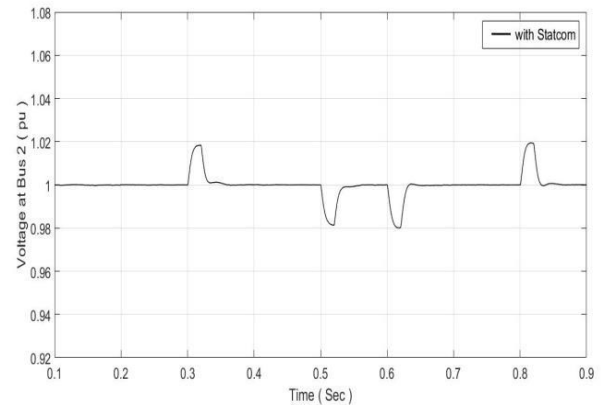
(a)   (b)

Fig(17): voltage profile at load bus for source voltage level disturbance

Case 3: When the technique of self-tuned for PI controller is used, the voltage profile will get enhanced and making the system voltage more stable. In this case, the disturbance accomplished in case 2 will be used as same in case 3 to analyze the difference between conventional and adaptive controller. Fig.(18) shows the voltage magnitude under source disturbance with self-tuned technique in STATCOM.
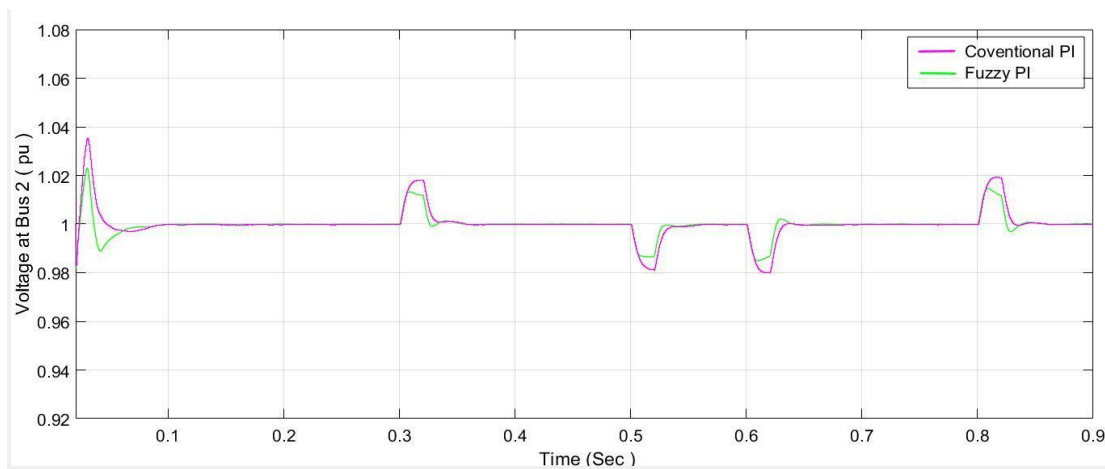
Fig(18): voltage profile enhancement in two control method

Figure (19) shows a zoom in for voltage signal. Obviously, the voltage profile can be enhanced by reducing the over shoot percentage when the magnitude of disturbance has been reduced by 0.005 pu and steady state achieved in less time than conventional PI controller. Figure (20) shows the same instantaneous voltage waveform at disturbance moment take place for phase (a).
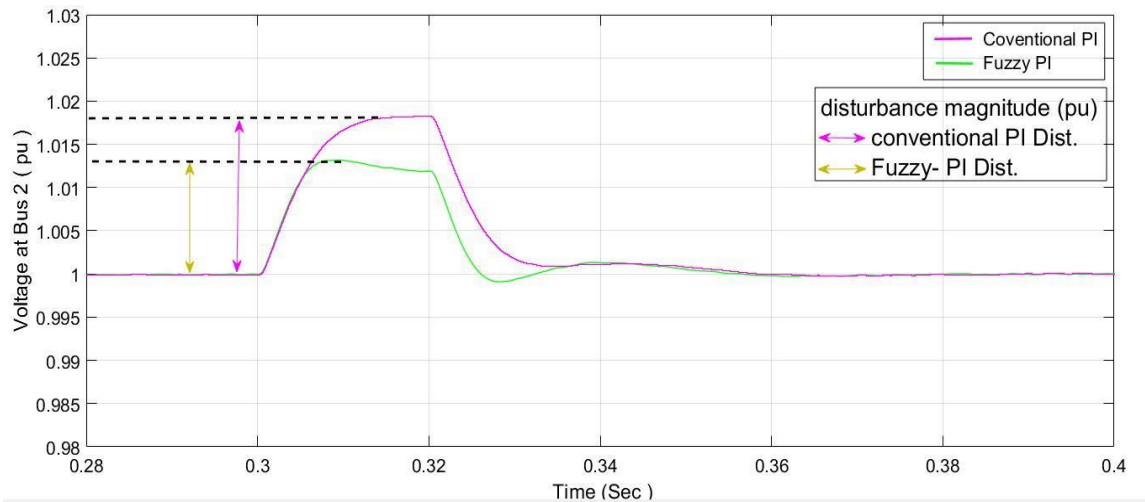
Fig(19): zoom in voltage profile enhancement in two control methods
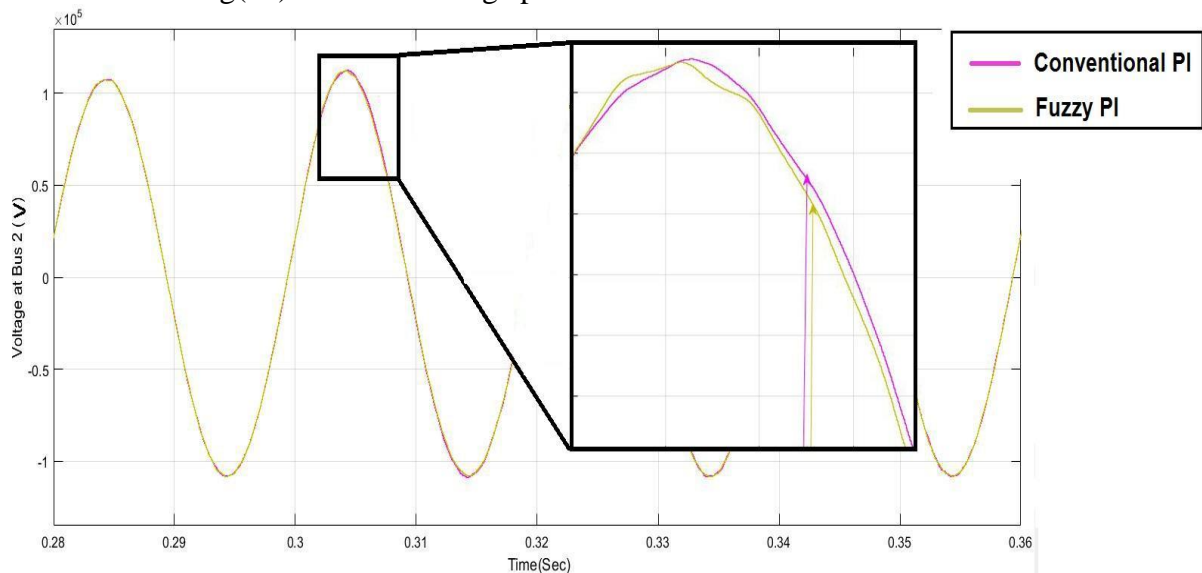
Fig(20): Instantaneous voltage waveform enhancement in two control methods for phase a

In any disturbance occur in this case, the value of ΔKi has been changed frequently depending on the error value as shown in figure (21).

Fig(21): the changing of ΔKi during disturbances occur as given in fig(18)

8.   List of Symbols:

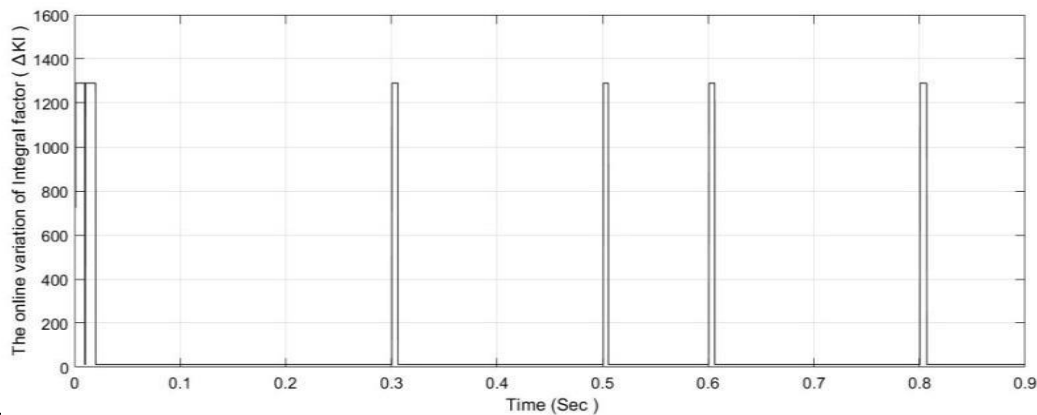| Symbol	Signification of Symbol	SI unit
C	Capacitor	μF
ea, eb,ec	three phase line to neutral output voltage of the STATCOM 's converter	V
ed,eq	Fundamental component of direct and quadrature axis voltage respectively	V
ia, ib, ic	Instantaneous line currents	A
id,iq	Fundamental component of direct and quadrature axis current respectively	A
Ki,Kp	Integral and Proportional gain respectively	
Ls	inductance of the transformer	H
M	Modulation Index	
Rs	Resistance of the transformer	Ω
Rp	Resistance defined the Overall losses in VSC	Ω
|v'|	Magnitude value of the voltage	V
va,vb,vc	Instantaneous line to neutral system voltage	V
vd,vq	Direct and quadrature axis voltage	V
Vdc	Voltage at DC side inverter	V
α	Firing angle of Converter	°
∅	Angle between instantaneous system voltage vector (d-axis) and a-phase axis of abc coordinate	°
ω	Angular velocity	rad/s

9.   Conclusion

FACTS device represented by STATCOM with self-tuned method is very important for improving of voltage profile. The contribution and conclusions can be summarized as follows:

1. The voltage level in the power system proposed at load busbar is improved and made it more stable when STATCOM with conventional PI equipped to the bus 2 under load and source disturbances.
    2. The technique of sinusoidal pulse width modulation (SPWM) has been used to drive the STATCOM. The total harmonic distorsion percent (THD %) achevied at reciveing end for phase voltage and current are 0.4% and 0.54% respectively, while it can be achevied at sending end a values of 0.45% and 0.34% for voltage and current waveforms respectively. These values are within the acceptable IEEE standards.
3.The STATCOM used in this work can be modified and improved to enhance the compensation process. In AC voltage regulator, the conventional PI controller can locate its integral gain (Ki) by using self-tuned method that uses fuzzy logic controller to detect the appropriate gain of integral

term. The results achieved a good response of STATCOM, minimizing over shoot and steady state reached faster than traditional PI controller.

References :

[1].N. G. Hingoranl and L. Gyugyi, 2000, Understanding FACTS, John Wiley & Sons Inc Publication, New York.

[2].S.Varma, 2015, FACTS Devices for Stability Enhancements, International Conference on Green Computing and Interest of Things, pp. 69-74.

[3].Dhiya. A. Al-Nimma, et al. 2011, Voltage Profile Improvements of Mosul City Ring System by STATCOM Reactive Power Control, International Aegean Conference on Electrical Machinesand Power Electronics, pp. 525-530.

[4].Tao Huang, et al. 2009, A Research on Fuzzy Control Method Used in STATCOM, Fuzzy Information and Engineering, Vol. 2, pp. 1119–1129.

[5].V. Ponananthi and B.R. Kumar, 2015, STATCOM with FLC and Pi Controller for a Three-Phase SEIG Feeding Single-Phase Loads, National Conference on Trends in Automotive Parts Systems and Applications, Vol. 4, Iss. 4,pp. 96-103.

[6].Naveen Goel, et al. 2010, Genetically Tuned STATCOM for Voltage Control and Reactive Power Compensation, International Journal of Computer Theory and Engineering, Vol. 2, No. 3, pp. 345-351.

[7].J. Vanishree and V. Ramesh, 2014, Voltage Profile Improvement in Power Systems – A Review, International Conference on Advances in Electrical Engineering.

[8].J. Dixon, L. Moran et al. 2005, Reactive Power Compensation Technologies: State of the Art Review, Proceedings of the IEEE, Vol. 93, No.12, pp. 2144 - 2164.

[9].Zhengping Xi, 2013, Control Strategies of STATCOM during System Faults", Ph.D thesis, North Carolina State University.

[10].Phinit Srithom, 2009, Control of a STATCOM with supercapacitor energy storage, Ph.D thesis, University of Nottingham.

[11].D.Masand, S. Jain and G. Agnihotri, 2006, Control Algorithms for Distribution Static Compensator, IEEE International Symposium on Industrial Electronics, pp. 1830-1834.

[12].D.Ganeshkumar, 2014, Virtual instrument system based arrangement for monitoring analysis and control of vibrations in rotating machinery, M.Sc Thesis, University of Anna.

[13].IEEE Std 519-1992, IEEE Recommended Practices and Requirements for Harmonic Control in Electric Power Systems.

Appendix – A

Parameters) :Base – 5MVA) , 5 MVAR STATCOM .

Converter parameters: two brides of IGBT – 12-pulse two level; nominal AC voltage =132 KV; DC link voltage = 2.4 KV; Capacitors (C) = 0.02 F.
Carrier frequency of SPWM= 1400 Hz.

Converter Transformer :Each one of 3-winding Transformer Rating: (5/3) MVA, 50Hz, 132 KV/1.25 KV, 3% (X(

PI-controller Gains: AC Voltage Controller: $K_{P1} = 0.5$, $K_{I1} = 2500$. DC Voltage Balancer: $K_{P2} = 0.001$, $K_{I2} = 0.15$. Decoupled Current Controller: d-axis controller: $K_{P3} = 0.8$, $K_{I3} = 1$; q-axis controller: $K_{P4} = 0.8$, $K_{I4} = 1$.

Thevenin's Equivalent Voltage Source: Nominal Voltage: 11kV; Source Resistance and inductance: R=0.121Ω, L=3.85mH, frequency: 50Hz; Short circuit level: 100 MVA

Step –up power transformer rating**:** Nominal power: 100MVA, 11KV/132KV, 50Hz, R_{pu}=0.002 pu, X_{pu}= 0.008 pu.

Power Quality Improvement of High Voltage DC Link using Modified Shunt Active Power Filter

Rakan Khalil Antar
Technical Engineering College
Northern Technical University
Mosul, Iraq
rakanpe@yahoo.com

Basil Mohammed Saied
Electrical Engineering Dept.
Mosul University
Mosul, Iraq
basilms2005@yahoo.com

Rafid Ahmed Khalil
Mechatronics Engineering Dept.
Mosul University
Mosul, Iraq
rafidamori@yahoo.com

Abstract: **A new control strategy for active power filters is proposed, modeled and implemented in order to improve the power quality of a line commutated converter High voltage DC link. The ability of reactive power and harmonics reductions are generally met by using passive and active power filters. In this paper, modified active power filter with a modified harmonics pulse width modulation algorithm is used to minimize the source harmonics and force the AC supply current to be in the same phase with AC voltage source at both sending and receiving sides of a line commutated converter high voltage DC link. Therefore, it is considered as power factor corrector and harmonics eliminator with random variations in the load current. The modified harmonics pulse width modulation algorithm is applicable for active power filter based on a three-phase five-level and seven-level cascaded H-bridge voltage source inverter. Simulation results show that the suggested modified multilevel active power filters improve total harmonics distortion of both voltage and current with almost unity effective power factor at both AC sides of high voltage DC link. Therefore, modified active power filter is an effective tool for power quality improvement and preferable for line commutated converter high voltage DC link at different load conditions.**

Keywords- Six-pulse line commutated converter HVDC, Power quality improvement, modified shunt active power filter, modified harmonics pulse width modulation, multilevel inverter.

1. INTRODUCTION

AC to DC converters, depending on thyristors, provide controllable active power in the rectification and inversion modes. But they consume reactive power and distort the supply current which affect on the power quality of the AC system. This effect can be treated by using passive and/or active power filters to reduce harmonics distortion of AC supply currents. High-voltage DC (HVDC) transmission system transmits a large amount of power over long distances [1]. HVDC converters produce harmonics in the AC power systems, which should be minimized by using power filters. Passive power filter can be used to reduce known harmonic components. While for unknown harmonic components, Active power filter (APF) is better in filtering performance than passive power filter [2].

The shunt APF (SAPF) is used to compensate harmonics current due to nonlinear system elements, improve effective input power factor and stabilize the three phase currents [3]. So, it acts as a controlled voltage source which forces the system line currents to become almost sinusoidal. This needs a complex regulation and control system [4]. The most control algorithms of three-phase shunt active power filters are based on instantaneous PQ theory, synchronous detection method and

using multilevel inverters. In [5, 6], the $I_1.\cos(\Phi)$ algorithm forces the supply current to be equal to the magnitude of the real component of fundamental load current, which is in same phase with the main sinusoidal supply voltage. This technique is applicable for three-phase voltage source inverters. In [7], the $\hat{I}_1.\cos(\Phi)$ algorithm is used with a 7-level shunt active filter as a controller based on multicarrier phase disposition pulse width modulation technique.

In this paper, for comparison of SAPF, five and seven level cascade H-bridge pulse width modulation voltage source inverters are investigated. The aim is to use modified SAPF (MSAPF) as harmonics injector and power factor corrector based on modified harmonics pulse width modulation (MHPWM) algorithm and therefore improving the power quality of 6-pulse line-commutated converter HVDC (LCC-HVDC) link as illustrated in Figure 1.
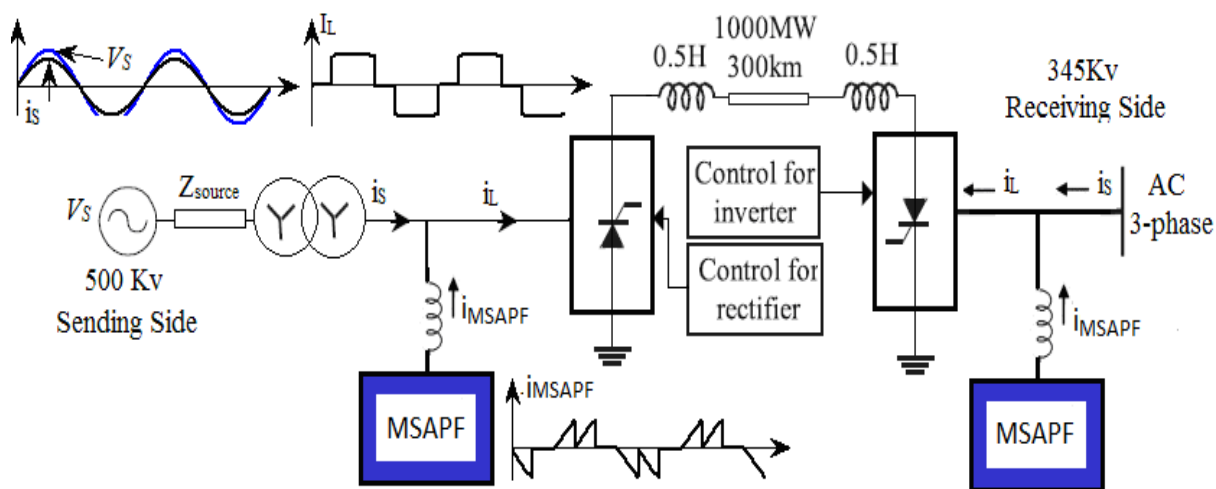
Fig(1): Three-phase 6-pulse LCC-HVDC link with the MSAPF circuit

2. HVDC LINK MODEL

2.1. HVDC Converter

In this paper, the 6-pulse LCC-HVDC link is used as shown in Figure 1. Converters of the LCC-HVDC link produce harmonics current at the AC sides and consume reactive power. In order to reduce the AC line current harmonics and correct effective input power factor, a MSAPF is used to improve the power quality at both sending and receiving sides. As a result, the shape of line current becomes almost sinusoidal which improves the performance of AC mains with keeping the DC link current smooth.

2.2.Filtering Principle

The principle operation of the MSAPF is to supply distortion current and reactive power components to the HVDC system to make the AC grid supplying only real power. Thus, the power distribution system on each side sees the nonlinear load with the MSAPF as a dynamic resistor. The power circuit of the MSAPF shown in Figure 2 is built depending on 5-level cascaded H-bridge voltage source inverter (5LCHBVSI) and 7-level cascaded H-bridge voltage source inverter (7LCHBVSI), respectively.

The MHPWM algorithm, which is suggested and used by [8, 9], computes the desired reference three phase AC currents ($i_{sa\text{-}ref}$, $i_{sb\text{-}ref}$, $i_{sc\text{-}ref}$) from the product of the real part of the fundamental load currents ($I_{La1(real)}$, $I_{Lb1(real)}$, $I_{Lc1(real)}$) in-phase with the corresponding AC voltages as shown in Figure 3. The compensation reference currents are formed as the difference between the actual load currents (i_{La}, i_{Lb}, i_{Lc}) and the desired reference AC supply currents. The compensation reference currents are compared with the MSAPF currents ($i_{MSAPF\text{-}a}$, $i_{MSAPF\text{-}b}$, $i_{MSAPF\text{-}c}$). The result signals, harmonics error signal (*HES*), are used as modulated reference signals which are compared with phase shifted multi-carrier signals to produce PWM signals and drive the IGBT's of the MSAPF.
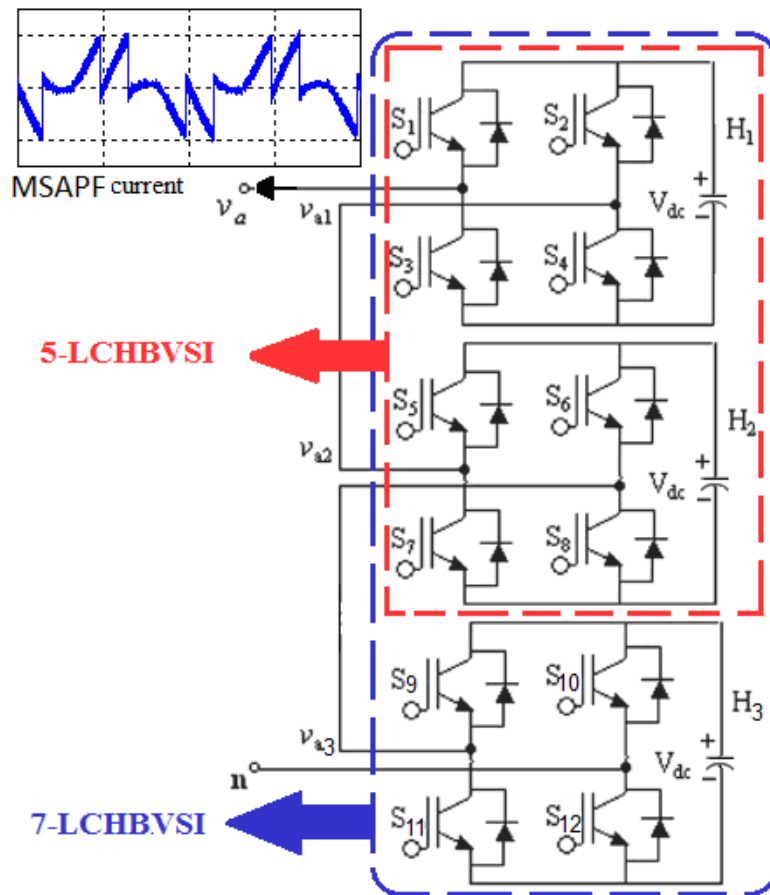
Fig(2): MSAPF configuration based on 5-level or 7-level cascaded H-bridge inverter per phase.
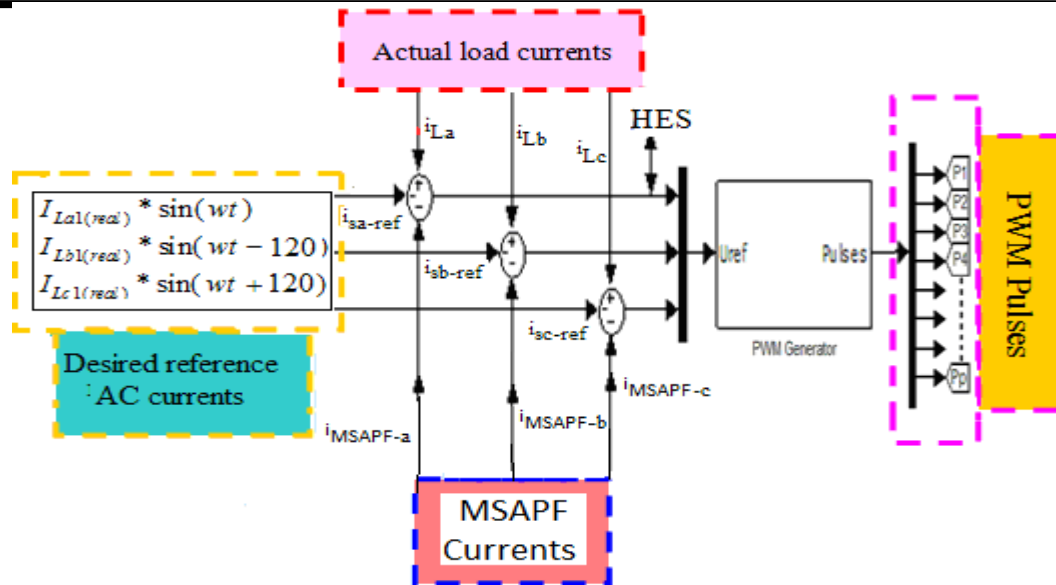
Fig(3): Control circuit of the MSAPF.

3. SIMULATION RESULTS

The 6-pulse LCC-HVDC link is modeled by MATLAB/SIMULINK/PSB as a 500kV-1000MW DC link to connect two AC systems, 500KV and 345kV, as shown in Figure 4. The DC sides of the HVDC converters have been modeled with 300Km transmission line and 0.5H smoothing reactor. The MSAPF is connected to AC system through coupling reactor (5mH). A DC capacitor (200μF per cell) is connected at the DC side of the MSAPF to store energy at the DC bus. The designed MSAPF is simulated to show its steady state and dynamic capability with the HVDC system.

Figure 5, Figure 6 and Figure 7 show the waveforms of the supply phase voltage (v_{sa}) and current (i_{sa}) at secondary side of the transformers at DC power flow (P_{dc}) equal to 0.7pu (700MW) without and with 5LCHBVSI and 7LCHBVSI MSAPF, respectively. The phase voltage and current at both sending and receiving sides are in phase with each other after connecting the MSAPF circuits. These figures show that the MSAPF gives acceptable THD and PF which makes the supply voltage and current in phase and almost free of harmonics. The distortion in the voltage and current waveforms is due to switching frequency of the inverter which can be eliminated simply by using a simple high pass filter as shown in Figure 8. The THD of the supply current waveform after connecting high pass filter with the 5LCHBVSI MSAPF is reduced from 1.27% to 0.8%. Figure 9, Figure 10 and Figure 11 illustrate the waveform of power factor, THD, and power utilization factor without and with the MSAPF at sending and receiving sides respectively. These results confirm that power factor stay at unity and THD improved at both sending and receiving sides. The MSAPF draws a small amount of the real power depending on the phase angle between the AC voltage and the MSAPF voltage which affect on the utilization factor of the system.
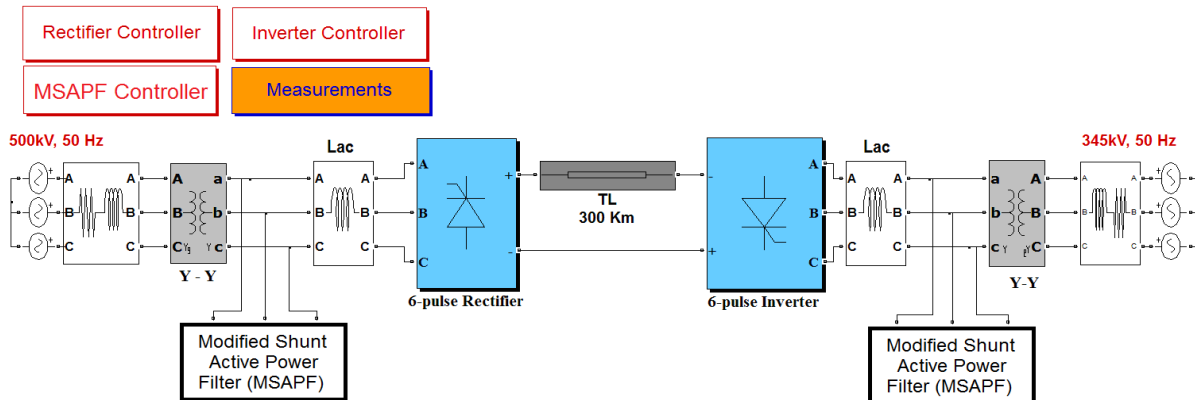
Fig(4): System overview of the 6-pulse LCC-HVDC system with the MSAPF at both sending and receiving sides.
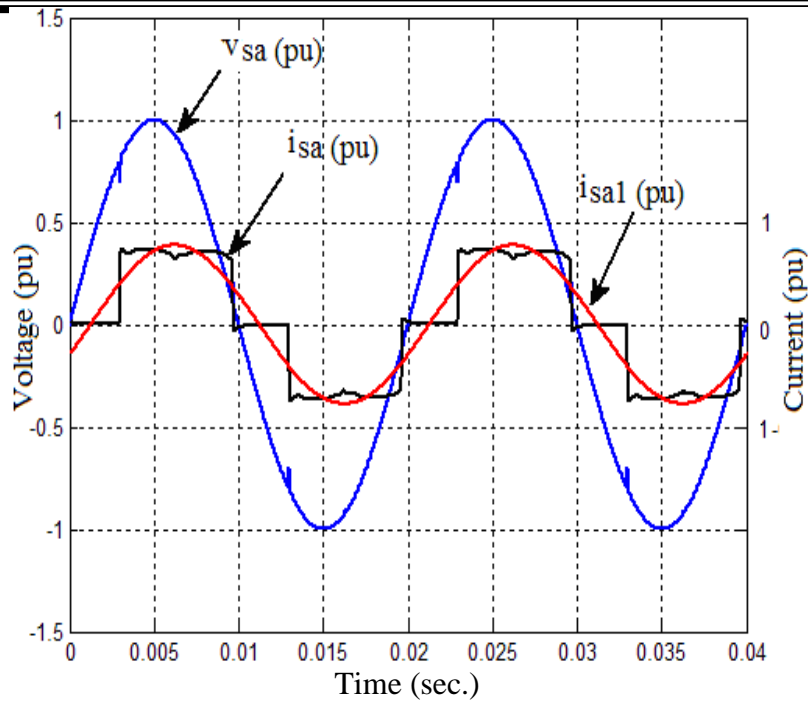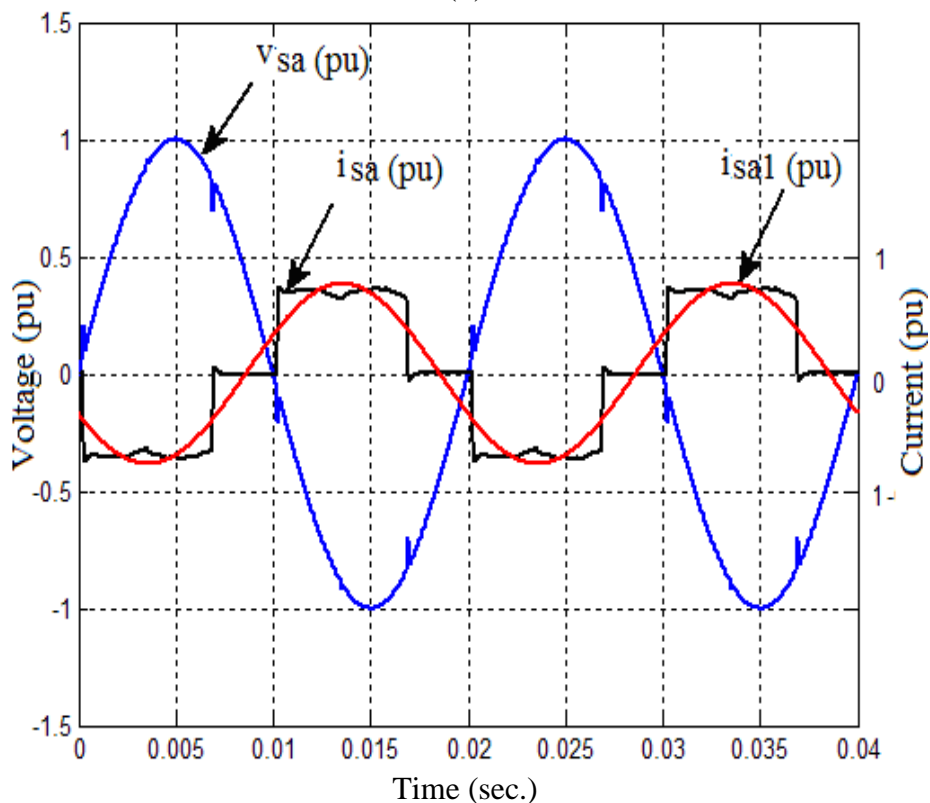
Fig(5): Phase voltage and current of the 6-pulse LCC-HVDC link without filters (P_{dc}=0.7pu) at (a) sending and (b) receiving sides
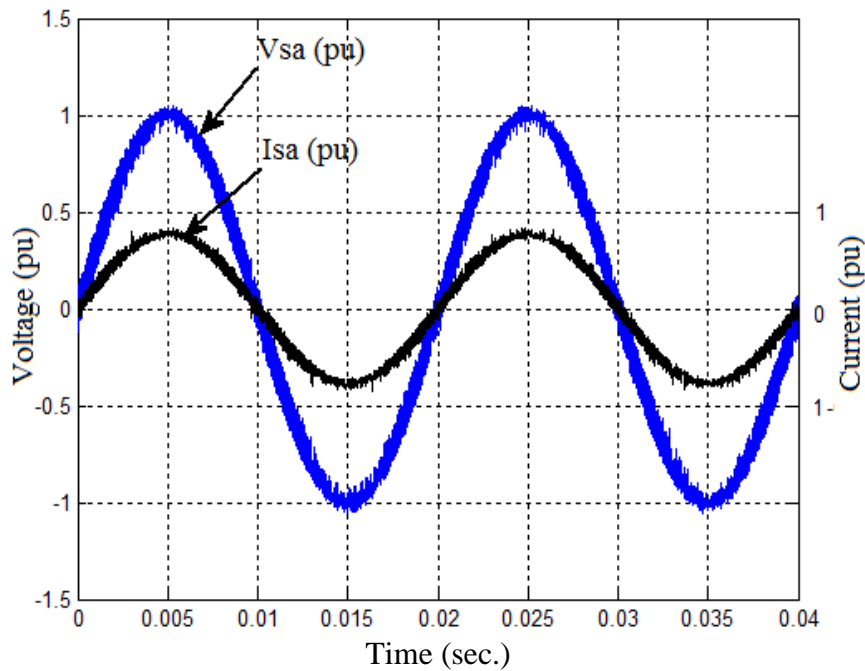
(a)
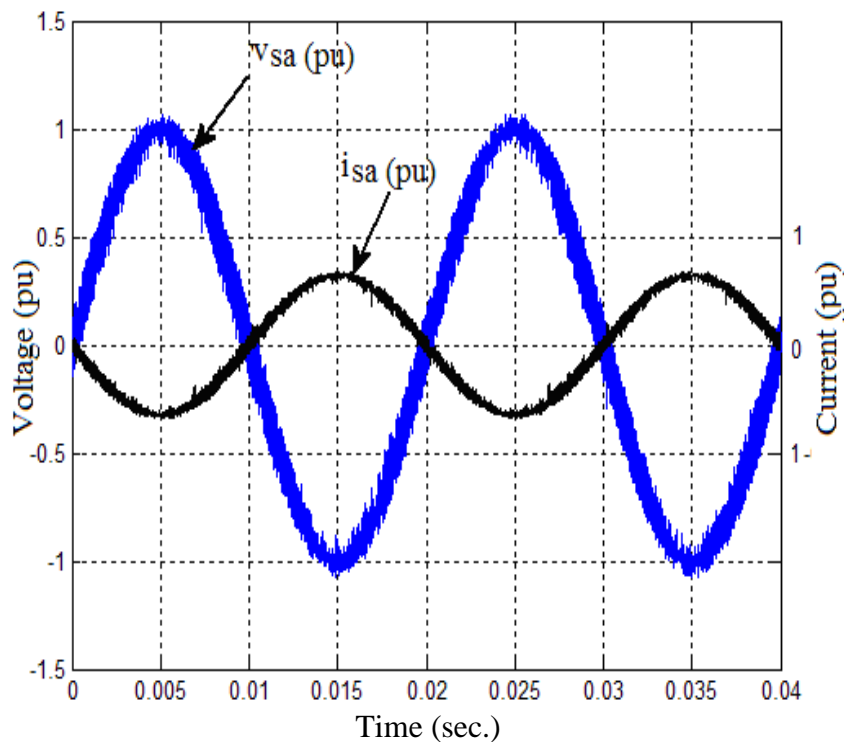
(b)

Fig(6): Phase voltage and current of the 6-pulse LCC-HVDC link with the   5-LCHBVSI MSAPF (P_{dc}=0.7pu) at (a) sending and (b) receiving sides
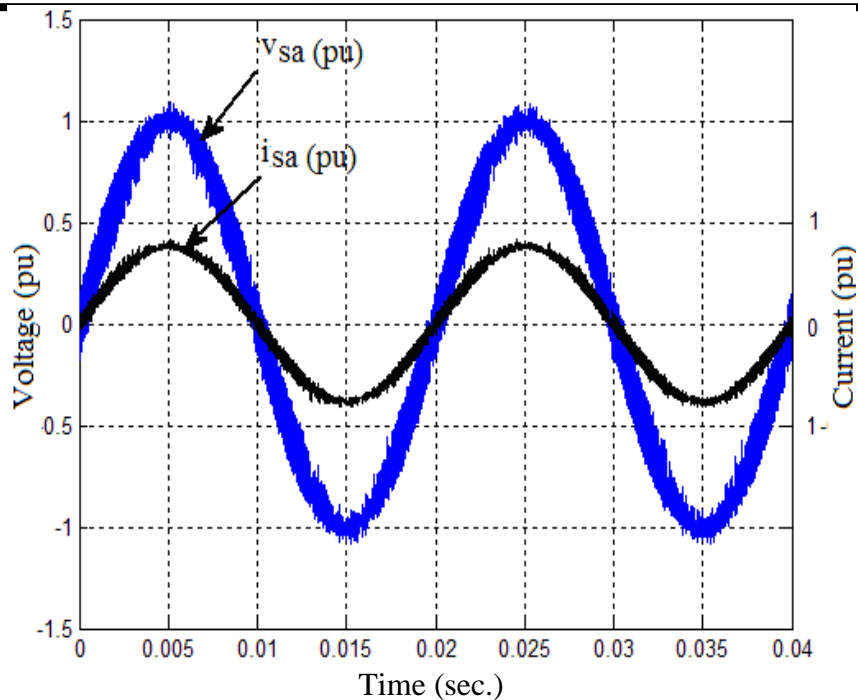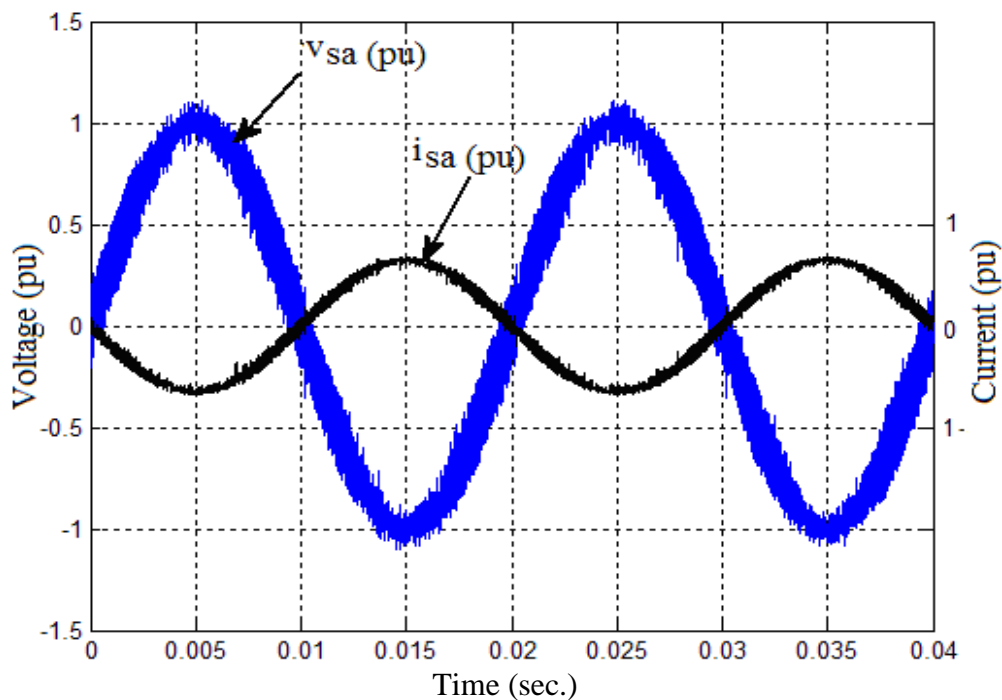
Fig(7): Phase voltage and current of the 6-pulse LCC-HVDC link with the   7-LCGBVSI MSAPF (P_{dc}=0.7pu) at (a) sending and (b) receiving side
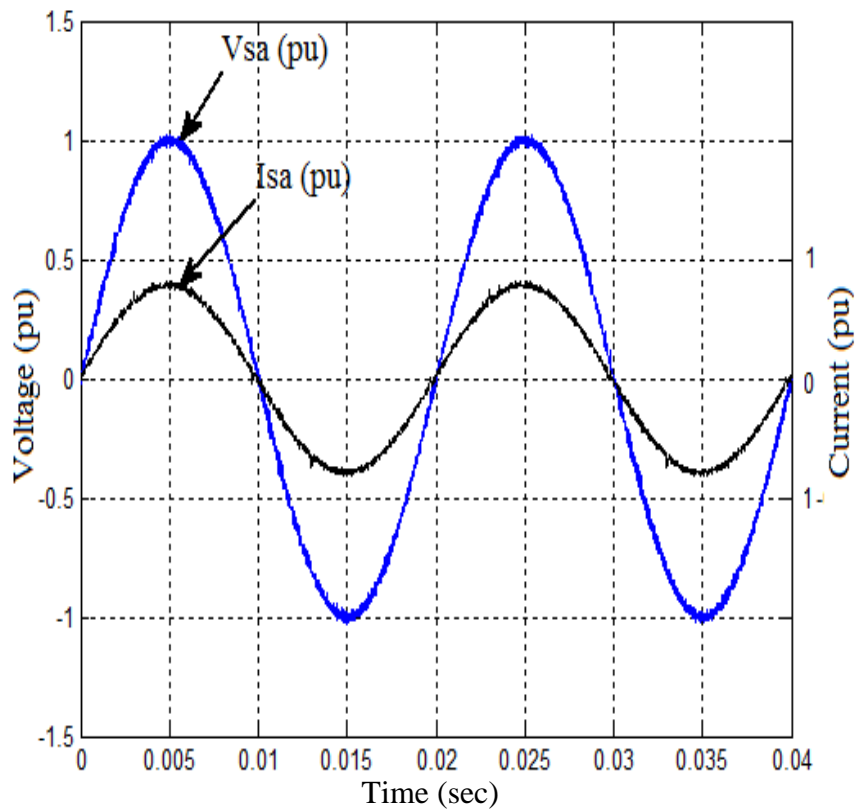
(a) 5-level MSAPF
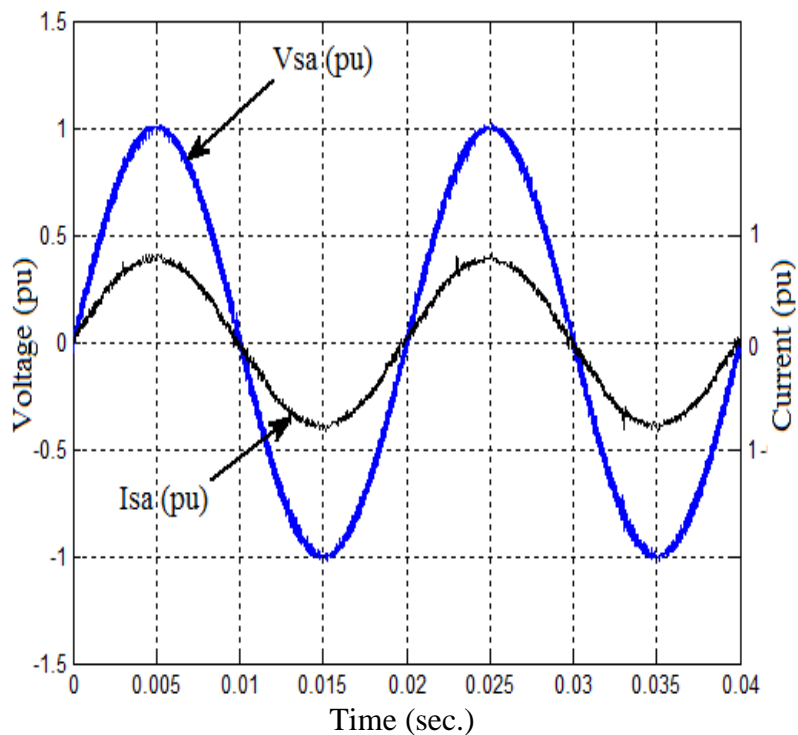
(b) 7-level MSAPF

Fig(8): Phase voltage and current of the 6-pulse LCC-HVDC system (P_{dc}=0.7pu) at sending side after connecting a small high pass filter
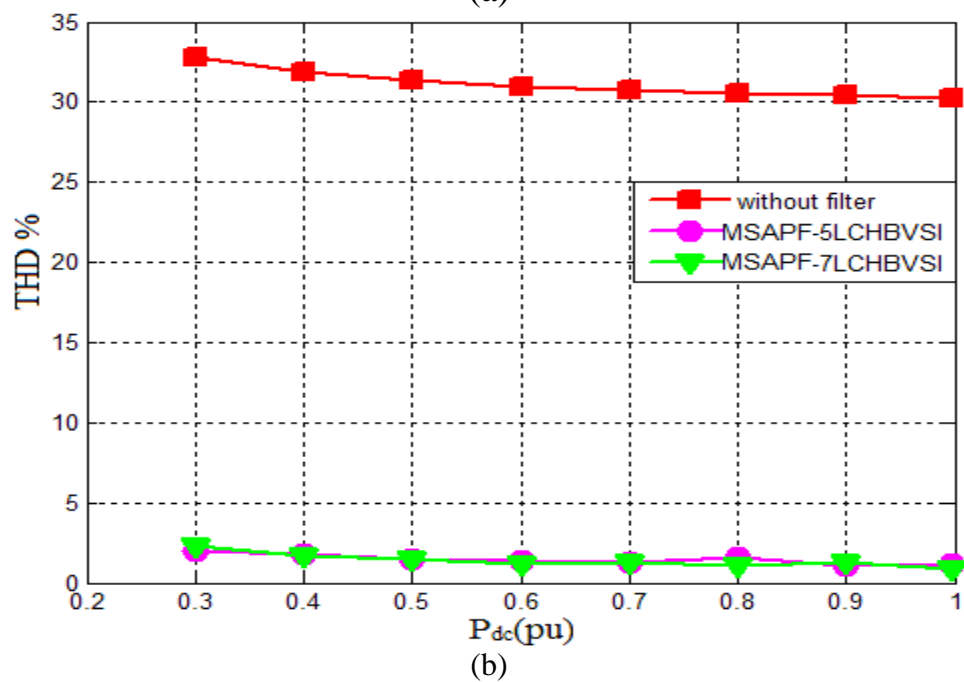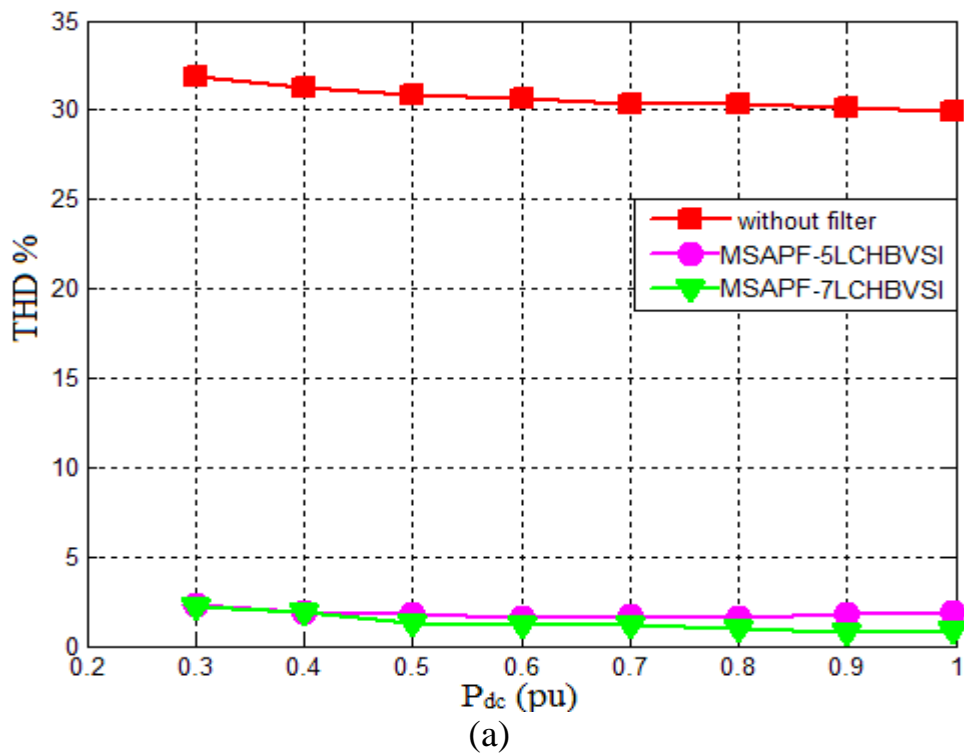
Fig(9): THD of the AC supply current of the 6-pulse LCC-HVDC system without and with MSAPF at (a) sending and (b) receiving sides.
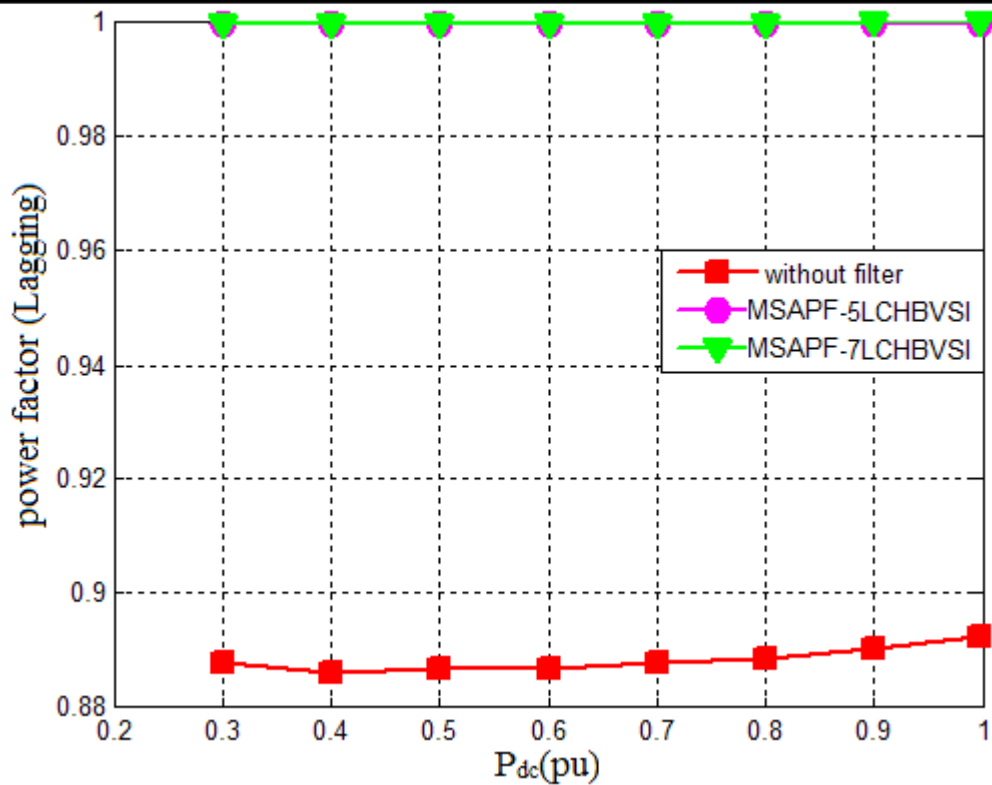
(a)
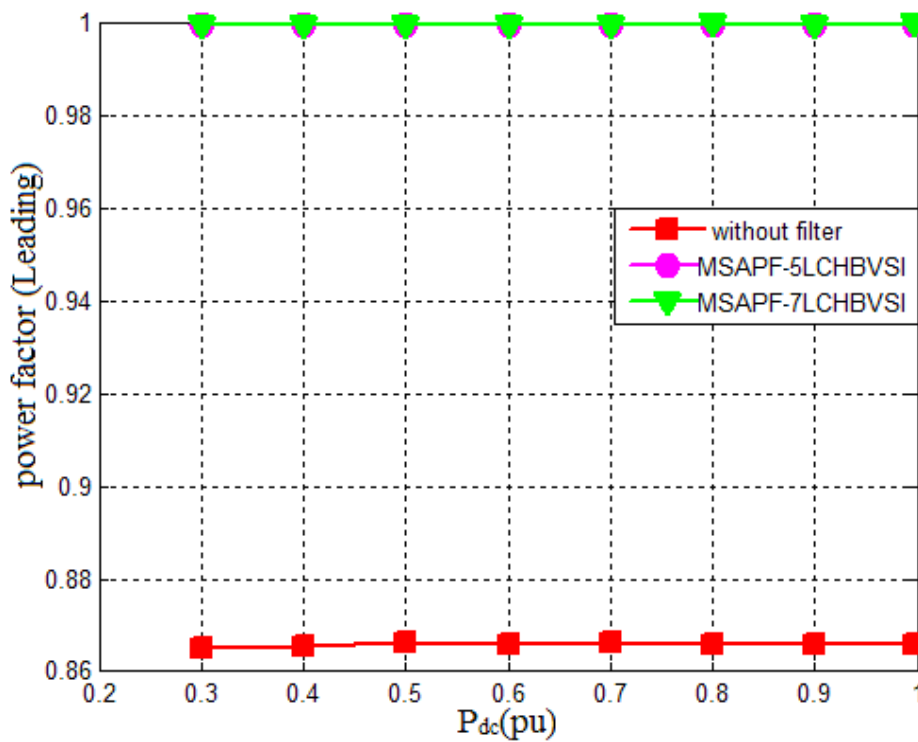
(b)

Fig(10): Simulation results of the effective input PF without and with the MSAPF at (a) sending and (b) receiving sides.
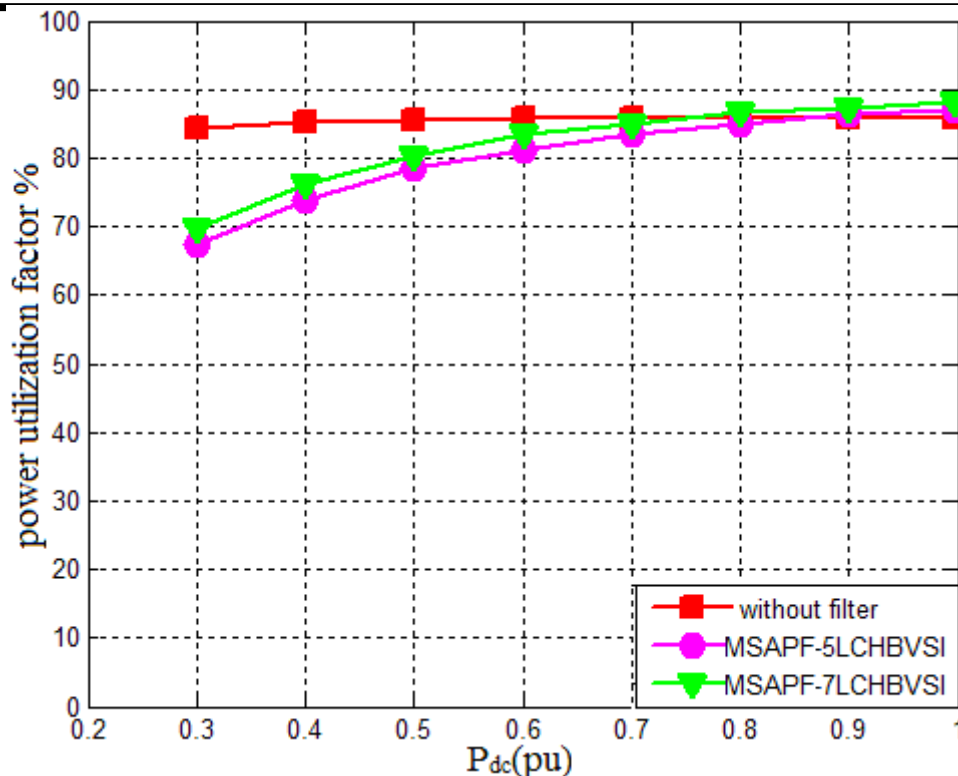
Fig(11): Power utilization factor of the 6-pulse LCC-HVDC link without and with filters.

4.CONCLUSIONS

The 6-pulse LCC-HVDC link model with five and seven level cascaded H-bridge inverters as a MSAPF at both sending and receiving sides have been analyzed, implemented and simulated. The MHPWM algorithm has been suggested to drive the suggested MSAPF. The simulation results proved that the designed active filter is applicable, reliable and effective for different operating conditions of the 6-pulse LCC-HVDC link. The designed filter with 5-level and 7-level give almost same results. These indicate that 5-level can be considered as a suitable type if the building cost and less complexity is taken into account. While for higher ratings power switching requirement 7-level is more convenient to be used. In both cases reliable power quality improvements have been achieved

5.REFERENCES

[1]-Mohan M, Singh B, Panigrahi K., 2010. Dynamic dead angle control of three-level voltage source converter based HVDC system. In: IEEE Indian International Conference on Power Electronics; 2010 (IICPE2010): IEEE. pp: 1-6.

[2]-Leng S, Liu W, Chung I, Cartes D., 2009. Active power filter for three-phase current harmonic cancellation and reactive power compensation. In: American Control Conference AACC. pp: 2140-2147.

[3]-Mihaela P, Alexandru B, Vlad S, Alexandra P., 2011. High Performance Shunt Active Power Filter. In: 7th international Symposium on Advanced Topics in Electrical Engineering (ATEE), Bucharest, Romania.

[4]-Luo L, Li Y, Xu J, Li J, Hu B, Liu F., 2008. A new converter transformer and a corresponding inductive filtering method for HVDC transmission system. IEEE Transactions on Power Delivery; Vol. 23; No. 3, pp: 1426-1431.

[5]-Charles.S, Bhuvaneswari G., 2010. Comparison of three phase shunt active power filter algorithms. International Journal of Computer and Electrical Engineering; Vol. 2; No. 1, pp: 175-180 .

[6]-Bhuvaneswari G, Nair G., 2008. Design, simulation, and analogue circuit implementation of a three-phase shunt active filter using the Icosϕ algorithm. IEEE Transactions on power delivery, Vol. 23, Issue 2; IEEE, pp:1222-1235

[7]-Rani S, Porkumaran K., 2010. Multilevel shunt active filter based on sinusoidal subtraction methods under different load conditions. International Conference on Computational Technologies in Electrical and Electronics Engineering (SIBIRCON), IEEE Region 8, Irkutsk Listvyanka, Russia.

[8]-Rakan Kh. Antar, Basil M. Saied, Rafid A. Khalil, 2012a. Modified Active Power Filter Based on Five-level Cascade H-Bridge PWM Voltage Source Inverter. In: 9th International Conference on Electronics, Computer and Computation (ICECCO), Turgut Ozel University, Ankara, Turkey.

[9]-Rakan Kh. Antar, Basil M. Saied, Rafid A. Khalil, 2012b. Using Seven-Level Cascade H-Bridge Inverter with HVDC System to Improve Power Quality, The 1st National Conference For Engineering Sciences, FNCES ,12'University of Al-Nahrain, Baghdad, Iraq.

تأثير الظروف المناخية على اداء التوربين الهوائي في مدينة كركوك

الدكتور سعاد حسن دانوك   السيد كمال جلال توفيق   اسراء عادل منصور

استاذ مساعد   استاذ مساعد   طالبة ماجستير

الجامعة التقنية الشمالية/الكلية التقنية كركوك

esraadil10@gmail.com   Kamal_19572003@yahoo.com   talebshebab@yahoo.com

الخلاصة:

يساهم هذا البحث في اعطاء تصور عن استخدام توربينات الرياح كمصدر بديل لمصادر الطاقة التقليدية , حيث تمت دراسة الية تحويل الطاقة الحركية الموجودة في الرياح الى طاقة كهربائية بالإضافة الى دراسة تأثير الظروف المناخية على اداء توربينات الرياح مثل درجة الحرارة , الرطوبة , وسرعة الرياح باستخدام برنامج التحليل الهندسي (الماتلاب) و مقارنته مع النتائج العملية التي تم التوصل اليها باستخدام توربين صغير من نوع FD1.5-400W حيث تبين بأن الزيادة في سرعة الرياح مع انخفاض درجات الحرارة والرطوبة يؤدي الى زيادة الاداء.

النقاط الدالة : التوربين الهوائي , الطاقة الحركية , سرعة الرياح , اداء التوربين , الظروف المناخية

Impact of environmental condition on the wind turbine performance

Dr.Suad Hassan Danook   **Mr.Kamal Jalal Tawfeeq**   **Esraa Adil Mansoor**

Assist Professor   *Assist Professor*   *M.Sc student*

Northern Technical University / Kirkuk Technical College

talebshebab@yahoo.com   Kamal_19572003@yahoo.com   esraadil10@gmail.com

Abstract:

This paper incorporates the utilization of the wind energy system as an alternative source for Traditional source of energy, where it has been studied convert the kinetic energy in the wind to electric energy and the impact of environmental condition like, temperature humidity and wind speed on turbines performance and analysis using MATLAB simulation. In addition the results were compared with the results obtained from the operation of the experimental turbine in the department and it turned out higher congruence results.

Key words: wind turbine, kinetic energy, wind speed, environmental condition, turbine performance.

1.المقدمة :-

يعتبر الهدف الاساسي من دراسة تأثير الظروف المناخية على الطاقة الميكانيكة التي يعقبها تحولها الى طاقة كهربائية لاظهار مدى حساسية التوربين الهوائي الى هذه المتغيرات في ظل سرع الرياح المختلفة , وتكمن اهمية هذا النوع من البيانات في الاختبارات العملية اللازمة لتركيب محطات الرياح بالاضافة الى مقارنة الربح الاقتصادي لنصب محطة الرياح مع التكاليف والخسائر ويعد استخدام بيئة الماتلاب للمحاكاة والحسابات الخاصة لتحسين نظم الطاقة الصغيرة الاكثر شيوعا في نمذجة ومحاكاة محطات الرياح في السنوات الاخيرة   (Florin Iov.et al 2004).

فقد استخدمت طاقة الرياح قديما في تسير القوارب الشراعية للنقل وذلك في عام 500 قبل الميلاد حيث استعملت الطاحونة الهوائية لسقي المحاصيل الزراعية عن طريق ضخ المياه من الجداول والابار في بلاد فارس 200 قبل الميلاد ولم تستخدم طاقة الرياح في

الانتاج الكهربائي الا في غضون عام 1888 في كليفلاند اوهايو بنموذج اولي ذو قدرة انتاجية ضعيفة بينما في عام 1891 تم استعمال الطاحونة الهوائية في اوربا لإنتاج الكهرباء باستخدام شفرات تم اختبارها بمرور الزمن من شأنها ان تدور بشكل اسرع وبالتالي توليد طاقة اكثر , ومع حلول الحرب العالمية الاولى انتشرت هذه الوحدات بشكل اكبر اذ غطت معظم انحاء الدنمارك(Ahmad .Y. Hassan.1987).

تعد الطاقة المتجددة ومن ضمنها الشمس , الرياح , المد والجزر, والطاقة الجوفية الارضية من الطاقات المستدامة وذلك لكونها قابلة للتجديد وصديقة للبيئة وتعتبر في الوقت الحالي من المصادر المهمة للطاقة بسبب نضوب الوقود الاحفوري وتزايد مشاكل التلوث (2009 Balasubramaniam Babypriya) لذلك طورت العديد من البحوث في هذا المجال فقد قدم الباحث Omar. B.et al 2012)) دراسة ذكرَ فيها ان استخدام طاقة الرياح لأغراض توليد الطاقة الكهربائية تحتل حصة كبيرة من الانتاج العالمي للكهرباء وهي في حالة تزايد مستمر لذا يجب الاخذ بنظر الاعتبار عند تصنيع وتركيب التوربينات الهوائية العديد من العوامل التي من اهمها (صلاحية التوربين للمنطقة, كثافة الهواء , سرعة الرياح , معامل القدرة , زاوية الميلان , سرعة طرف النصل.

اما الباحث(Mohammed G Khalfallah.2007) فقد استخدام مختلف الطرق لتحسين اداء قدرة توربينات الرياح بشكل تجريبي ونظري في منطقة الغردقة بمصر وذلك باستخدام توربينة من نوع (Nordtank300KW) وقد استنتج بأنه عند تصميم التوربينات الهوائية يجب ان يؤخذ بنظر الاعتبار كيفية الوصول الى اعظم اداء لمنحني القدرة بالاضافة الى الموقع المناسب لنصب المحطات الهوائية

2. المنهجية:-

2-1 نمذجة عمل التوربين الهوائي

2-1-1 سرعة طرف النصل

يبين الشكل (1-1) القدرة المستخرجة من الرياح القادرة على تدوير شفرات التوربين الهوائي, حيث يعتبر حساب سرعة طرف النصل من العوامل الرئيسة في تصميم الشفرات الخاصة بالتوربين الهوائي اذ تعرف على انها (النسبة بين سرعة اطراف شفرات العنفة الهوائية الى سرعة الرياح) (TSR) وكما مبين في المعادلة ادناه (2008.Shackleton, Jonathan)
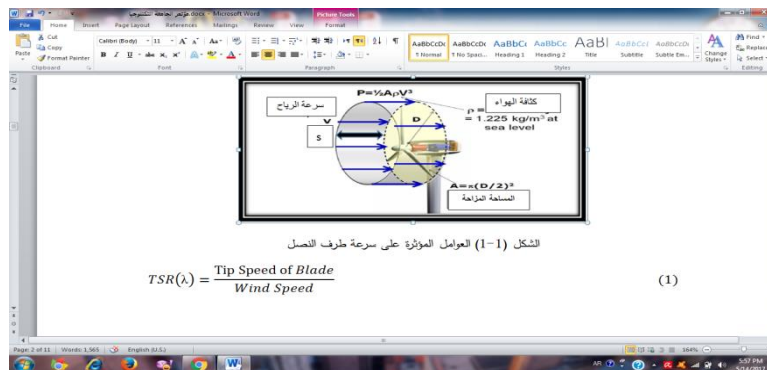
الشكل (1): العوامل المؤثرة على سرعة طرف النصل

$$TSR(\lambda) = \frac{Tip\ Speed\ of\ Blade}{Wind\ Speed} \quad \dots\dots\dots\dots(1)$$

في حالة دوران شفرات العنفة الهوائية بسرعة بطيئة جدا فان معظم الرياح ستمر بشكل مستقيم عبر الثغرات ما بين الشفرات والتي بدورها تؤدي الى انعدام القدرة اما في حالة الدوران بسرع عالية جدا فأن الشفرات ستتشوه وتمثل حاجزا صلبا للرياح مما يؤدي الى اضطراب حركتها (Luke Hagedorn.2011) لذلك يجب مراعاه الزمن اللازم للشفرات لا كمال الدورة الواحدة ومن ثم حساب سرعة طرف النصل (المسافة مقسومة على الزمن اللازم للشفرة لتقطع محيط الدائرة التي ترسمها الريشة) $(A\pi r^2)$ حسب المعادلة التالية

$$V=2\pi r\ T(time) \qquad \ldots\ldots\ldots\ldots\ldots (2)$$

حيث تمثل

V : سرعة طرف النصل (m/s)

πr2: المسافة (m)

T : الزمن اللازم لقطع دورة واحدة كاملة (sec)

عندما تكون سرعة طرف النصل أكبر من واحد، فان ذلك يشير الى الحاجة لزيادة ارتفاع البرج لجعل عجلة التوربينات تدور بسرعة مطلوبة لتوليد القدرة، وإذا كانت أقل من واحد، فهذا يعني، انه توجد مقاومة كبيرة ضد الهواء مما يشكل عقبة في طريق عجلة الدوران (Charles F. Brush.2007) ولمعرفة مقدار القيمة المثالية لسرعة طرف النصل للحصول على اعلى قيمة للقدرة الناتجة يتم استخدام هذه الصيغة التالية التي تم اثبات صحتها تجريبيا (Warnes, Kathy.2013)

$$\lambda(max\ power)=4\pi n \qquad \ldots\ldots\ldots\ldots\ldots (3)$$

حيث تمثل n. عدد الشفرات

الجدول رقم (1-1) يمثل بعض النتائج التجريبية

نسبة TSR المثالية	عدد الشفرات
حوالي 6	2
حوالي4-5	3
حوالي 3	4
حوالي 2	6

2-1-2 : معامل بيتز ومعامل القدرة

قام العالم الالماني البرت بيتز (Albert Betz) في عام 1919 بالتوصل الى قانون يجمع عددا من المبادئ التي تشمل (حفظ الكتلة وحفظ الطاقة لجريان الهواء عبر قرص) ينص القانون على انه لا يمكن لأي توربين هوائي تحويل اكثر من 59,3% من الطاقة الحركية للرياح الى طاقة ميكانيكية تعرف هذه القيمة (بمعامل بيتز) . حيث ان (اقصى كفاءة للطاقة المستخرجة من اي توربين هوائي من الناحية النظرية تكون قيمتها(0,59) في الحالة المثالية, بينما من الناحية العملية تكون ضمن الحدود (45-50)%

فرضيات الجريان:

- الجريان غير انضغاطي (عدم وجود انتقال للحرارة و كثافة ثابتة للهواء)
- اجزاء التوربين في حالة مثالية تقوم بتحويل طاقة الرياح الى طاقة ميكانيكية دون وجود خسائر بسبب الاحتكاك او التصميم الهندسي
- تدفق الهواء محوري ومركز باتجاه المروحة الهوائية وانه غير قابل للتشتت

ان الطاقة الميكانيكية التي يقابلها محول على شكل قرص ناتج من تدفق الهواء عبر التوربينة ينتج عنه فرق طاقة لتيار الهواء قبل الدخول وبعد الدخول(Erich Hau.2005) كما مبين بالشكل (1-2)
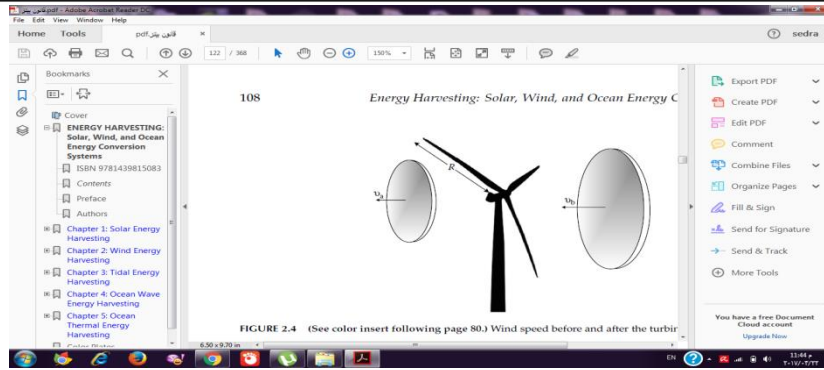
الشكل (2-1) فرق التيار الهوائي بين الدخول والخروج(Alroza Khaligh and Omar G. Onar 2009).

$$E = \frac{1}{2}\rho A_1 v_1^3 - \frac{1}{2}\rho A_2 v_2^3 = \frac{1}{2}\rho(A_1 v_1^3 - A_2 v_2^3) \quad (w) \quad \ldots\ldots\ldots\ (4)$$

وبتطبيق معادلة حفظ الكتلة

$$\rho A_1 v_1 = \rho A_2 v_2 \quad (kgs) \quad \ldots\ldots\ldots\ (5)$$

لذلك تكون

$$E = \frac{1}{2}\rho v_1 A_1 (v_1^2 - v_2^2)$$

او

$$E = \frac{1}{2}m(v_1^2 - v_2^2)$$

فأن متوسط السرعة للتوربين (العضو الدوار) هي

$$v = \frac{1}{2}(v_1 + v_2) \quad \ldots\ldots\ldots\ (6)$$

$$E_{kin} = \frac{1}{2}*\rho*A*[v_1 + v_2^2]*[v_1^2 - v_2^2]$$
$$= \frac{1}{4}\rho*A*[v_1^3 - v_2^3 - v_1*v_2 + v_1^2*v_2]$$
$$= \frac{1}{4}\rho*A*v_1^3*[1 - (\frac{v_2}{v_1})^3 - (\frac{v_2}{v_1})^2 + (\frac{v_2}{v_1})]$$

ولمعرفة النقطة التي تتحقق عندها القدرة العظمى نشتق علاقة القدرة بالنسبة لـ (v_2) ونساويها للصفر

$$\frac{dE_{kin}}{dv_2} = \frac{1}{4}*\rho*A*(-3*v_2^2 - 2v_1*v_2 + v_1^2) = 0$$
$$(3v_2 - v_1)(v_2 + v_1) = 0$$
$$3v_2 = v_1 \quad \rightarrow \quad v_2 = \frac{1}{3}v_1$$
$$E_{max} = (0.5925)*\frac{1}{2}\rho A v_1^3 \quad \ldots\ldots\ldots\ (7)$$

ان الطاقة الحركية التي يكتسبها التوربين الهوائي هو جزء من الهواء وان العامل الذي يدخل في تحديد كفاءة انتاج الطاقة التي يولدها التوربين الهوائي هو معامل القدرة power coefficient of the rotor)(cp) للعضو الدوار وتعرف بانها: النسبة بين القدرة الفعلية للعضو الدوار نسبة الى القدرة المتاحة او التي تمتلكها الرياح (Horikiri Kana 2011، Martin O. L.2008)

$$cp = \frac{2P}{\rho A v^3} \quad \ldots\ldots\ldots\ (8)$$

حيث (p) القدرة الكلية المتولدة

2-2: الجانب العملي

2-2-1 : الاجهزة المستخدمة

تم استعمال البيانات الناتجة من نصب توربين صغير صالح للاستعمال المنزلي نوع fd1.5-400w في موقع الكلية التقنية / كركوك واخذ قراءات باستخدام تقنية برمجة المتحكم الدقيق نوع (ATMEG328P-PU) بلغة (MICRO-C). البرنامج

الخاص بالتحكم الدقيق يحتوي على المعادلات الخاصة لحساب القدرة اضافة الى قراءة المتغيرات الجوية (درجة الحرارة, الرطوبة, وسرعة الرياح) الشكل (1-3), تبين الاجهزة المستخدمة

الشكل (1-3) التوربين الهوائي وادوات القياس

2-2-2 : النتائج العملية

من خلال النتائج المستحصلة عمليا لقياس اداء التوربين الهوائي في ظل الظروف المناخية الخاصة بمحافظة كركوك حيث تم تمثيلها على شكل منحنيات خلال فترة مناسبة لتشغيل التوربين واعتبارا من الساعة التاسعة صباحا لحد الساعة الثانية بعد الظهر وكما هو مبين في الاشكال التالية
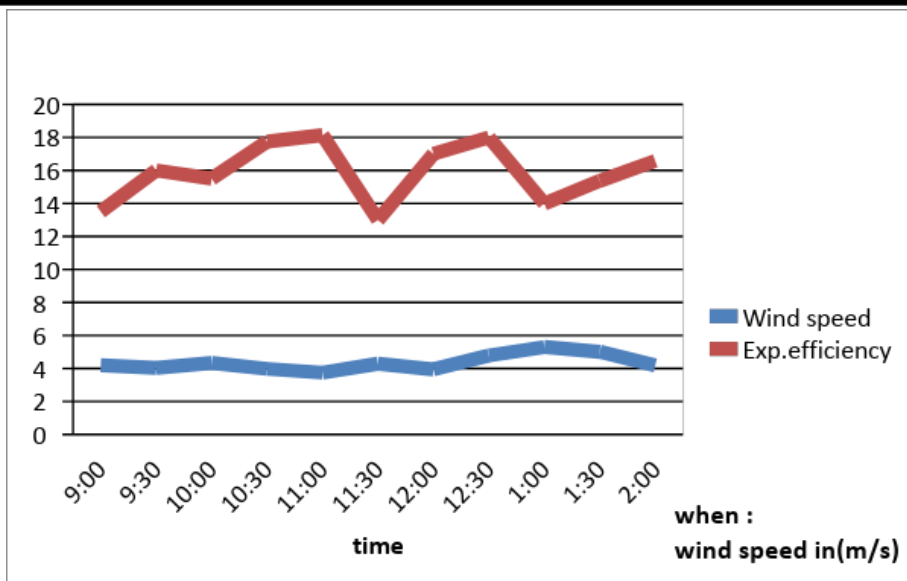
الشكل (1-4) النتائج العملية لكفاءة التوربين وسرعة الرياح
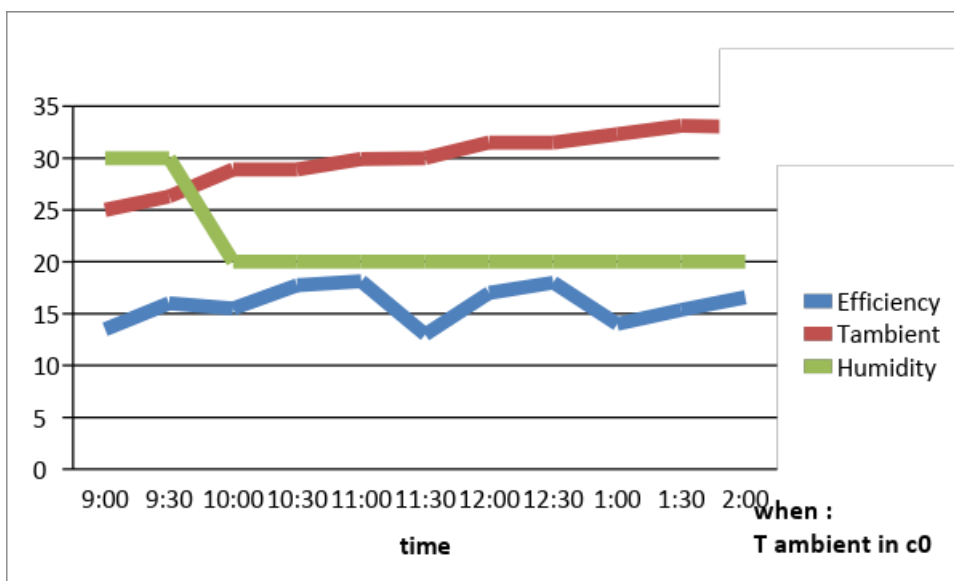
الشكل (1-5) النتائج العملية لرطوبة ودرجة الحرارة و الكفاءة
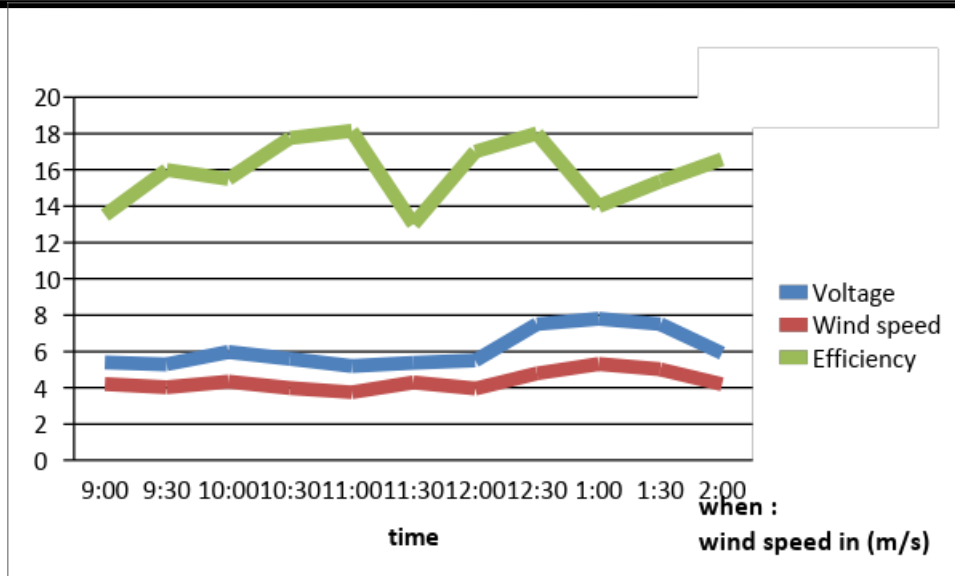
الشكل (1-6) النتائج العملية لفولطية المتولدة وسرعة الرياح والكفاءة
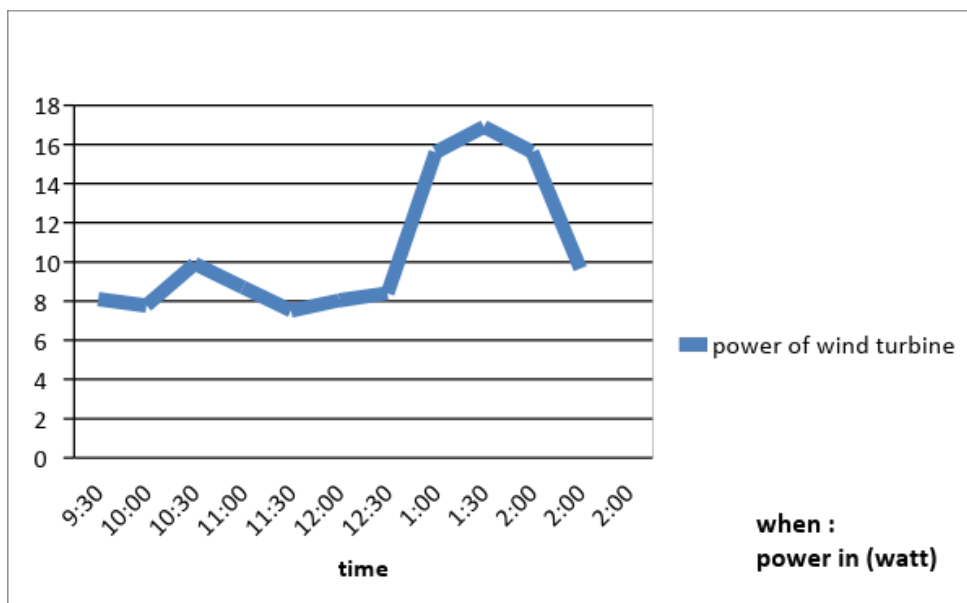
الشكل (1-7) القدرة المتولدة من النتائج العملية

3-2 : نتائج المحاكاة من خلال محاكاة النتائج العملية باستخدام برنامج التحليل الهندسي الماتلاب وفق معادلات رياضية لحساب القدرة المتولدة على مرحلتين تتضمن اعلى قيمة وادنى قمة لمعامل القدرة التي تتدرج ضمن الحدود (0.59-0.25) كما مبين في المنحنيات المرفقة
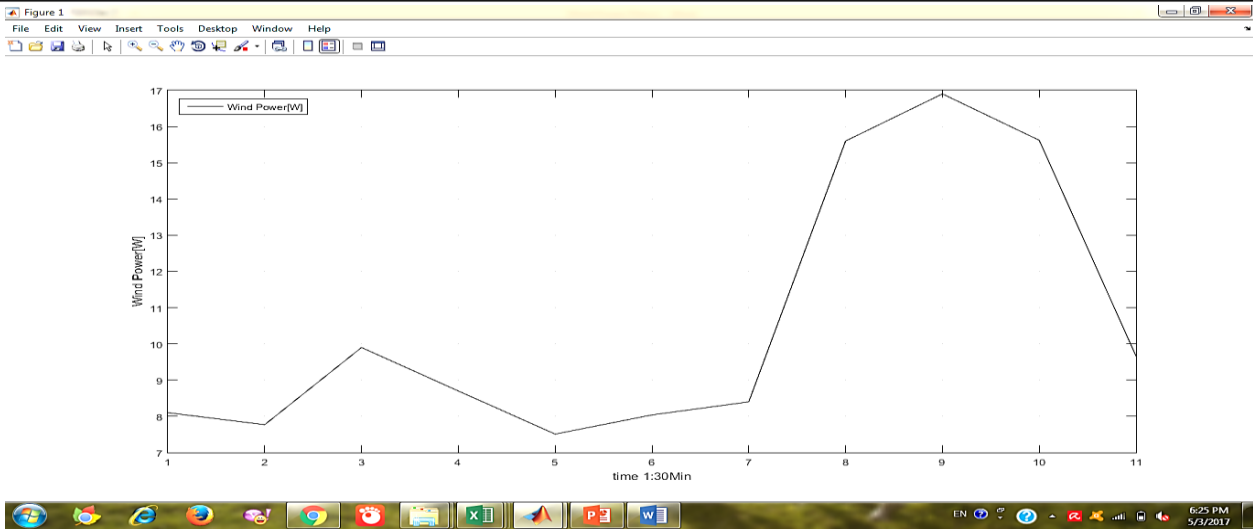
الشكل (1-8) يوضح القدرة الناتجة عمليا
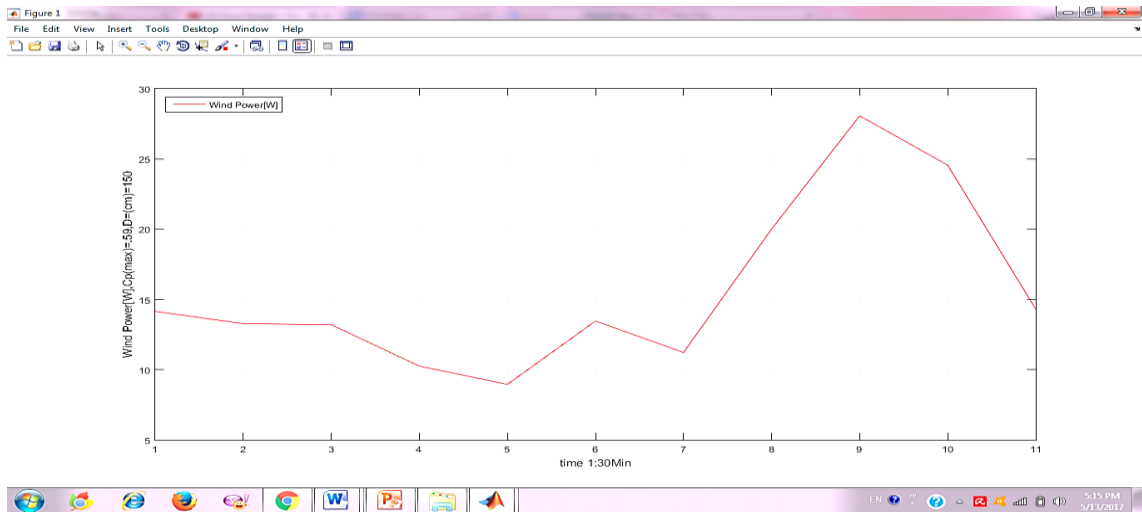
الشكل (1-9) القدرة المتولدة باستخدام المحاكاة بمعامل قدرة 0.59
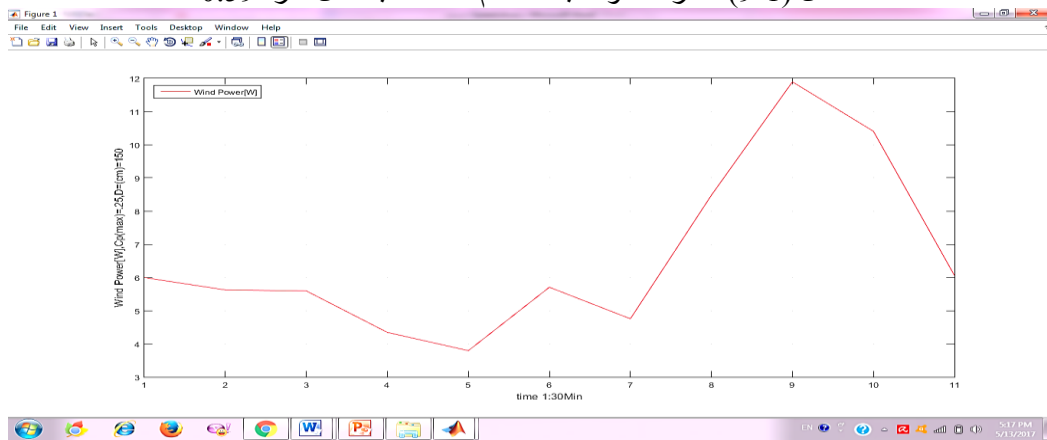
الشكل (1-10) القدرة المتولدة باستخدام المحاكاة بمعامل قدرة 0.25

4. الاستنتاجات و المناقشة

من موازنة الطاقة الحركية للرياح اتضح بأن الطاقة المستخلصة من استعمال التوربين الهوائي لا يمكن ان تتجاوز اكثر من(0.59) وان السرعة الخطية لرأس الريش تعادل 1/3 (ثلث) سرعة الرياح قبل دخول التوربين الهوائي.

ومن خلال التجربة والمحاكاة تبين ان الطاقة التي من الممكن الحصول عليها بوساطة التوربين الهوائي تزداد بانخفاض درجات الحرارة والرطوبة المؤثرة على كثافة الهواء وهو ما يؤكد الحقيقة الفيزيائية التي تشير الى ان الهواء الجاف اكثر كثافة من الهواء الرطب وان انخفاض درجات الحرارة يزيد من كثافة الهواء المؤثر بصورة مباشرة على الطاقة الناتجة من التوربين الهوائي والذي اتضح جليا في النتائج التجريبية والمحاكاة عن طريق برنامج الماتلاب

5. المصادر

Ahmad Y Hassan, Donald Routledge Hill. Islamic Technology: An illustrated history, p. 54. Cambridge University Press. ISBN 0-521-42239-6.) (1986).

Alroza Khaligh Omar G. Onar,2009 " ENERGY HARVESTING Solar, Wind, and Ocean Energy Conversion Systems"

Balasubramaniam Babypriya, Rajapalan Anita. 2009" Modeling, Simulation and Analysis of Doubly Fed Induction Generator for Wind Turbine" , Journal of Electrical Engineering, Vol. 60, no. 2, pp.79–85,

Charles F. Brush, Accessed 2007-05-02 Danish Wind Industry Association A Wind Energy Pioneer..

Erich Hau, .2005 wind turbine fundamental technology application economic

Florin Iov, Anca Daniela Hansen, Poul Sørensen, Frede. "Wind Turbine Block set in Kana Horikiri , January 2011 "Aerodynamics of wind turbines" A thesis submitted for the degree of Master of Philosophy to the University of London

Luke Hagedorn on July 28, 2011 "Mr. Brush's Windmill Dynamo', Scientific American.

Martin O. L. Hansen.2008 " Aerodynamics of Wind Turbines "Second Edition

Matlab/Simulink",, March 2004 Institute of Energy Technology, Aalborg University.

Mohammed G. Khalfallaha*, Aboelyazied M. Koliubb.2007. Suggestions for improving wind turbines power curves

Omar Badran, Emad Abdulhadi, Rustum Mamlook. 2012"Evaluation of parameters affecting wind turbine power generation", Internet Survey.

Shackleton, Jonathan. "World First for Scotland Gives Engineering Student a History Lesson". The Robert Gordon University. Retrieved 20 November 2008.
URL:http://www.ontariosea.org/Storage/27/1883

Warnes, Kathy, Retrieved 20 January 2013 "Poul la Cour Pioneered Wind Mill Power in Denmark". History, because it's there..

النمذجة الرياضية باستخدام المعادلات الضبابية مع التطبيق

أ.د. باسل يونس ذنون الخياط   *إسراء محمد بشير جقماقجي*

كلية علوم الحاسوب والرياضيات

جامعة الموصل

الخلاصة:

يتناول هذه البحث الحلول الضبابية لمعادلات تفاضلية وفروقية خطية من المرتبة الأولى ذات المعاملات الثابتة بوجود شروط ابتدائية ضبابية. يُستهل البحث بالمعادلة التفاضلية وتُستعرض طريقة حلها عندما تكون دالة انتمائها مثلثية وشبه منحرف ودالة كاوس. ثم يتناول المعادلة الفروقية الخطية وتُعرض طريقة حلهاعندما تكون دالة انتمائها دوال الانتماء الثلاثة آنفة الذكر. وتطبق النتائج النظرية على مسألة نمذجة عدد سكان العراق. ويتضح من خلال التطبيق العملي أن نماذج المعادلات التفاضلية والفروقية ذات القيم الإبتدائية الضبابية متفوقة في مجال التنبؤ عن مثيلاتها النماذج غير الضبابية.

Mathematical Modeling Using Fuzzy Equations

Abstract:

This research deals with the solutions of first order fuzzy differential and difference equations with constant confections with fuzzy initial conditions. We start with the differential equation and explain their solution when their membership functions are triangular, trapezoidal and Gaussian. Then we explain the solution of fuzzy difference equation in similar way. The obtained results are then applied on the problem of modeling of the population of Iraq. The practical application indicated that differential and difference equations with fuzzy initial conditions are superior in prediction than ordinary once.

1- مقدمة:

لقد اهتم بعض الباحثين في الآونة الأخيرة بدراسة المعادلات التفاضلية الضبابية، انظر على سبيل المثال [الكاتب، 2013]، كما اهتم بعض الباحثين مؤخرا بدراسة المعادلات الفروقية الضبابية، انظر Buckley and Feuring (2000). وقد قام بعض الباحثين بدراسة معادلات تفاضلية/ فروقية عندما تكون القيم الابتدائية أعدادا ضبابية، وقام البعض الآخر بدراسة معادلات تفاضلية/ فروقية عندما تكون معاملاتها أعدادا ضبابية. وحسب علمنا لم نجد أي باحث قام بدراسة معادلات تفاضلية أو فروقية عندما تكون متغيراتها ضبابية.

2- المجموعة الضبابية:

المجموعة الضبابية Fuzzy Set عبارة عن مجموعة حدودها مرنة وليست قطعية Crisp، ولا يمكن تعريف حدودها بصورة واضحة ودقيقة، أي يتم فيها الابتعاد عن المنطق الحدي (ينتمي أو لا ينتمي)،لأن الغموض يكون موجود دائما فيها. فلو كانت X تمثل المجموعة الشاملة Universal Set فإن المجموعة الضبابية A في X هي عبارة عن مجموعة الأزواج المرتبة Ordered Pairs والمعرّفة بالصيغة الآتية لكل عنصر x في X، [Sivanandam et al.; 2007]:

A(x)}،،A={x

حيث أن A(x) هي دالة انتماء العنصر x في A وأن A(x)Э[0،1].

1-2 دوال الانتماء Membership Functions:

يرتكز مفهوم المنطق الضبابي على أنه لا يوجد انتماء تام للعناصر في المجموعات، أو بالعكس، فهناك ثمة انتماء أو انتماء جزئي بمستوى يتحدد من خلال المعالجة المعرفية، وقد أطلق على هذه المستويات اصطلاح دالة الانتماء أو دالة العضوية Membership من خلال هذه الدالة تحديد نسبة الانتماء إلى المجموعة، والشرط الأساس المعمول به حاليا على هذه الدالة أن يقع مداها بين الصفر والواحد، كما أن لها أشكالاً متعددة منها [الدباغ، 2003]:

1. الدالة المثلثية **Triangular** Function: وصيغتها الرياضية:

$$A(x) = \begin{cases} 0 & ; & x \leq a \\ \dfrac{x-a}{b-a} & ; & a \leq x \leq b \\ \dfrac{c-x}{c-b} & ; & b \leq x \leq c \\ 0 & ; & c \leq x \end{cases} \qquad (1)$$

إذ إن a و b و c هي معلمات للدالة، و a و c تمثلان قوائم الدالة المثلثية وأن b تمثل رأس المثلث.

1- دالة شبه المنحرف Trapezoidal Function: وصيغتها الرياضية:

$$A(x) = \begin{cases} 0 & ; & x \leq a \\ \dfrac{x-a}{b-a} & ; & a \leq x \leq b \\ 1 & ; & b \leq x \leq c \\ \dfrac{d-x}{d-c} & ; & c \leq x \leq d \\ 0 & ; & d \leq x \end{cases} \qquad (2)$$

حيث أن كل من a و b و c و d هي معلمات للدالة وأن a و d تمثلان الرؤوس السفلى للشكل في حين b و c تمثلان الرؤوس العليا.

1- دالة كأوس Gaussian Function: وصيغتها الرياضية:

$$A(x) = e^{-\frac{(x-\mu)^2}{2\sigma^2}} \qquad (3)$$

إن المعلمتين μ و σ تمثلان على التوالي الرأس العلوي للشكل وبُعد الأطراف عن مركز الشكل.3.
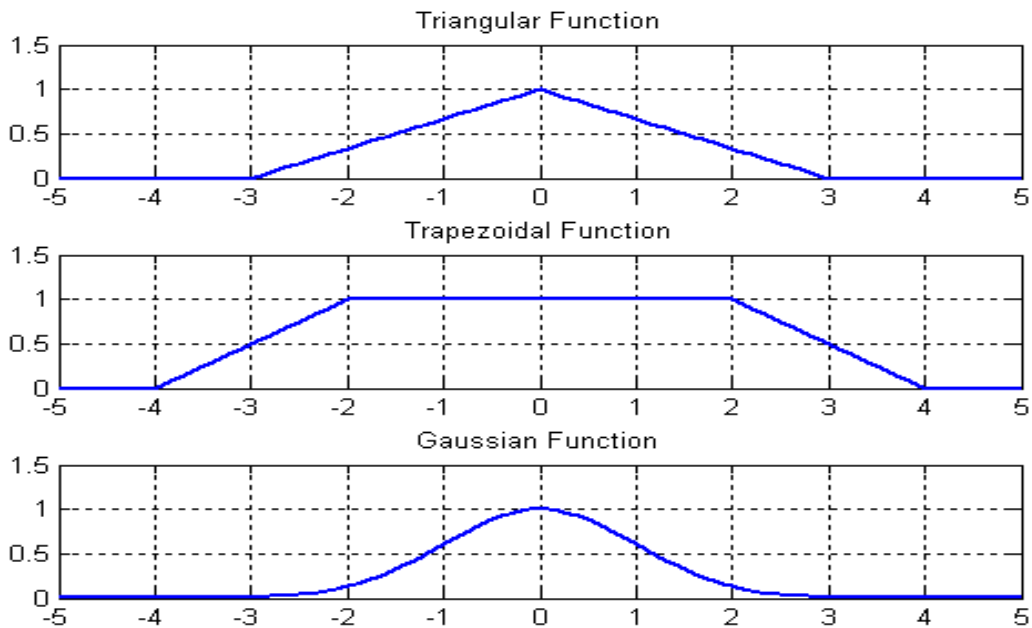
الشكل (1): دوال الانتماء : الدالة المثلثية وشبه المنحرف ودالة كأوس.

2-2 الحساب الضبابي Fuzzy Arithmetic:

هناك العديد من الظواهر الكمية لا يمكن التعبير عنها بدقة من خلال أعداد دقيقة مطلقة مما يجعل استخدام أعداد ضبابية Fuzzy Numbers أكثر واقعية للتعامل معها. ويلعب مفهوم قطع ألفا دورا أساسيا في الحساب الضبابي. فإذا كانت A مجموعة ضبابية في المجموعة الشاملة X بدالة انتماء A(x))، فإن القطع ألفا α-Cut للمجموعةA، يرمز له $^\alpha$A ويُعرّف على النحو الآتي، [الخياط وقاسم، 2017]:

$^\alpha$A={x∈X:A(x)≥α}, 0≤x≤1}.

إن العدد الضبابي Fuzzy Number هو عبارة عن مجموعة ضبابية تتميز بما يأتي:

1. الأعداد الضبابية عبارة عن مجموعات ضبابية دالة انتمائها محدَّبة Convex Sets ومتناظرة Symmetric تبلغ ذروتها في مركزها ثم تتناقص نحو الصفر.
2. تكون الأعداد الضبابية طبيعية Normal: بمعنى أن لب Core العدد لا يكون خاليا.
3. قطوع ألفا α-Cutsلكل عدد ضبابي هي عبارة عن فترات مغلقة Closed Intervals لأعداد حقيقية.
4. يمكن تمثيل العدد الضبابي بطريقة وحيدة بواسطة القطع ألفا الخاص به والذي يكون عادة فترة مغلقة من الأعداد الحقيقية.

يمكن إجراء عمليات الحساب الضبابي على الأعداد الضبابية يدويا باستخدام قواعد معينة أو حاسوبيا باستخدام برامج جاهزة، كما هو موجود مثلا في MATLAB. فلو كان A و B عددان ضبابيان لهما قطع ألفا $^\alpha$A و $^\alpha$B، على التوالي، فيمكن أيجاد العدد الضبابي الناجم من العملية الحسابية * من خلال العلاقة العامة الآتية ، [الخياط وقاسم، 2017]:

$^\alpha$(A*B)= $^\alpha$A * $^\alpha$B،   (4)

إذ إن* ممكن أن تكون أي من العمليات الحسابية الأربع: الجمع، الطرح، الضرب أو القسمة.

2-3 أنظمة الاستدلال الضبابي Fuzzy Inference Systems:

هي أنظمة مستندة على القواعد الضبابية Fuzzy- Rules. ونظام الاستدلال الضبابي هو اسم عام للنظام الذي يستخدم التفكير الضبابي لتحويل فضاء الإدخال إلى فضاء الناتج أو الإخراج. إن الغموض يكون موجود دائماً في أي عملية واقعية، وهذا الغموض قد ينشأ نتيجة تفسير بيانات الإدخال والقواعد المستخدمة لوصف العلاقة بين الخواص الغنية بالمعلومات في تلك الإدخالات، كما أن المنطق الضبابي يزودنا بنظام استدلال ضبابي يشابه قابليات الاستنتاج البشرية، وهذا النظام يمثل العملية الكاملة لاتخاذ القرارات باستعمال المنطق الضبابي. وهنالك نوعان أساسيان من نظم الاستدلال الضبابي هما:

1. الاستدلال الضبابي من نوع مامداني Mamdani Fuzzy Inference.
2. الاستدلال الضبابي من نوع تاكاجي- سوجينو Takagi- SugenoFuzzy Inference.

2-4عكس التضبيب Defuzzification:

هي عملية استبدال فترة ضبابية Fuzzy Interval بعدد حقيقي مفرد يمثلها أفضل تمثيل. من أكثر طرائق عكس التضبيب شيوعا هي طريقة Centroid. فإذا كانتA(x) فترة ضبابية، فإن عكس تضبيبها، يرمز له d(A)، ويُعرَّف لأي مجموعة شاملةX كما يأتي [Klir,2006]:

$$d(A) = \frac{\int_R xA(x)dx}{\int_R A(x)dx}.$$

(5)

وعندما تكون A معرفة في مجموعة شاملة محدودة X فإن عكس التضبيب يُعرَّف كما يأتي:

$$d(A) = \frac{\sum_{x \in X} xA(x)}{\sum_{x \in A(x)} A(x)}.$$

(6)

2-5 الاستدلال الضبابي من نوع مامداني:

في هذا الإستدلال يتم تطبيق عملية عكس التضبيب Defuzzification على المجموعة الضبابية الناتجة من حاصل جمع المجموعات الضبابية لكل قاعدة في جزء التابع Consequent، إذ يتم تمثيل الإخراج فيه بشكل مجاميع ضبابية. كما أن المعدل الموزون للقواعد يحسب من خلال المعادلة الآتية :

$$Y = \frac{\sum_{i=1}^{K} A_i(x)y_i}{\sum_{i=1}^{K} A_i(x)} = \frac{\sum_{i=1}^{K} A_i(x)(a_i^T x + b_i)}{\sum_{i=1}^{K} A_i(x)},$$

(7)

إذ إن $A_i(x)$ تمثل دالة الانتماء، [الخياط وقاسم،2017].

3- المعادلات التفاضلية الضبابية:

سنقوم في هذا المبحث بدراسة المعادلة التفاضلية الضبابية من المرتبة الأولى ذات المعاملات الثابتة وعندما تكون القيم الابتدائية بشكل أعداد ضبابية. لنفرض أن لدينا المعادلة التفاضلية ذات المعاملات الثابتة من المرتبة الأولى الآتية :

$$\frac{dx(t)}{dt} = cx(t) + b.$$

(8)

فكما هو معروف جيدا فإن حل هذه المعادلة التفاضلية يكون على النحو الآتي:

$$x(t) = x(0)e^{ct} + \frac{b}{c}(e^{ct} - 1).$$

(9)

إذ إن(0)x تمثل القيمة الابتدائية.

لنحاول الآن دراسة حل المعادلة التفاضلية السابقة عندما تكون القيمة الابتدائية (0)x عددا ضبابيا، وليكن (0)$\tilde{x}$. والمبرهنة الآتية تعود للباحث [Barnabas Bede, 2007] وتوضح كيفية الحصول على حل المعادلة التفاضلية السابقة عندما تكون القيمة الابتدائية عددا مثلثيا، وليكن (0)$\tilde{x}$=(α،β،γ) ، إذ إن α و β و γ أعداد حقيقية تمثل رؤوس المثلث$\alpha, \beta, \gamma \in \mathbb{R}$.

المبرهنة (1): [Barnabas Bede, 2007]
إذا كان لدينا المعادلة التفاضلية الضبابية(8) فيمكن الحصول على الحل من إحدى الحالتين الآتيتين:
1. إذا كان c>0 فإن:

$$x(t) = e^{c(t-t_0)}[x(0) + \int_{t_0}^{t}(b(s)) \cdot e^{-c(s-t_0)} ds] \qquad (10)$$

هو حل للمعادلة التفاضلية الضبابية (8) وأن x(t) دالة قابلة للاشتقاق بقوة من النوع (1).

2. إذا كان c<0 وكان فرق H- للمقدار $x(0) - \int_{t_0}^{t}(-b(s)) \cdot e^{-c(s-t_0)} ds$ موجوداً فإن:

$$x(t) = e^{c(t-t_0)}[x(0) + \int_{t_0}^{t}(-b(s)) \cdot e^{-c(s-t_0)} ds] \qquad (11)$$

هو حل للمعادلة التفاضلية الضبابية (8) وإن x(t) دالة قابلة للاشتقاق بقوة من النوع (2).

لقد قامت الباحثة [الكاتب، 2013] بتطوير المبرهنة السابقة عندما تكون القيمة الابتدائية (0)x عددا ضبابيا شبه منحرف وقامت بإيضاح منهجيتها من خلال مثال عددي. وفي ضوء ما تقدم يمكن تعميم النتائج السابقة للوصول إلى النتائج الآتية والتي تبين حل المعادلة التفاضلية الضبابية (8) عندما تكون القيمة الابتدائية (0)x عددا ضبابيا دالة انتمائها مثلثية وشبه منحرف ودالة كاوس.

النتيجة(1): إذا كانت القيمة الابتدائية (0)x عددا ضبابيا مثلثيا، وليكن (0)$\tilde{x}$=(α،β، γ) ، إذ إن α و β و γ أعداد حقيقية تمثل رؤوس مثلث، $\alpha, \beta, \gamma \in \mathbb{R}$، فإن حل المعادلة التفاضلية الضبابية (8) يكون على النحو الآتي:

$$\tilde{x}(t) = (α +1، β +1، γ +1)e^{ct} + \frac{b}{c}(e^{ct}-1). \qquad (12)$$

البرهان: حسب المبرهنة (1) وبالتعويض عن القيمة الابتدائية بالعدد الضبابي (0)$\tilde{x}$=(α،β، γ) ، وبعد الاستفادة من الحساب الضبابي يكتمل البرهان.

النتيجة(2): إذا كانت القيمة الابتدائية (0)x عددا ضبابيا شبه منحرف وليكن (0)$\tilde{x}$=(α،β، γ، δ) ، إذ إن α و β و γ و δ أعداد حقيقية تمثل رؤوس شبه المنحرف، $\alpha, \beta, \gamma, \delta \in \mathbb{R}$، فإن حل المعادلة التفاضلية الضبابية (8) يكون على النحو الآتي:

$$\tilde{x}(t) = (α +1، β +1، γ +1، δ+1)e^{ct} + \frac{b}{c}(e^{ct}-1). \qquad (13)$$

البرهان: حسب المبرهنة (1) وبالتعويض عن القيمة الابتدائية بالعدد الضبابي (0)$\tilde{x}$=(α،β،γ، δ) ، وبعد الاستفادة من الحساب الضبابي يكتمل البرهان.

النتيجة(3): إذا كانت القيمة الابتدائية (0)x عددا ضبابيا بشكل دالة كاوس، وليكن (0)$\tilde{x}$=G(μ،σ) ،إذ إن المعلمتين μ و σ تمثلان على التوالي الرأس العلوي للشكل وبُعد الأطراف عن مركز الشكل، فإن حل المعادلة التفاضلية الضبابية(8) يكون على النحو الآتي:

$$\tilde{x}(t) = \left[e^{-\frac{1}{2\sigma^2}(t-\mu)^2}\right]e^{ct} + \frac{b}{c}(e^{ct} - 1). \qquad (14)$$

البرهان: حسب المبرهنة (1) وبالتعويض عن القيمة الابتدائية بالمقدار $(0)\tilde{x} = e^{-\frac{1}{2\sigma^2}(x-\mu)^2}$، وبعد الاستفادة من الحساب الضبابي يكتمل البرهان.

4

ـ المعادلات الفروقيه الضبابيه:

سنقوم في هذا المبحث بدراسة المعادلة الفروقية من المرتبة الأولى ذات المعاملات الثابتة وعندما تكون القيم الابتدائية أعداد ضبابية. إن المعادلات الفروقية تماثل المعادلات التفاضلية وأن الفارق بينهما أن المعادلات التفاضلية تكون في الزمن المستمر في حين أن المعادلات الفروقية تكون في الزمن المتقطع، أنظر رسالة الماجستير للباحث الثاني للتفاصيل.

لو فرضنا أن لدينا المعادلة الفروقية من المرتبة p ذات المعاملات الثابتة الآتية :

$$x_{k+1} = a_1 x_k + a_2 x_{k-1} + \cdots + a_p x_{k-p} + b; \ k = 0، 1، 2، \ldots \qquad (15)$$

حيث أن $a_p، \ldots ،a_2،a_1$ وb ثوابت. فكما هو معروف فإن الشروط الابتدائية هي عبارة عن أعداد حقيقية وأن الحل العام للمعادلة (15) يكون، انظر على سبيل المثال[الخياط، 2012]:

$$x_k = x_{hk} + x_{pk}، \qquad (16)$$

إذ إن x_{hk} يمثل الحل المتمم complementary function للمعادلة المتجانسة:

$$a_1 x_k + a_2 x_{k-1} + \cdots + a_p x_{k-p} + b = 0$$

و x_{pk} يمثل الحل الخاص للمعادلة .

لنفرض الآن أن لدينا المعادلة الفروقية الاعتيادية من المرتبة الأولى ذات المعاملات الثابتة:

$$x_{k+1} = a x_k + b; \ k = 1, 2, \ldots \qquad (17)$$

إذ إن a و b ثابتان. فكما هو معروف فإن الحل النهائي للمعادلة (17) هو [الخياط، 2012]:

$$x_k = a^k x_0 + b \sum_{i=1}^{k} a^{i-1} \ ; \ k = 1، 2، \ldots$$

ويمكن تبسيط المعادلة الأخيرة لتصبح:

$$x_k = \begin{cases} \dfrac{b(1-a^k)}{1-a} + x_0 a^k & ; a \neq 1 \\ kb + x_0 & ; a = 1 \end{cases}, \ k = 1, 2, \ldots \qquad (18)$$

إذ إن x_0 تمثل القيمة الابتدائية. ويمكن كتابة الحل العام للمعادلة (17) بالشكل الآتي:

$$x_k = x_{hk} + x_{pk} ، \qquad (19)$$

حيث أن x_{hk} يمثل الحل المتمم (complementary function) للمعادلة المتجانسة:

$$x_{k+1} + a x_k = 0 \qquad (20)$$

و x_{pk} يمثل الحل الخاص للمعادلة (17). ويمكن استخدام الشرط الابتدائي لإيجاد القيم من الثوابت الموجودة في x_k للحصول على الحل الوحيد للمعادلة (17).

لنحاول الآن دراسة حل المعادلة الفروقية السابقة عندما تكون القيمة الابتدائية x_0 عددا ضبابيا، وليكن $\tilde{x}_0$. وباستخدام الحساب الضبابي يمكن أن نجد حل المعادلة الفروقية الضبابية (17) عندما تكون القيمة الابتدائية $\tilde{x}_0$ عددا ضبابيا وكما مبين في النتائج الآتية .

النتيجة(3): إذا كانت القيمة الابتدائية $\tilde{x}_0$ عددا ضبابيا مثلثيا، وليكن $\tilde{x}_0 = (\alpha، \beta، \gamma)$، إذ إن α و β و γ أعداد حقيقية تمثل رؤوس مثلث، $\alpha، \beta، \gamma \in \mathbb{R}$، فإن حل المعادلة الفروقية الضبابية (17) يكون على النحو الآتي:

$$\tilde{x}_t = (\alpha، \beta، \gamma)[a^k x_0 + b \sum_{i=1}^{k} a^{i-1}]$$

أي إن

$$\tilde{x}_t = [\alpha \, (a^k x_0 + b \sum_{i=1}^{k} a^{i-1})، \beta(a^k x_0 + b \sum_{i=1}^{k} a^{i-1})، \gamma(a^k x_0 + b \sum_{i=1}^{k} a^{i-1})]. \qquad (21)$$

النتيجة(4): إذا كانت القيمة الابتدائية $\tilde{x}_0$ عددا ضبابيا شبه منحرف، وليكن $\tilde{x}_0 = (\alpha، \beta، \gamma, \delta)$، إذ إن α و β و γ و δ أعداد حقيقية تمثل رؤوس شبه المنحرف، $\alpha، \beta، \gamma، \delta \in \mathbb{R}$، فإن حل المعادلةالفروقية الضبابية (17) يكون على النحو الآتي:

$$\tilde{x}_t = (\alpha، \beta، \gamma، \delta)[a^k x_0 + b \sum_{i=1}^{k} a^{i-1}]$$

أي إن

$$\tilde{x}_t = [\alpha\,(a^k x_0 + b\sum_{i=1}^{k} a^{i-1})، \beta(a^k x_0 + b\sum_{i=1}^{k} a^{i-1})، \gamma(a^k x_0 + b\sum_{i=1}^{k} a^{i-1})، \delta(a^k x_0 + b\sum_{i=1}^{k} a^{i-1})].$$

$$(22)$$

النتيجة(5): إذا كانت القيمة الابتدائية $\tilde{x}_0$ عددا ضبابيا بشكل دالة كأوس، وليكن $\tilde{x}_0 = G(\mu،\sigma)$، إذ إن المعلمتين μ و σ تمثلان على التوالي الرأس العلوي للشكل وبُعد الأطراف عن مركز الشكل، فإن حل المعادلة الفروقية الضبابية (17) يكون على النحو الآتي:

$$\tilde{x}_t = e^{-\frac{1}{2\sigma^2}(t-\mu)^2}\left(a^k x_0 + b\sum_{i=1}^{k} a^{i-1}\right).$$

$$(23)$$

3-5 النمذجة الضبابية لعدد سكان العراق:

لقد اجريت خمسة تعددات رسمية في العراق في العصر الحديث، بواقع تعداد لكل عشر سنين، وكما مبين في الجدول اللاحق [الخياط، 2012].

الجدول (1): عدد سكان العراق حسب تعدادات السكان الرسمية.

عدد السكان (مليون نسمة)	السنة
4.564	1947
6.34	1957
9.255	1967[(*)]
12.17	1977
16.34	1987
22.02	1997

(*) لا يوجد تعداد سكان في هذا العام، والقيمة المذكورة تقديرية.

وقد عرض [الخياط، 2012] مسألة نمذجة عدد سكان العراق باستخدام المعادلات الفروقية والتفاضلية الاعتيادية. وسنقوم في هذا المبحث بتطوير تلك النماذج وذلك باستخدام نماذج ضبابية.

عند اختيار سنة الأساس لتكون سنة 1947 فقد وجد المصدر السابق أن المعادلة التفاضلية الآتية مناسبة لنمذجة عدد سكان العراق في الزمن المستمر:

$$x(t) = x(0)e^{ct}$$ $$(24)$$

إذ إن c=0.3287 و x(0)=4.564. وأن المعادلة الفروقية الآتية مناسبة لنمذجة عدد سكان العراق في الزمن المتقطع:

$$x_k = \tilde{x}_0 a^k; \; k = 1،2، ...$$ $$(25)$$

إذ إن a=1.3891 و x_0=4.564.

وبفرض أن القيمة الابتدائية $x(0)$ هي كمية ضبابية تقع بين 4 و 5، فإننا سنحاول أن نجد القيم التقديرية لعدد سكان العراق للسنوات 1967، 1977، 1987، 1997 باستخدام كل من المعادلة التفاضلية الضبابية:

$$\tilde{x}(t) = \tilde{x}(0)e^{ct}$$ $$(26)$$

والمعادلة الفروقية الضبابية

$$x_k = \tilde{x}_0 a^k; \; k = 1، 2، \dots \qquad (27)$$

إذ إن a=1.3891 و x₀=4.564.

لقد تم استخدام ثلاث دوال انتماء هي: دالة شبه المنحرف والدالة المثلثية ودالة كاوس. ونشير إلى أن معلمات دالتي الانتماء شبه المنحرف والمثلثية قد تم اختيارها ضمن فترات قريبة تقع فيها القيم الضبابية، في حين أن معلمتي دالة كأوس قد تم اختيارهما على النحو الآتي: معلمة الرأس العلوي μ قد اختيرت لتكون المعلمة المراد تضبيبها ومعلمة بُعد الأطراف قد ثُبتت عند $\sigma = 1$. علما أن جميع البرامج الحاسوبية المستخدمة موجودة في الملحق A برسالة الماجستير للباحثة الثانية.

إن القيمة الابتدائية $x(0)$ و x₀ لنموذجي المعادلة التفاضلية والمعادلة الفروقية السابقتين هي قيمة تقريبية. لذا سنحاول الآن تضبيب هذه القيمة بالقيمة الضبابية 4.5 = $\tilde{x}_0 = \tilde{x}(0)$ والتي يُنظر اليها بوصفها عددا ضبابيا. وقد تم كتابة برنامج حاسوبي بلغة MATLAB يقوم بتضبيب القيمة الابتدائية ثم عكس تضبيبها ومن ثم استخدام حل المعادلة التفاضلية الضبابية للتنبؤ بعدد بتضبيب سكان العراق للسنوات1967، 1977، 1987، 1997 وذلك باستخدام ثلاث دوال انتماء مختلفة وهي:

1- دالة انتماء شبة منحرف trapmf.
2- دالة انتماء مثلثية trimf.
3- دالة انتماء كأوس gaussmf.

كما يقوم البرنامج بحساب معدل مربع الخطأ MSE ومعدل الخطأ المطلق MAE.

$$MSE = \frac{\sum_{i=1}^{n}(x_i - \hat{x}_i)^2}{n}, \qquad (28)$$

$$MAE = \frac{\sum_{i=1}^{n}\left|x_i - \hat{x}_i\right|}{n}, \qquad (29)$$

إذ إن $x_1, x_2, \dots, x_n$ تمثل أعداد السكان الواقعية و $\hat{x}_1, \hat{x}_2, \dots, \hat{x}_n$ تمثل أعداد السكان المتنبأ بها من النموذج الرياضي و n تمثل عدد القيم.

الجدول(2): عدد سكان العراق باستخدام المعادلة التفاضلية التقليدية والمعادلة التفاضلية الضبابية.

عدد السكان المتوقع باستخدام نموذج المعادلة التفاضلية الضبابية (مليون نسمة)			عدد السكان المتوقع باستخدام نموذج المعادلة التفاضلية التقليدية (مليون نسمة)	عدد السكان الملاحظ فعليا (مليون نسمة)	السنة
دالة انتماء كاوس	دالة انتماءمثلثية	دالة انتماء شبة منحرف			
8.4457	8.8075	8.3182	8.8075	9.255	1967
11.7324	12.2350	11.5553	12.2350	12.17	1977
16.2983	16.9964	16.0521	16.0521	16.34	1987
22.6409	23.6107	22.2990	23.6107	22.02	1997
0.3084	0.7914	0.3541	0.7914		MSE
0.4774	0.6899	0.5296	0.6899		MAE

الجدول (3): عدد سكان العراق باستخدام المعادلة الفروقية التقليدية والمعادلة الفروقية الضبابية (مليون نسمة) .

عدد السكان المتوقع نموذج الفروقية الضبابية	عدد السكان المتوقع باستخدام نموذج المعادلة الفروقية الضبابية	عدد السكان المتوقع باستخدام نموذج المعادلة الفروقية الضبابية	عدد السكان المتوقع باستخدام نموذج المعادلة الفروقية التقليدية	عدد السكان الملاحظ فعليا (مليون نسمة)	السنة
دالة انتماء كاوس	دالة انتماء مثلثية	دالة انتماء شبة منحرف			
8.3887	8.8067	8.3174	8.8067	9.255	1967
11.6528	12.2334	11.5537	12.2334	12.17	1977
16.1869	16.9934	16.0493	16.9934	16.34	1987
22.4852	23.6055	22.2941	23.6055	22.02	1997
0.3144	0.7864	0.3546	0.7864		MSE
0.5004	0.6876	0.5297	0.6876		MAE

وكما هو واضح من الجدولين السابقين فإن نموذجي المعادلة التفاضلية التقليدية والضبابية اعطيا نتائج تنبؤ متماثلة عند دالة الانتماء المثلثية، أما نتائج دالتي الانتماء شبه المنحرف وكأوس فمتفوقتان على النموذجين الآخرين. ومن خلال معياري معدل مربع الخطأ ومعدل الخطأ المطلق يتضح أن المعادلة التفاضلية الضبابية بدالة انتماء كاوس متفوقة في كفاءتها على المعادلة التفاضلية الاعتيادية وكذلك على كل من المعادلة التفاضلية الضبابية بدالة انتماء شبة منحرف وبدالة انتماء مثلثية. على نحو مماثل فإن نموذجي المعادلة الفروقية التقليدية والضبابية أعطيا نتائج تنبؤ متماثلة عند دالة الانتماء المثلثية، أما نتائج دالتي الانتماء شبه المنحرف وكأوس فمتفوقتان على النموذجين الآخرين. ومن خلال معياري معدل مربع الخطأ ومعدل الخطأ المطلق يتضح أن المعادلة الفروقية الضبابية بدالة انتماء كاوس متفوقة في كفاءتها على المعادلة الفروقية الاعتيادية وكذلك على كل من المعادلة الفروقية الضبابية بدالة انتماء شبة منحرف وبدالة انتماء مثلثية.

المصادر

[1].الدباغ، سفيان سالم (2003) **"تصميم نظام حاسوبي لتقدير قوة مقاومة انضغاط الإسمنت البورتلندي"**، رسالة ماجستير غير منشورة، كلية علوم الحاسوب والرياضيات، جامعة الموصل.

[2].جقماقجي، اسراء محمد بشير (2017) **"النمذجة الرياضية باستخدام المعادلات الضبابية مع التطبيق"**، رسالة ماجستير غير منشورة، كلية علوم الحاسوب والرياضيات، جامعة الموصل.

[3].الخياط، باسل يونس (2012) **" مدخل الى النمذجة الرياضية باستخدام MATLAB"**، دار ابن الأثير للطباعة والنشر، جامعة الموصل.

[4].الخياط، باسل يونس ذنون وقاسم، عمر صابر (2017) **"الرياضيات الضبابية وتطبيقاتها باستخدام "MATLAB**، كتاب قيد الإعداد.

[5].الكاتب، اسماء زياد (2013) **" حول بعض المعادلات المضببة "**، اطروحة دكتوراه غير منشورة، كلية علوم الحاسوب والرياضيات، جامعة الموصل.

[6].Barnabas Bede (2007), Imre J. Rudas and Attila L. Bencsik **"First order linear fuzzy differential equations under generalized differentiability"**, Inf. Sci.177(7), pp.1648-1662.

[7].James J. Buckley and Thomas Feuring (2000) **"Fuzzy differential equations"**, Elsevier Fuzzy Sets and Systems, 110, pp. 43-54.

[8].Jang, J.S.R.,(1993) **"ANFIS : Adaptive– Network - Based Fuzzy Inference System",** IEEE Trans Actions on Systems, Man, and Cybernetics, VOL. 23, NO. 3.

[9].Klir, George J. (2006) **"Uncertainty and Information: Foundations of Generalized Information Theory"**, John Wiley & Sons, Inc.

[10]. Sivanandam, S. N., Sumathi, S. and Deepa , S. N. (2007) **"Introduction to Fuzzy Logic Using MATLAB"**, Springer-Verlag Berlin Heidelberg, Berlin.

دراسة العوامل المؤثرة على السلوك المميعة وانتقال الحرارة في وحدات المميعة

أ.م احسان فاضل عباس   ساره برهان عزت

(المشرف)   (طالبة ماجستير)

الجامعة التقنية الشمالية/الكلية التقنية كركوك

burhan2014@gmail.com   ehsanfadhil@ntu.edu.iq

الخلاصة:

تهدف هذه الدراسة تأثير كل من سرعة الجريان الغاز، حجم جسيمات الرمل والمسافة بين الاعمدة الساخنة المغمورة في الطبقة المميعة على معامل انتقال الحرارة. حيث تضمنت الدراسة على اجراء اختبارات على منشأ تجريبي يتكون من حاوية البلاستيكية وتحتوي هذه الحاوية على حزمة من أنابيب نحاسية بقطر(12.5)ملم وطول(320)ملم، موزعة على شكل مصفوفة (17×9) مرتبة بشكل متعرج، وثلاث انابيب منها استخدمت كمصدر حراري بشكل عمودي وبقدرة (366) واط، حيث تم تنفيذ الاختبارات على قياسين من حبيبات الرمل بقطر (0.15 و 0.3)ملم وبكمية (25kg)، وباستخدام ست سرع لجريان الغاز(0.16، 0.2، 0.221، 0.254، 0.3, 0.338)م/ثا . أظهرت النتائج بأن أعلى قيمة لـ (Nu) قد حصلت عند العمود HT3 في جميع الاختبارات عند نموذج الرمل بقطر(0.15)ملم وبنسبة الزيادة 300% عن نموذج الرمل (0.3) ملم. وكانت النتائج متطابقة عند مقارنتها مع الدراسات الأخرى في نفس المجال من حيث التطبيق ولكن اختلاف قطر الحبيبات الرمل.

الكلمات الدالة: الطبقة المميعة, معامل انتقال الحرارة, حد التمييع

المقدمة:

تدخل التقنية المميعة الان في جميع الصناعات سواء بترولية منها اوغيرها، وتستعمل بشكل مكثف في صناعات كيميائية، كذلك استخدم التقنية المميعة كتكنولوجيا الثانية في عملية الاحتراق (كتلة الحيوية) وانتاج الغازات. اول التقنية المميعة تم انتاجها بنجاح من قبل الكيميائي الماني (Fritz Winkler) في المانيا سنة (1922م) لإنتاج الغاز، و استخدم في عمليات التكسير الحراري بالولايات المتحدة الامريكية سنة (1942م)(Basu P. 2006). بغية تطوير واستفادة من هذه التقنية قي مجال تحسين الاداء الحراري للمبادلات الحرارية، فقد اجريت عدد من الدراسات النظرية والعملية من قبل باحثين معظم الدول ومنها:

قدم الباحث (Xu G. et al. 2004) دراسة عملية عن تأثير تغير تركيز الفراغات أثناء عملية التمييع وذلك باستخدام عمود التمييع قطره(90)ملم وطوله(11)م غمر في طبقة من جسيمات المائع التكسير تحفيزي(FCC) بقطره(54)مايكرومتر وكثافته(929.5)كغم/م³. اظهرت النتائج بان تركيز الفراغات ينخفض بانخفاض سرعة الغاز وبالعكس. اما الباحثة (.Salwe A. M et al. 2014) فقد قدمت دراسة عن تأثير كل من سرعة وحجم جسيمات على معامل انتقال الحرارة في مبادل حراري من نوع الطبقة المميعة. حيث اجريت الاختبارات على ثلاث طبقات مميعة والتي تم اختيارها حسب المعاير(Geldart)،و استخدم ثلاث نماذج اقطار من جسيمات الرمل بقياسات تتراوح ((300_450)، (425_650) و(600_850)) مايكرومتر،

و عرضت هذه النماذج الى عشر سرع مختلفة للهواء. استخدمت مسخنات كهربائية لتسخين الطبقة المميعة. اظهرت نتائج الاختبارات بان معدل انتقال الحرارة يزداد في جسيمات الرمل ذات احجام صغيرة بالنسبة لسرعة الهواء. تمكن الباحثان (Sunderson & Clark 1995) من تقديم دراسة تطبيقية لحساب معامل انتقال الحرارة موضعياً على محيط الانبوب في الطبقة المميعة من الغاز ، وذلك باجراء اختبارات على انبوب ساخن مغمور في طبقة مميعة متكونة من(التراب وحبيبات الزجاج) و باستخدام اربع قياسات للطبقة المميعة. اظهرت من النتائج بأن هنالك منطقة الركود في اعلى انبوب اضافة الى السرعات السطيحة المنخفضة والحصول على علاقة رياضية تربط معدل معامل انتقال الحرارة بالجذر التربيعي لمعامل انتقال الحرارة انتقالي. قدم الباحث (Masoumifard N. et al. 2008) تحققاً مختبرياً لانتقال الحرارة بين انبوب افقي والطبقة(غاز- صلب) المميعة. استخدمت في هذه الدراسة انبوب افقي ساخن بقطر(8)ملم مغمور في طبقة مميعة واجريت الاختبارات في ثلاث انواع من طبقات مميعة اقطار حبيبات الرمل ذات اقطار(750,490,280) مايكرومتر وتم اسالتها بتدفق الهواء. اظهرت النتائج بان معامل انتقال الحرارة يزداد بتقليل حجم الجسيمات الرمل , وكذلك يزداد بزيادة سرعة الهواء الى اعلى قيمة ومن ثم ينخفض قليلا , اما بالنسبة لتأثير موقع المجسات على معامل انتقال الحرارة فانه يعتبر ضعيف. قام الباحث (Johansson K. et al. 2004) بدراسة تطبيقية عن اليه عمل الطبقة المميعة من النوع الفقاعي وذلك من خلال اجراء عدد من التجارب في الدرجة الحرارة ثابتة (550)مئوية باستخدام جسيمات الرمل بقطر(0.7_ 0.8)مايكرومتر في ثلاث سرع مختلفة(0.7,0.4,0.15)م/ثا. بينت من النتائج العملية بان سرعة الغاز المثالية بالنسبة لهذه الدراسة كانت (0.4)م/ثا. اما الباحث (Al-Tamimi et al. 2000) فقد قدم دراسة عملية على مبادل الحراري يعمل بالأنبوب الحراري المغمور بالطبقة المميعة ويعتبر اول من اقترح الاستعمال الطبقة المميعة مع الانابيب الحرارية في العراق من خلال تصنيع المبادل الحراري فريد من نوعه في اجهزة التي تولد الحرارة، واما سبب استخدام هذه التقنية كانت لزيادة كفاءة لانتقال الحرارة، تصغر الحجم ومنع تراكم مخلفات على سطوح الانابيب، حيث هذه المخلفات تؤدي الى انخفاض قيم معاملات انتقال الحرارة و فرق بدرجات الحرارة. حيث تضمنت هذه الدراسة، استخدم انابيب من النحاس بقطر خارجي(22.2)ملم وطول(600)ملم ومثبتة في مجرى

معدني بابعاده(150×300)ملم بارتفاع (650)ملم واما حبيبات الرمل المستخدمة فقد كانت بقطر(652,420,274) مايكرومتر، وفي مدى لسرعة الكتلة تراوحت بين (0.302_0.542)كغم/م^2.ثا، ودرجات الحرارة تراوحت بين (120_ 200)مئوية. حيث اظهرت النتائج بان معامل انتقال الحرارة يزداد بزيادة درجة الحرارة والسرعة التدفق الهواء ويقل بزيادة قطر حبيبات الرمل.

الجانب العملي:

تم بناء منشأ تجريبي لأجراء التجارب كما مبين في الشكل(1) مكون من حاوية مصنوعة من الواح بلاستيكية بسمك(6)ملم بأبعاد (30×60)سم وارتفاع(100)سم مثبتة على هيكل من الحديد الزاوية قياس (25)ملم، ثبت فيها الانابيب النحاسية بقطر(12.5)ملم وبطول(32)سم على شكل مصفوفة متعرجة قياس(17×9)، حيث كانت ثلاثة انابيب منها استخدمت فيها مسخنات كهربائية بالقدرة (366)واط. لضمان سريان الهواء بشكل منتظم الى داخل الحاوية فقد تم تصنيع الصندوق مخروطي الشكل اسفل الحاوية ومحتواهُ:

أ-   طبقة من الاسفنج التجاري لمنع عبور دقائق الرمل من الحاوية الى الصندوق.

ب-   مرشحات كارتونية (تمنع دخول جسيمات الرمل الى منظومة الهواء).

ج- موزع الهواء مصنوع من لوح خشبي بأبعاد(26×56)سم وبسمك(2)سم يحتوي على(263) ثقب قطره(10)ملم,لضمان التوزيع الهواء بصورة متساوية في جميع انحاء الطبقة المميعة).

د- اربع قنوات تنقل الهواء الى مخمده للهواء(وذلك لإعطاء تدفق مستقر للهواء في منطقة التمييع لمنع حدوث تدفق غير مستقر(Air jets)). استخدمت في الاختبارات ثلاث انواع من الرمل بعد غسل وجفف ونخل حسب اقطار مطلوبة.

كذلك استخدام جهازين لقياس الفرق الضغط، احدهما ثبت على قرص المثقوب (Orifice disk) للاستفادة منه لقياس سرعة الهواء والاخر ثبت في الطبقة المميعة لقياس فرق الضغط فيها، اما بالنسبة قياس درجات الحرارة فقد استخدم جهاز مسجل درجات الحرارة ذو (32) قناة، وزعت المزدوجات الحرارية نوع (K)على نحو الاتي:

1. ثبت خمس عشر مزدوج حرارى في الاعمدة (HT3,HT2,HT1) و بواقع خمس مزدوجات لكل عمود.

2. ثبت خمس عشر مزدوج حراري وزعت داخل الطبقة المميعة في اماكن مختلفة.

3. ثبت مزدوجين حرارين عند الدخول والخروج الهواء الى طبقة المميعة.

خطوات العمل:

1- تثبيت الحاوية في المنشأ وبشكل محكم لمنع تسريب جسيمات الرمل الى الصندوق او خارج الحاوية، ومن ثم ادخال الانابيب في امكانها وتثبيتها في الجدار الحاوية.

2- ادخال المسخنات الحرارية في العمود الاول(X1) من مجموعة الاعمدة كما مبين في الشكل (2).

3- تعبئة الحاوية البلاستيكية بكمية (25) كغم رمل قياسه (0.15) ملم وكان ارتفاع الرمل بمستوى الصف الاول من الانابيب.

4- تجهيز الانابيب الساخنة بالطاقة الكهربائية من خلال مجهز القدرة والانتظار لفترة زمنية حتى وصل سطح المسخنات الى درجة حرارة (200) مئوية.

5- تشغيل منفاخ الهواء والسيطرة على سرعة تدفق الهواء من الصمام الرئيسي والبوابة المثبتة عند مدخل الهواء، واختيار اربع سرع وهي(0.16، 0.2، 0.221، 0.254) م/ثا لنموذج الرمل ($d_p = 0.15mm$) و(0.221، 0.254, 0.3, 0.338)م/ثا لنموذج الرمل ($d_p = 0.3mm$)، وقد خصص فترة(15) دقيقة لوصول جريان الهواء الى حالة من الاستقرارية في الطبقة المميعة.

6- يتم اتباع الاجراءات من (1 الى 8) في الاختبارات على موقع المسخنات من العمود(X2) الى العمود الاخير(X5).

7- بعد انتهاء من نموذج الرمل قياس (0.15) ملم، يتم تغير النموذج الى قياس (0.3) ملم ويتبع الاجراءات من (1 الى 6) لاكمال الاختبارات.
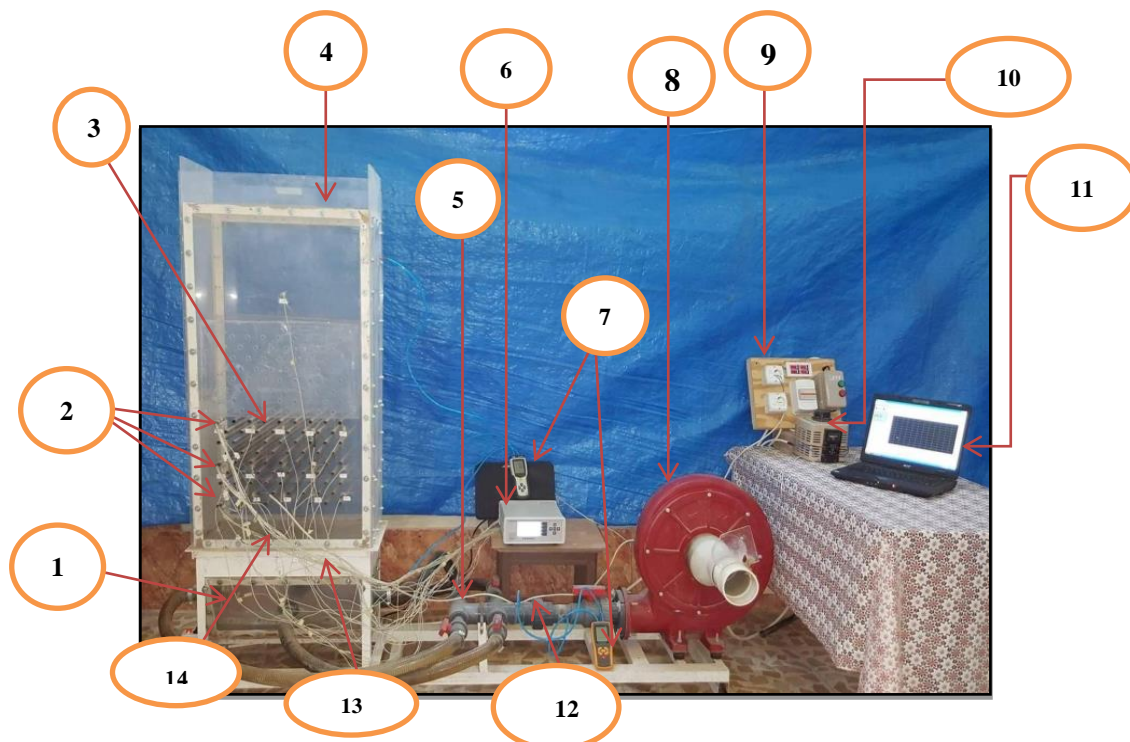
شكل(1): صورة فوتوغرافية لجهاز الاختبار

\   جدول(1): أجزاء الجهاز اختبار

اسم جزء	ت	اسم جزء	ت	اسم جزء	ت
الة الحاسوب	11	مسجل درجات الحرارة	6	الصندوق مخروطي	1
فوهه مترية	12	جهازي قياس الفروق الضغط	7	الانابيب الساخنة	2
موزع الهواء وفلتر	13	منفاخ نوع طاردة المركزية	8	الانبوب نحاسي	3
مزدوجات الحرارية	14	لوحة تجهيز القدرة الكهربائية	9	حاوية بلاستيكية	4
		مجهز قدرة	10	منظومة الانابيب	5

الحسابات:

تحسب قيمة معدل معامل انتقال الحرارة في كل عمود ساخن على اساس معدل درجات الحرارة فيها واعتبار القدرة الكلية تتوزع بشكل متساوي على مسخنات الكهربائية الثلاث لانها مربوطة على التوالي مع بعضها، حيث ان

$$Q = \frac{Q_t}{3}$$ ....(1)

$$h = \frac{Q}{A\,(\overline{T_w} - T_m)}$$ ....(2)

حيث ان

$$A = \pi\,d_t\,L$$ ....(3)

$$\overline{T_w} = \frac{\sum_{i=1}^{i=5} T_{w.i}}{5}$$ ....(4)

$$T_m = \frac{T_{in} + T_{out}}{2}$$ ....(5)

اما بالنسبة لايجاد الخواص (k, μ, ρ) للهواء عند (T_f) من جدول خواص الفيزياوية للهواء في الضغط الجوي (Holman 2010):

$$T_f = \frac{T_m + \overline{T_w}}{2}$$ ....(6)

اما لايجاد سرعة الغاز فقد تم الاعتماد على قانون البرنولي في تحويل فرق الضغط إلى السرعة، كما موضح في المعادلة (7) (Al-Mola 2008):

$$U = \sqrt{2gH}$$ ....(7)

ويتم احتساب عدد رينولد وعدد نسلت على اساسي قطر الانبوب وقطر جسيمات الرمل ، كما في ادناه (Moawed et al. 2010):

$$Re_t = \frac{\rho_a\,U\,d_t}{\mu_a}$$ ....(8)

$$Re_p = \frac{\rho_a\,U\,d_p}{\mu_a}$$ ....(9)

$$\overline{Nu_t} = \frac{\overline{h}\,d_t}{k_a}$$ ....(10)

$$\overline{Nu_p} = \frac{\overline{h}\,d_p}{k_a}$$ ....(11)

النتائج ومناقشة:

النتائج التي حصلت عليها من الاختبارات التي اجريت على نموذج الرمل (0.15) ملم لمختلف المواقع للاعمدة الساخنة من (X1 الى X5) والتي عبرت عنها بالعلاقة بين (Nu_t وRe_t)، كما موضح في الاشكال من (3) الى (5)، حيث يلاحظ فيها تأثير كبير لكل من موقع العمود وسرعة الهواء على قيم Nu_t. في الشكل (3) يلاحظ بأن اعلى قيم لـ(Nu_t) حصلت في (HT1) عند (X5) و تراوحت قيمتها من (34.5 الى 36.5)، بينما المواقع الاخري لعمود (HT1) كانت متقاربة من بعضها محصورة بين (28 <Nut> 32). اما بالنسبة للعمود (HT2)، فقد حصلت اعلى مستوى لقيم (Nu_t) عند موقع (X5) ايضا" و تروحت بين (30.7 الى 33.7). حيث يلاحظ مستوى قيم (Nu_t) عند جميع المواقع للعمود (HT2) اقل مستوى من قيم المواقع المنظرة للعمود (HT1) كما مبين في الشكل (4). في حين مستوى القيم (Nu_t) عند العمود (HT3) كانت عالية جدا في جميع المواقع مقرنتا" بالعمودين السابقين، والسبب هو غمور العمود (HT3) بالكامل داخل الطبقة المميعة في جميع الحالات وهذا ما ادى الى حصول على قيم عالية لـ(Nu_t). كما مبين في الشكل (5) اعلى مستويات لقيم (Nu_t) حصلت عند موقع (X1) عكس ما جاء في الحالتين السابقتن وتراوحت بين (234.5 الى 247.5)، اما في موقع (X5) حصلت عندها ادنى مستويات لقيم (Nu_t) في مدى لـ(Re_t) اقل من 190.

اما الاختبارات التي اجريت على نموذج الرمل (0.3) ملم عبرت عن نتائجه بالاشكال من (6 الى 8)، يلاحظ فيها مستويات لقيم (Nu_t) اقل بكثير للعمودين (HT1 و HT3) عن ما حصلت عليها من نموذج الرمل (0.15) ملم، بينما حصل العكس عند العمود (HT2)، كانت مستوى قيم (Nu_t) اعلى من القيم التي حصلت في المواقع المناظرة في عند (HT2) في نموذج الرمل (0.15). حيث كانت حصلت اعلى مستوى لقيم (Nu_t) في الاختبارات على نموذج الرمل (0.3) في العمودين (HT1 و HT2) عند موقع X5 وتراوحت

تقريباً بين (30-32) و (32- 34) على التوالي، بينما عند العمود (HT3) كانت قيم (Nu_t) لجميع الاعمدة محصورة بين (35 الى 50) لمدى (Re_t) اقل من 150، اما ان في المديات اعلى منها كانت لموقعين X2 و X4زيادة كبيرة في قيم (Nu_t) لكليهما وكانت بحدود (70).

اما عند تحليل نتائج الاختبارات على اساس قطر الجزيئي للرمل والتي عبرت عنها في الاشكال (9 الى 11) للاختبارات على نموذج الرمل (0.15) ملم ، عند مقارنة قيم (Nu_P) فيها، يلاحظ مستوى القيم التي عليها لجميع المواقع للعمود (HT3) اعلى بكثير من العمودين (HT1 وHT2) والتي تقدر بـ (ثلاث الى 8) اضعاف، حيث كانت اعلى مستوى لقيم (Nu_P) عند العمودين (HT1 و HT2) في موقع X5 وتراوحت بين (0.38 الى 0.41) و (0.36 الى 0.41) على التوالي, بينما عند عمود (HT3) تراوحت بين (2.5 الى 3) عند موقع X1. في حين الاشكال (12 الى 14) للاختبارات على نموذج الرمل (0.3) ملم، يلاحظ فيها تقارب كبير بين قيم (Nu_P) للعمودين (HT1 و HT2) مع قيم النموذج السابق للرمل، بينما مستوى قيم التي حصلت عليها في العمود (HT3) كانت اقل بكثير مقارنتا" بقيم نفس العمود في نموذج الرمل (0.15) ملم وتقدر بـالحد الادنى الى (30%).

حيث قورنت النتائج في الدراسة الحالية مع نتائج التي توصل اليه الباحث(Moawed et al. 2010) تبين بأنها تتطابق من حيث التطبيق ولكن باختلاف اقطار الجسيمات الرمل.
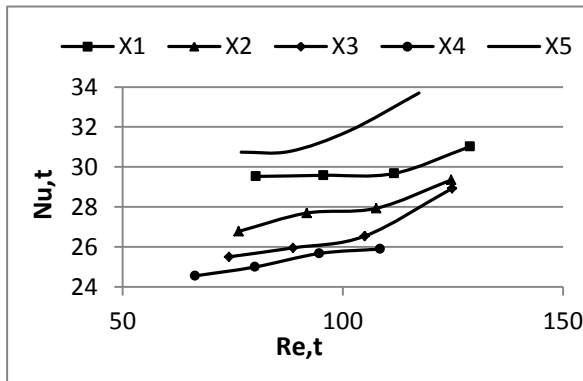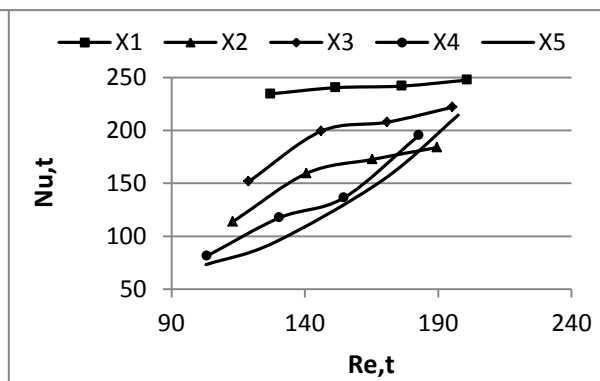

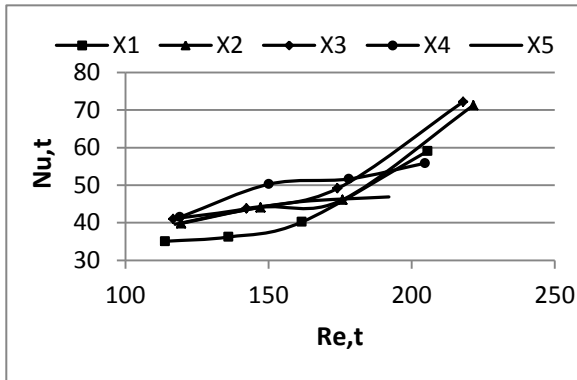شكل(4) علاقة معدل عدد نسلت بعدد رينولد عند (HT2) و($d_p = 0.15mm$)
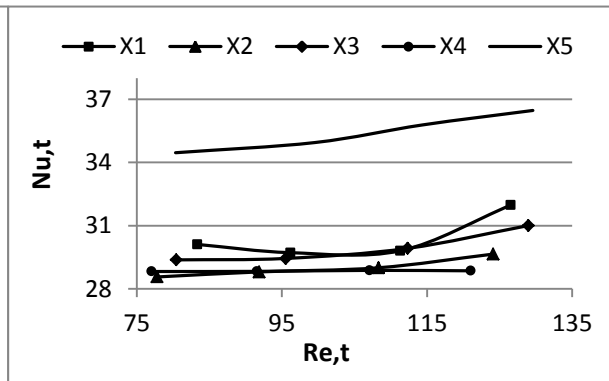
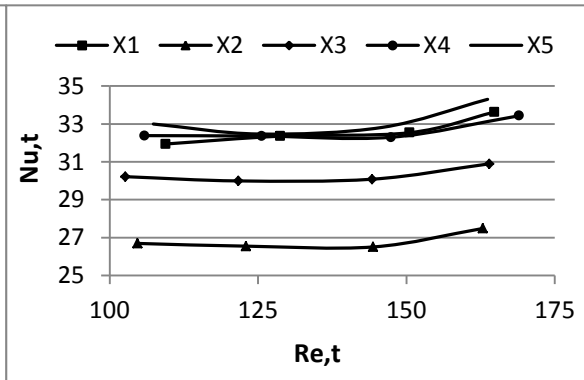شكل(3) علاقة معدل عدد نسلت بعدد رينولد عند (HT1) و($d_p = 0.15mm$)
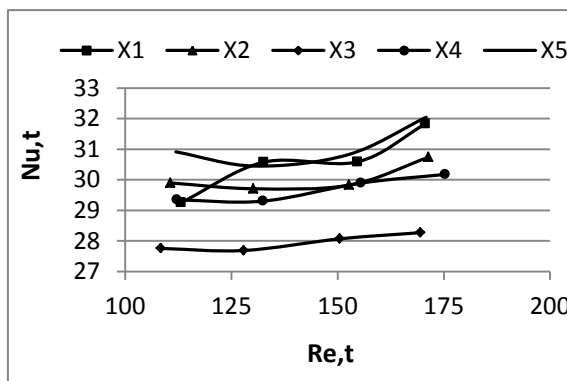
شكل(6) علاقة معدل عدد نسلت بعدد رينولد عند (HT1) و($d_p = 0.3mm$)

شكل(5) علاقة معدل عدد نسلت بعدد رينولد عند (HT3) و($d_p = 0.15mm$)

شكل(8) علاقة معدل عدد نسلت بعدد رينولد عند
(HT3) و($d_p = 0.3mm$)

شكل(7) علاقة معدل عدد نسلت بعدد رينولد عند
(HT2) و($d_p = 0.3mm$)

شكل(10) علاقة معدل عدد نسلت بعدد رينولد عند
(HT2) و($d_p = 0.15mm$)

شكل(9) علاقة معدل عدد نسلت بعدد رينولد عند
(HT1) و($d_p = 0.15mm$)

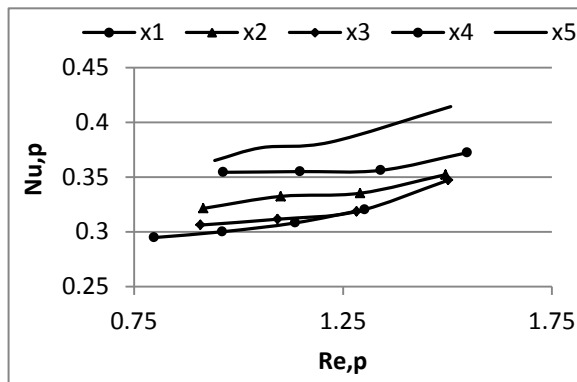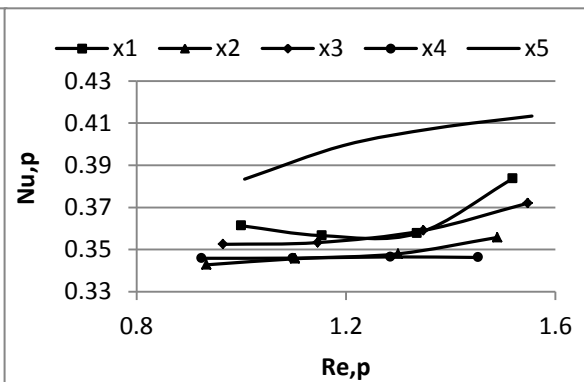شكل(12) علاقة معدل عدد نسلت بعدد رينولد عند
(HT1) و($d_p = 0.3mm$)

شكل(11) علاقة معدل عدد نسلت بعدد رينولد عند
(HT3) و($d_p = 0.15mm$)

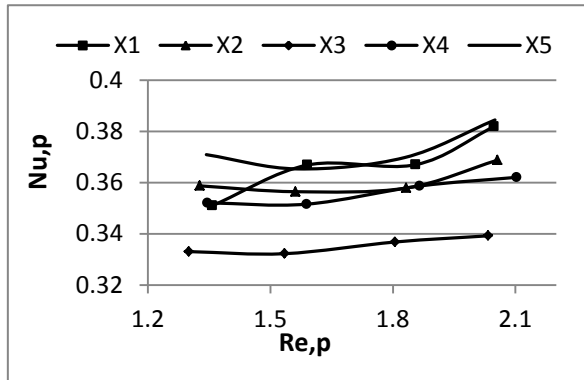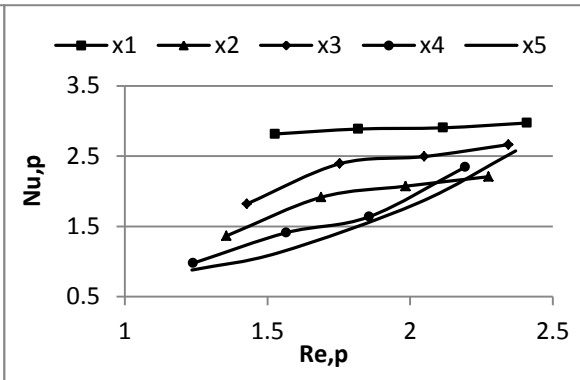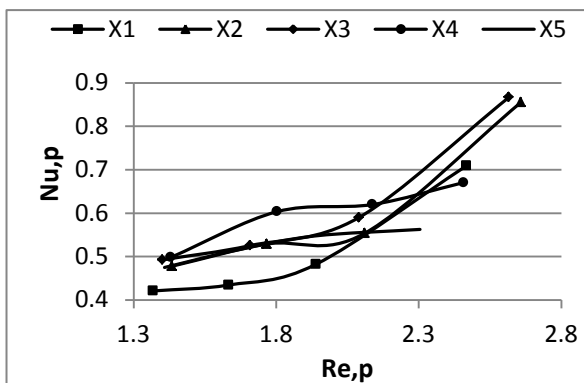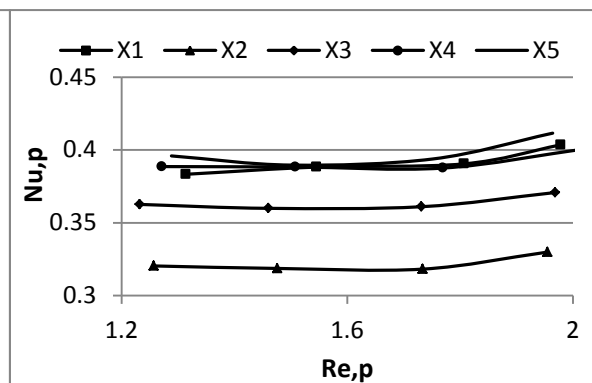شكل(14) علاقة معدل عدد نسلت بعدد رينولد عند
(HT3) و($d_p = 0.3mm$)

شكل(13) علاقة معدل عدد نسلت بعدد رينولد عند
(HT2) و($d_p = 0.3mm$)

الاستنتاجات:

من خلال استعراض النتائج التى اجريت على نموذجين من الرمل (0.15 و 0.3) ملم في وحدة التمييع المشار اليها في اعلاه وفي الظروف التشغيلية الموضحة في الجانب العملي، استنتجت مايلي:

1. قيم كل من الـ(Nu_tوNu_P) عند العمود HT3 في جميع المواقع اعلى بكثير من العمودين (HT1 وHT2) والسبب هو الغمور التام للعمود HT3 داخل الطبقة المميعة بشكل مستمر، بينما العمودين (HT1 وHT2) كانت تتناثر على اسطحهما حبيبات الرمل اثناء الاختبار.

2. تأثير كبير لقطر حبيبات الرمل على قيم كل من الـ(Nu_tوNu_P)، حيث كانت القيم عند قطر (0.15) ملم اكبر مما حصلت عليها عند قطر (0.3) ملم وهذا يدل على زيادة قيمة معامل انتقال الحرارة عند نموذج الرمل (0.15) ملم بنسبة ما لا يقل عن 300%, عدد نسلت يتناسب طردياً مع قيمة معامل انتقال الحرارة.

3. اما بالنسبة لتاثير موقع الاعمدة فانه واضح، حيث لم يحصل أي من الاعمدة على قيم نفسها او المقاربة للمواقع التي اجريت لها الاختبار.

المصادر :

[1].Al-Tamimi , Tareef N. M., 2000, "*Fluidized Bed Heat Pipe Heat Exchanger*" MSc Thesis, Mechanical Eng. Dep. University of Technology.

[2].Basu P., 2006. *"Combustion and gasification in fluidized beds"*,   Boca Raton: CRC/Taylor & Francis.

[3].Holman J. P., 2010. " *Heat Transfer*", Magraw Hill, 758pp.

[4].Johansson K., Norlingb R., Hjornhede A., Almstedt A. E., Johansson F., Nylund A., 2004.*"Hydrodynamics and steel tube wastage in a Fluidized bed at elevated temperature"*, Chemical Engineering Science, Vol. 59,Issue 1,pp:31-40.

[5].Masoumifard N., Mostoufi N., Hamidi A., Sotudeh-Gharebagh R., 2008."*Investigation of heat transfer between a horizontal tube and gas-solid fluidized bed"* International Journal of Heat and Fluid Flow, Vol. 29, Issue 5, pp: 1504-1511.

[6].Moawed M. A. , Berbish N. S., Allam A. A. , El-Shamy A. R., El-Shazly K. M.,2010.*"Heat Transfer between Fluidized Bed and Horizontal Bundle of Tubes in a Vertical Channel"*, International Journal of Chemical Reactor, Vol. 8, Article A105, Issue 1542-6580.

[7].Salwe A. M., Pande S. Sh., Khan S. J., 2014.*"Effect of Velocity and Particle Size on the Coefficient of Heat Transfer in Fluidized Bed Heat Exchanger"* International Journal of Engineering Research and General Science, Vol: 2, Issue 2, pp: 230-234.

[8].Sunderesan, S. R., Clark N. N., 1995. *"Local heat transfer coefficients on the circumference of a tube in a gas fluidized bed"* International Journal of Multiphase Flow, Vol. 21, Issue 6, pp: 1003-1024.

[9].Xu G., Sun G., Gao Sh., 2004.*"Estimating radial voidage profiles for all fluidization regimes in circulating fluidized bed risers"* Powder Technology, Vol: 139, Issue 2, pp: 186-192.

:

الكتاب الجامعة في مسيرتها العلمية ، اسوة بغيرها من المؤسسات الاكاديمية الحكومية وغير الحكومية بجهود حثيثة لإصدار مجلة علمية محكمة تختص بالعلوم الإنسانية، لتضطلع بمهمة النتاجات والبحوث العلمية الرصينة كثمار للجهود الفكرية والعلمية للباحثين الأفاضل في صرحنا الاكاديمي والعلمي هذا ، فضلا عن المؤسسات الاكاديمية والمراكز العلمية الاكاديمية الاخرى لتصب في معين العلم والمعرفة الواسعين .

إن هدف مجلتنا (مجلة الكتاب للعلوم الإنسانية) هو تقييم بحوث الأكاديميين والباحثين ونشرها فضلا عن بحوث طلبة الدراسات العليا. ونظراً الى كثرة التفرعات العلمية واختصاصات العلوم الانسانية ، فقد أقرت هيئة التحرير الموقرة أن تصدر هذه المجلة لتهتم بنشر النتاجات والبحوث العلمية المختلفة والتي تعنى بالعلوم الادارية والمالية, والعلوم القانونية ,والعلوم التربوية وفي المجالات المرتبطة بها كافة.

تتمركز مهمة هيئة تحرير المجلة باستلام البحوث من الباحثين وتدقيقها من حيث مطابقتها لشروط النشر وتسجيل البحوث واعطائها رقم خاص وتحديد المقومين في حقل الاختصاص كما تقوم هيئة التحرير بارسال البحوث الى المقومين ومتابعتها. واستلام البحوث العائدة من التقييم وتسليمها الى الباحث لغرض اجراء التعديلات المقرَرة من المقيمين ومن ثم تزويدهم بقبول نشر بعد اجراء التعديلات المطلوبة ثم القيام بنشر البحوث باعداد المجلة كل حسب اختصاصة وتسلسله.

التدقيق اللغوي

أ.د. عباس جودة رحيم   /تدقيق اللغة الانكليزية

أ.م.د. ابراهيم احمد العميري/تدقيق اللغة العربية

اللجنة الفنية

رئيسا   م.م عمر عادل محمد علي

عضوا   م. محمد نعمان مراد

عضوا   م.م. مروان حازم احمد علي

عضوا   عامر سعد صالح

مثال:

[1] P. Ring and P. Schuck, "*The Nuclear Many-Body Problem*", First Edition, Springer-Varlag, New York (1980).

ب) إذا كان المرجع عبارة عن ورقة بحث أو مقال في مجلة: يجب كتابة اسم المؤلف أولاً ، عنوان المقالة (غامق ومائل) بين فارزتين مرفوعتين ، اسم المجلة ، المجلد (العدد) ، الصفحة (السنة).

[2] Ali H. Taqi, R. A. Radhi, and Adil M. Hussein, "*Electroexitation of Low-Lying Particle-Hole RPA States of 16O with WBP Interaction*", Communication Theoretical Physics, 62(6), 839 (2014).

ج) إذا كان البحث عبارة عن رسالة ماجستير أو رسالة دكتوراه ، فيجب كتابة اسم الباحث يليه اللقب ، وعنوان الرسالة (غامق ومائل) بين فارزتين مرفوعتين ، اسم الجامعة ، والبلد (السنة).

[3] R. A. Radhi, "*Calculations of Elastic and Inelastic Electron Scattering in Light Nuclei with Shell-Model Wave Functions*", PhD Thesis, Michigan state University, USA (1983).

د) إذا كان المرجع من مؤتمرفيكتب اسم المؤلف ، "عنوان البحث" (غامق ومائل) بين فارزتين مرفوعتين ، اسم المؤتمر ، البلد ، جهة النشر ، المجلد ، الصفحة (السنة).

مثال:

[4] Ali H. Taqi and Sarah S. Darwesh, "*Charge-Changing Particle-Hole Excitation of 16N and 16F Nuclei*", 3rdInternational Advances in Applied Physics and Materials Science Congress, Turkey, AIP Conf. Proc., 1569, 27 (2013).

ه) بعد نشر الورقة وعرضها في صفحة المجلة ، فان المؤلف ليس لديه الحق في طلب اللاوراق الاصلية التي قدمها في أي حال من الاحوال.

بيان الخصوصية

سيتم استخدام الأسماء وعناوين البريد الإلكتروني التي تم إدخالها في موقع المجلة بشكل حصري للأغراض المذكورة لهذه المجلة ولن يتم توفيرها لأي غرض آخر أو لأي طرف آخر.

ملاحظة : للمزيد من المعلومات يمكن زيارة رابط المجلة:

Note: For more information, visit www.uoalkitab.edu.iq

http://www.isnra.com/ojs/index.php/KJPS

كما ويمكن مراسلة المجلة على البريد الالكتروني: kjps@uoalkitab.edu.iq

او بريد مدير التحرير: sameersaadoon@yahoo.com

<div dir="rtl">

قواعد و تعليمات النشر في
مجلة الكتاب للعلوم الصرفة

المتطلبات العامة

1. يتم تقديم البحث الى سكرتارية تحرير المجلة بشكل مباشر باربع نسخ مع قرص مدمج او عبر البريد الاليكتروني للمجلة بصورة ملف (MS-Word) وملف (PDF).
2. تخضع البحوث قبل ارسالها الى المقومين العلميين الى برنامج الاستلال Turnitin
3. تقبل البحوث للنشر بعد تحكيمها من قبل مقيمين علميين وحسب الاصول.
4. تبلغ اجور النشر في المجلة (75000) دينار للباحث من داخل كلية الكتاب الجامعة و(125000) دينار للباحثين من خارج الكلية و(125$) للباحث الاجنبي.

ثانيا: لإعداد بحث للنشر ، يجب على المؤلفين اتباع الإجراءات التالية.

1. المقالة

يجب كتابة المقالة على جانب واحد من الورق A4 : الهامش الأيمن = 2.5 سم ، الهامش الأيسر = 2.5 سم و 2 سم للأعلى والأسفل) مع مسافة 1.5 ويجب ترقيم الصفحات.

2.تنظيم المحتوى:

MS Word لاستخدامه على النحو التالي: الخط "Simplified Arabic" للورقة العربية ، و "Times New Roman" للمقالات الإنجليزية.

3.حجم الخط:

- العنوان الرئيسي للبحث 18 غامق
- اسماء المؤلفين عربي او انكليزي 11 غامق
- العناوين الرئيسية 14 غامق.
- العناوين الفرعية 12 غامق.
- الملخص 12.
- النص (متن البحث) 12.

4.الترتيب (تسلسل المحتويات)

يكون ترتيب محتوى البحث كما يلي: عنوان المقالة ، أسماء المؤلفين وعناوينهم ، الملخص باللغة العربية و الإنجليزية (كلاهما مطلوبان) ثم متن البحث.

5.عنوان ورقة البحث: يجب أن يكون العنوان قصيرًا قدر الإمكان ويشير إلى محتويات الموضوع مع اسم (أسماء) المؤلفين. كما ان المؤلف الذي ستتم المراسلات معه تظهر معه اشارة (*) مع إظهار بريده الإلكتروني.

6. عدد الصفحات: يجب ألا تحتوي الورقة على أكثر من 15 صفحة من صفحات المجلة ، بما في ذلك المخططات والرسوم البيانية. سيتم تحميل 5000 دينار عراقي (3 دولار) لكل صفحة إضافية, علما ان اجور النشركالاتي:

للباحثين من كلية الكتاب الجامعة: 75 ألف دينار

لبقية الباحثين: 125 ألف دينار

7. الملخص: لا يزيد على 250 كلمة على أن يشتمل على الغرض والنتائج والاستنتاجات الاساسية. يجب أن يحتوي أيضًا على قيم المعرفة لموضوع البحث و التركيز على محتوى الموضوع ويتضمن الكلمات الأساسية المستخدمة في جميع أنحاء الصحيفة.

8.الاشكال و الرسوم البيانية: يجب أن يحتوي كل رسم بياني على عنوانه أسفل الرسم التخطيطي بحجم 12. يجب أن يكون الرسم التخطيطي قابلاً للتحرير, التكبير و التصغير.

9. الجداول: يجب أن تحتوي الجداول على عناوين بحجم 12. يجب أن يكون النص المستخدم داخل الجداول بحجم 12.

10. المراجع: تذكر المراجع المستخدمة في البحث بالترتيب وأعدادها تُعطى داخل قوسين مربّعين [ ]. يجب اتباع الإرشادات التالية:

(أ) إذا كان المرجع عبارة عن كتاب ، فيجب كتابة اسم الباحث الاول متبوعًا بالأسماء الأخرى. ثم عنوان الكتاب (غامق ومائل) بين فارزتين مرفوعتين، ثم الطبعة ، الناشر ، مكان النشر (سنة النشر).

</div>

هيئة التحرير

1- أ. د. أياد غني أسماعيل .   رئيساً
2- أ. م. د. سمير سعدون مصطفى .   مدير التحرير
3- أ. د. عبد الرسول خضر عباس .   عضواً
4- أ. د. علي اسماعيل عبد الله .   عضواً
5- أ. ضياء اسماعيل ابراهيم .   عضواً
6- أ. م. د. نهاد عبد الوهاب محمد .   عضواً
7- أ. م. د. هيثم عبد العال عبود .   عضواً
8- أ. م. د. وفيقة تايه ذياب .   عضواً
9- أ. م. د. محمد فوزي عبد الله .   عضواً
10- أ. م. د. كاظم محمد حسين .   عضواً

الهيئة الاستشارية :

1- أ. د. باسل محمد سعيد .   جامعة الموصل / العراق
   رئيساً
2- أ. د. خديجة أحمد اسماعيل .   جامعة الإسكندرية / مصر   عضواً
3- أ. د. عبد المنعم ابو طبيخ .   الجامعة التكنلوجية / العراق   عضواً
4- أ. د. محمد الجرادين .   جامعة لوند / السويد   عضواً
5- أ. د. سالمة عبد الكريم أبو خطوة .   الجامعة الطبية الوطنية الليبية/ليبيا   عضواً
6- أ. د. علي حسين تقي .   جامعة كركوك / العراق   عضواً
7- أ. د. عزيز ابراهيم عبد الله .   جامعة تكريت / العراق   عضواً
8- أ. د. رامي عبد القادر ماهر .   جامعة الاسراء / الاردن   عضواً
9- أ. د. قاسم موسى العبيدي .   جامعة فيلادلفيا / الاردن   عضواً
10 - أ. د. غانم بطرس اليشع .   جامعة نورثمبريا نيوكاسل/بريطانيا عضوا

رئيس التحرير

أ.د. اياد غني اسماعيل

(عميد كلية الكتاب الجامعة)

مدير التحرير

أ.م .د .سمير سعدون مصطفى